CHEMICAL REVIEWS

pubs.acs.org/CR

Review

Versatile Tools for Understanding Electrosynthetic Mechanisms

Eric C. R. McKenzie,[§] Seyyedamirhossein Hosseini,[§] Ana G. Couto Petro, Kelly K. Rudman, Benjamin H. R. Gerroll, Mohammad S. Mubarak, Lane A. Baker, and R. Daniel Little*

Cite This: https://doi.org/10.1021/acs.chemrev.1c00471

Read Online

ACCESS | Metrics & More | Article Recommendations

ABSTRACT: Electrosynthesis is a popular, green alternative to traditional organic methods. Understanding the mechanisms is not trivial yet is necessary to optimize reaction processes. To this end, a multitude of analytical tools is available to identify and quantitate reaction products and intermediates. The first portion of this review serves as a guide that underscores electrosynthesis fundamentals, including instrumentation, electrode selection, impacts of electrolyte and solvent, cell configuration, and methods of electrosynthesis. Next, the broad base of analytical techniques that aid in mechanism elucidation are covered in detail. These methods are divided into electrochemical, spectroscopic, chromatographic, microscopic, and computational. Technique selection is dependent on predicted reaction pathways and electrogenerated intermediates. Often, a combination of techniques must be utilized to ensure accuracy of the proposed model. To conclude, future prospects that aim to enhance the field are discussed.

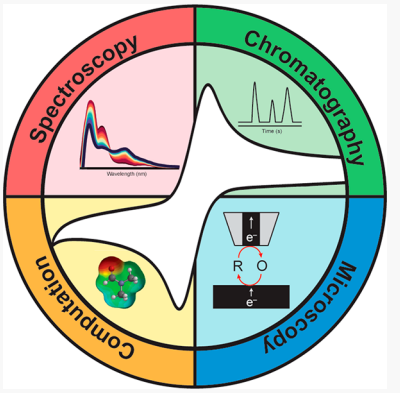

CONTENTS

Received: June 1, 2021

1. INTRODUCTION

Organic electrosynthesis has experienced a surprising, yet gratifying, revival that extends beyond established venues to garner more interest from traditional synthetic chemists. Recent collections have highlighted this interest and underscored the inherent benefits of electrochemical synthesis.[1−3] The growth in popularity of electrochemically driven transformations arises from opportunities in green chemistry, improved atom economy, and control over reaction landscapes.[4,5] Fundamental organic transformations, including C−C coupling,[6−9] C−H activation,[10−14] and stereoselective heterocyclic reactions,[15,16] have been explored electrochemically. Indeed, a broad base of applications in electrosynthesis continues to grow.[17−20]

As with any chemical reaction, mechanistic studies are key and may be understood through identification of intermediates and elucidation of reaction kinetics. To this end, a host of in situ and ex situ analytical techniques are employed. Analysis of electrosynthetic reactions can benefit from these techniques but often requires unique approaches. To date, published reviews have focused primarily on methods of electrosynthesis and electrochemical tools for mechanistic studies.[21,22] Electrochemical approaches combined with complementary tools, such as spectroscopic, spectrometric, or chromatographic techniques, along with computational analysis and simulation comprise the larger toolbox. This review seeks to survey the complete analytical toolbox accessible to the electrosynthetic chemist to include hybrid approaches that extend beyond traditional electroanalytical methods. Fundamentals of electrosynthetic reactions are first described, followed by a detailed account of the wide array of available experimental and computational approaches.

2. FUNDAMENTALS OF ELECTROSYNTHESIS

2.1. Instrumentation

Electrolyses can be performed either chronoamperometrically (potentiostatic control) or chronopotentiometrically (galvanostatic control), as illustrated in Figure 1. In potentiostatic electrolysis, a potentiostat applies a fixed potential to the working electrode (WE) vs a reference electrode (RE) and current flows between the WE and the counter electrode (CE). Under galvanostatic control, a galvanostat, which can be as simple as a 9-V battery or a photovoltaic panel, passes a fixed current through the cell.[18,23] In this case, the WE potential is allowed to float, necessitating only two electrodes. Each technique differs in terms of instrumentation and power requirements, as detailed below. In-depth discussions of electronic circuitry and control hardware can be found elsewhere.[24−26]

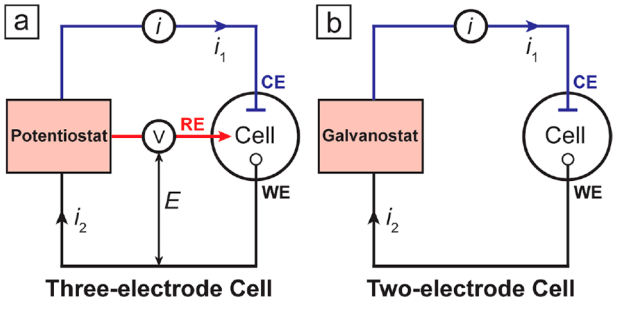

Figure 1. (a) Three-electrode configuration for potentiostatic electrolysis, and (b) two-electrode configuration for galvanostatic electrolysis. WE = working electrode, CE = counter electrode, RE = reference electrode.

Practicalities of two- and three-electrode electrochemical instrumentation are important to consider. For instance, large-scale electrolyses at constant potential require a potentiostat with electronic control units capable of establishing stable potentials for extended periods of time. In practice, the potential applied by the potentiostat may differ slightly from the intended potential as a result of solution resistance. Electric resistance within the electrolysis cell can be lowered through minimization of the WE and RE separation and selecting a solvent-supporting electrolyte with high conductivity (section 2.3). Potentiostats for electrosynthesis typically include high-voltage compliance and are rated for significant current (i.e., >200 mA) relative to electroanalytical equipment. Potentiostats can be acquired commercially or manufactured in house. Home-built potentiostats have been employed mostly for field analysis of various analytes or teaching purposes.[27−29]

2.2. Electrodes

2.2.1. Working Electrodes. Proper selection of the WE material is pivotal for optimization of product yield and selectivity in electrosynthesis. Some requirements for WEs include (1) high conductivity, (2) wide exploitable potential range, (3) chemical inertness, (4) physical stability under various conditions (temperature, pressure, solvents), (5) rapid charge transfer, and (6) low residual current. In addition, the electrode material should be inexpensive and preferably nontoxic.[30,31] In most purely electrosynthetic applications, the WE should have a high surface area for increased mass transport. In contrast, and as is discussed below, smaller electrode areas can provide special opportunities for electroanalytical applications of synthetic reactions.[32−36] An overview of common electrode materials related to electrosynthesis is described below.

Carbon Electrodes. Carbon is a popular, relatively inexpensive electrode material that exists in many forms with a wide potential window from ca. −2 to 2 V vs Ag/AgCl in aqueous media.[37−40] Glassy (vitreous) carbon is a hard, strong, chemically stable material resistive to corrosion and oxidation.[31,41] Reticulated vitreous carbon (RVC) electrodes consist of glassy carbon manufactured as foam and have an open, honeycomb structure with increased surface area.[42,43] Carbon felt[44,45] can be utilized as a highly porous electrode and consists of randomly distributed fibers. These electrodes have exceptionally large surface areas as well as high conductivity and chemical stability. Graphite is less expensive and more conductive than glassy carbon but is less chemically stable and can be prone to chemical modification.[31,46] Structural differences between the edge and the basal planes are caused by stacked graphene planes and result in different reactivities.[47] For example, alkanes have been shown to have a strong affinity toward the basal plane, while polar solutes have a strong affinity toward edge sites.[48] For electrosynthesis, RVC and carbon felt electrodes are more efficient as mass transfer is enhanced as electrode porosity increases.

Boron-doped diamond (BDD) is a semiconductor electrode that is becoming increasingly popular.[49−52] Diamond alone is a

https://doi.org/10.1021/acs.chemrev.1c00471
Chem. Rev. XXXX, XXX, XXX−XXX

chemically inert insulator with a large band gap of 5.45 eV at 300 K. To impart conductivity, diamond must be doped with boron at a concentration of 5×10^{20} atoms cm^{-3}. A BDD electrode can be manufactured with a conductivity as high as 10^{-5} S cm^{-1}.[50,53,54] BDD electrodes are appealing due to their low background currents, rapid electron transfer, and chemical stability in corrosive and high-temperature environments.[54] Moreover, these electrodes have potential windows of 3.2 and 4.6 V in aqueous and organic media, respectively.[55] Large overpotentials for hydrogen evolution (ca. −1.5 V vs Ag/AgCl)[56,57] and oxygen reduction (ca. 1−2 V vs Ag/AgCl, dependent on doping treatment)[56−58] in aqueous media also make BDD electrodes popular. This suppresses competing processes and provides access to a wider operational potential window. Furthermore, increased overpotential for oxygen reduction allows for formation of hydroxyl radicals, which can be used for electrochemical cleaning of the electrode surface and degradation of organic compounds.[59] Though expensive, BDD electrodes have been used for a variety of electrosynthetic reactions, such as oxidation of alcohols to reactive alkoxyl intermediates, as well as anodic or cathodic coupling reactions of aryl molecules.[50,54] Notably, alcohol oxidation at BDD electrodes is preferred relative to glassy carbon electrodes, where such reactions are difficult to achieve since oxidation of the glassy carbon anode is more facile.[60] Reviews and monographs offer more detailed descriptions of carbon electrode materials.[32,48,50,61]

Metal Electrodes. General features of metal electrodes include fast electron-transfer kinetics for many redox systems and relatively wide anodic potential windows.[62] Platinum and platinum alloys are popular as they are robust, easy to clean, chemically (and electrochemically) stable, and resistive to corrosion.[31,63,64] In aqueous media, Pt has a high overpotential for oxygen evolution but is limited by proton reduction in the cathodic range. In aprotic media, Pt has large cathodic and anodic windows. Pt is commonly employed in electrosynthesis for oxidation of organic compounds, such as methanol to CO_2.[65] Furthermore, oxygen reduction at Pt cathodes forms superoxide in organic media, which can react with organic compounds at electron-deficient carbon centers.[64] Despite these advantages, widespread and large-scale use is limited by the high cost and poisoning of the electrode surface by unintended adsorbates, such as water or supporting electrolyte.[65]

At cathodic potentials, mercury electrodes have special historical significance[66] and are popular because of the exceptionally large overpotential for hydrogen evolution.[40] In addition, liquid mercury provides a reproducible, renewable surface. Mercury has been used for various electrosynthetic reactions,[67] such as intramolecular addition or cyclization,[68−71] and dimerization.[72,73] Dropping mercury electrodes (DMEs) have been used traditionally for electroanalytical applications such as stripping analysis[74,75] and polarography.[76,77] However, these electrodes are highly toxic and limited to reductive potentials as mercury is easily oxidized. As a result, mercury electrodes have been phased out recently.[32] Silver continues to grow as a popular replacement, particularly due to the catalytic features of these electrodes. The strong affinity of halides for silver allows carbon−halogen bond reduction to occur at more positive potentials.[78] While these electrodes are used almost exclusively for cathodic processes, the ease of silver oxidation can be exploited for techniques such as stripping analysis.[79]

Modified Electrodes. Electrode surfaces can be modified either chemically (covalently)[80,81] or physically (noncovalently)[82] to increase electrode reactivity through analyte binding to the modified surface. Various alterations of electrode surfaces have been reported in the literature, including addition of self-assembled monolayers (SAMs), biofilms, or redox polymers.[83−85] Moreover, metal alloys have been employed to maintain desired electrochemical properties while minimizing corrosion of the electrode surface.[86] Modification pathways have been described extensively by Murray.[87] Das and Stahl[88] reported a remarkable application of modified electrodes through construction of a TEMPO-immobilized electrode for alcohol oxidation. 4-Amino-TEMPO coupled with 1-pyrenebutyric acid generates a pyrene-linked 4-acetamido-TEMPO species. Modification of a glassy carbon electrode is achieved through interaction between a drop-cast layer of multiwalled carbon nanotubes and the 4-acetamido-TEMPO species. The robustness of this process results from $\pi-\pi$ stacking between pyrene and the nanotubes. This modified electrode was employed to perform electrocatalytic oxidation of various alcohols. Synthetic applications of modified electrodes have also involved asymmetric synthesis of organic compounds.[89,90] However, their use in organic electrosynthesis has not been fully exploited.[40]

In selecting a suitable WE, the overpotential for competing reactions (e.g., hydrogen evolution) as well as the propensity of organic molecules to adsorb to the electrode surface are important considerations. The latter can prove problematic in instances where adsorption is so strong that electrode passivation terminates the electrolysis as unreacted substrate cannot reach the surface. In cases where adsorption is deleterious and a WE of different composition cannot be implemented, addition of a redox mediator can prevent adsorption from occurring.[31]

2.2.2. Counter Electrodes. The CE should be in close proximity to the WE to minimize ohmic drops, thereby allowing accurate determination of the applied potential. In the case of a reversible redox process, the CE is often stored in a separate compartment (section 2.4) to ensure that no competitive reactions occur and the desired product does not reoxidize or rereduce.[91] In standard applications, CEs are typically made from carbon or a metal other than mercury.

Although specific reactions at the CE can often be disregarded, these electrodes may function as a sacrificial anode to balance ion exchange. In this case, CEs are composed of easily oxidized metals (e.g., Al, Mg, Zn), which generate metal ions in solution as reduction occurs at the WE. Sacrificial anodes have been utilized for reduction of haloorganic compounds, especially in carboxylic acid, alcohol, and ketone synthesis.[92−97] Metal ions are proposed to participate in the reaction by catalyzing electron transfer or stabilizing anionic intermediates.[98,99] In a similar fashion, electroreduction of triphenylphosphine oxide to triphenylphosphine was achieved with the aid of a sacrificial Al anode.[100] Introduction of Al^{3+} was beneficial for the selective reduction of P−O bonds over P−C bonds and demonstrates a novel technique to recycle widely used industrial feedstock.

Reactions at the CE can also be coupled with reactions at the WE through paired electrosynthesis (section 2.5.3), where both reactions work synergistically to drive the overall reaction forward.[101−103] A successful paired electrolysis optimizes the energy efficiency of the cell, which minimizes the potential

https://doi.org/10.1021/acs.chemrev.1c00471
Chem. Rev. XXXX, XXX, XXX−XXX

difference between the WE and the CE. In many cases, this is done by selecting a reaction that readily occurs at the CE.[104]

2.2.3. Reference Electrodes. If accurate knowledge of the WE potential is required, a RE is incorporated into the electrochemical cell.[32,91,105] REs have a fixed potential set by a defined composition and electrochemical reaction. For a given experiment, a RE must be selected with careful consideration of the electrolyte solution in which the experiment will be conducted. Ideally, the RE is of similar composition to the electrolyzed solution; however, in practice, the composition of the RE may vary slightly from that of the solution to be analyzed. If the two solutions are too different, formation of liquid junction potentials must be accounted for in reporting accurate potentials.[91]

Aqueous Reference Electrodes. Reference electrodes derived from the H^+/H_2 redox couple include the normal hydrogen electrode (NHE), the standard hydrogen electrode (SHE), and the reversible hydrogen electrode (RHE). Detailed descriptions of the construction and potential measurements of the RHE and SHE can be found elsewhere.[106] Briefly, the SHE electrode is composed of a platinum wire immersed in an aqueous solution containing H_3O^+ at unit acidity ($a_{H_3O^+} = 1$) and $H_2(g)$ at a pressure of 1 bar. By definition, a SHE has a standard potential (E^0) of 0.00 V.

While electrochemical half-reactions are measured against the SHE, these electrodes are not used in practice as it is difficult to maintain a solution at unit acidity and $H_2(g)$ at 1 bar. Instead, silver/silver chloride (Ag/AgCl) REs are used frequently for electrochemical studies in aqueous solution owing to stability and ease of construction. A typical procedure to fabricate Ag/AgCl REs involves immersion of a Ag wire, coated with a thin layer of AgCl, in saturated KCl. However, other sources of chloride (e.g., 1 M NaCl) have also been employed to make Ag/AgCl REs. Silver chloride can be deposited by placing a silver wire in a freshly prepared 0.1 M Fe^{III} chloride solution or electrooxidation for a short duration in 1.0 M KCl solution.[107] For accurate potential reporting, the potential of a home-built Ag/AgCl RE must be verified against another standard RE. Other common aqueous REs require use of mercury, such as the saturated calomel electrode (SCE), mercury/mercury(I) sulfate (Hg/Hg_2SO_4), and mercury/mercuric oxide (Hg/HgO). Table 1 contains a list of these REs, net electrode reactions, and potentials vs SHE. Procedures for preparation of these electrodes can be found elsewhere.[40]

Organic Reference Electrodes. For experiments in organic solvents, nonaqueous REs must be used to prevent water contamination and minimize liquid junction potentials.[91] Table 2 contains a list of commonly utilized organic REs. The most popular is a silver−silver ion electrode (Ag/Ag^+), which is employed widely in MeCN-based solutions.[109] However, Ag/Ag^+ REs show relatively poor stability due to silver ions leaching from the electrode into solution. As a result, the potential of the Ag/Ag^+ RE must be measured against a stable RE before and after the experiment to monitor possible drift. In cases where silver ions react with the solvent, such as DMF, silver−silver cryptate (Ag/AgCryp)[110] or cadmium-amalgam (Cd/Hg)[111,112] REs are more appropriate.

In some instances, the electrochemical cell design or conditions (e.g., use of ultrasound) may be too complex to incorporate a traditional reference electrode. As an alternative, a quasi-reference electrode (QRE) can be incorporated to provide potential measurement.[113] These electrodes are often as simple as a glass body containing a silver wire immersed in electrolyte solution. A frit located at the bottom of the glass body establishes an electrical connection between the RE and the solution. The potential of this reference must be measured before and after any electrochemical experiment. If a QRE cannot be utilized, in situ references (e.g., Fc^+/Fc) can also be used for potential reporting. This is advantageous as RE potentials can drift with time and junction potential correction is difficult. Incorporation of these references as an internal standard improves reproducibility and allows for more accurate reporting of redox potentials.[114]

Table 1. Aqueous Reference Electrode Potentials[40,91,108]

electrode	net electrode reaction	potential (V vs SHE)
silver chloride (Ag/AgCl, saturated KCl)	$AgCl(s) + e^- \rightleftharpoons Ag(s) + Cl^-(aq)$	+0.197
saturated calomel electrode (SCE) (Hg/Hg_2Cl_2)	$Hg_2Cl_2(s) + 2e^- \rightleftharpoons 2Hg(l) + 2Cl^-(aq)$	+0.241
mercury(I) sulfate (Hg/Hg_2SO_4, saturated K_2SO_4)	$Hg_2SO_4(s) + 2e^- \rightleftharpoons 2Hg(l) + SO_4^{2-}(aq)$	+0.640
mercuric oxide (Hg/HgO, 0.1 M NaOH)	$HgO(s) + H_2O(l) + 2e^- \rightleftharpoons Hg(l) + 2\ OH^-(aq)$	+0.926

Table 2. Organic Reference Electrode Potentials[109,110]

electrode	net electrode reaction	potential (V vs SHE)[a]
silver−silver ion (Ag/Ag^+, 0.1 M $AgNO_3$−MeCN)	$Ag^+(solv) + e^- \rightleftharpoons Ag(s)$	−0.579
silver−silver cryptate ($Ag/AgCryp^+$, 0.005 M $AgClO_4$, 0.01 M Cryp(2,2), 0.05 M Et_4NClO_4 in MeCN)	$AgCryp^+(solv) + e^- \rightleftharpoons Ag(s) + Cryp(solv)$	−0.112
cadmium mercury amalgam (Cd/Hg, $CdCl_2$-saturated DMF)	$Cd^{2+}(solv) + 2e^- \rightleftharpoons Cd(s)$	−0.526

[a]Electrode potentials are dependent on solvent and supporting electrolyte.

2.3. Solvents and Supporting Electrolytes

Use of an electrolyte solution is beneficial to maintain charge neutrality, minimize solution resistance, and provide a medium for movement of species to and from the WE.[40,115,116] Important considerations when choosing a solvent−electrolyte system include: (1) binding affinity or buffer capacity of the electrolyte, (2) electrolyte influence on the double-layer structure, (3) possible reactions with electrogenerated intermediates, (4) solvent potential range, and (5) ease of electrolyte recrystallization.[19,32,111,117] Good solvents should be chemically and electrochemically stable, able to solubilize the analyte, and with notable exceptions[118] have a reasonably large dielectric constant so that high concentrations of supporting electrolyte can be dissolved.[119−121] Organic solvents must also be easily purified and dried.[111,116]

Common supporting electrolytes in aqueous media are inorganic salts, acids, and bases. Before dissolving the supporting electrolyte, water is purified by passing through ion-exchange columns until a specific resistance (nominally 18.2 MΩ cm^{-1}) is attained.[40] The potential window for water is pH dependent and limited by water splitting into hydrogen and oxygen gases at the cathode and anode, respectively. Table 3 depicts the potential windows for various aqueous electrolytes at different electrodes.[40]

https://doi.org/10.1021/acs.chemrev.1c00471
Chem. Rev. XXXX, XXX, XXX−XXX

Table 3. Functional Ranges of Working Electrodes in Aqueous Electrolytes[40,122]

electrode	electrolyte[a]	anodic limit (V vs SCE)	cathodic limit (V vs SCE)
Pt	$HClO_4$	1.30	−0.25
	NaOH	0.50	−1.15
	KCl (0.1 M)	1.00	−1.20
C	$HClO_4$	1.40	−1.00
	NaOH	0.90	−1.50
	KCl (0.1 M)	1.00	−1.30
Hg	$HClO_4$	0.50	−1.10
	NaOH	0.00	−2.80
	KCl	0.30	−1.90

[a]Electrolyte concentrations are 1 M, unless otherwise specified.

Organic solvents are classified as protic or aprotic and have a characteristic potential range.[40,111,120] Typically, low-pH solvents are not favored as hydrogen evolution occurs readily. For weakly acidic solvents, solvent reduction is difficult, which allows for access of more negative potentials. Solvent oxidation is difficult for basic solvents and thereby extends the potential window to more positive values.[111] Appropriate pH selection is also important in consideration of electrogenerated intermediates. Protic solvents (e.g., HFIP) can serve as a proton source during electrolysis to quench carbanion intermediates, whereas aprotic solvents can undergo hydrogen atom transfer (HAT) to quench radical species.[78] Solvent selection also influences the reaction course by stabilizing electrogenerated intermediates and preventing overreaction of products.[121] For example, oxidation of cyclopropane carboxylic acids in basic aqueous solution affords a Kolbe-dimerized product. However, a similar reaction in methanol in the presence of sodium methoxide results in decarboxylation.[123]

Tetraalkylammonium salts are commonly employed as supporting electrolytes when used with organic solvents.[40] However, these compounds can coordinate with the metal centers of electrocatalysts or react with electrogenerated intermediates. As shown in Scheme 1, tetraalkylammonium

Scheme 1. Reaction Mechanism of Tetraalkylammonium Salts to Alkenes[a]

$$R_4N^+ + e^- \rightarrow R_4N^\bullet \quad (A)$$

$$R_4N^\bullet \rightarrow R^\bullet + R_3N \quad (B)$$

$$R^\bullet + e^- \rightarrow R^- \quad (C)$$

$$R^- + H_2O \rightarrow RH + OH^- \quad (D)$$

$$R_4N^+ + OH^- \rightarrow R_3N + R(-H) + H_2O \quad (E)$$

$$R^- + R_4N^+ \rightarrow RH + R(-H) + R_3N \quad (F)$$

$$H_2O + e^- \rightarrow {}^1/_2\,H_2 + OH^- \quad (G)$$

[a]Adapted with permission from ref 119. Copyright 1996 Elsevier.

cations can react with electrogenerated radical intermediates to afford trialkylamine and the corresponding alkene moiety. This has been exemplified by Dahm et al., where purposeful reduction of TEA^+ and TBA^+ in DMF resulted in formation of ethene and butene, respectively.[119]

2.4. Electrochemical Cell Designs

Prior to construction of a cell for electrosynthesis, a decision between batch or flow electrolysis must be made. For small-scale applications, batch electrolysis is more commonly used as cells for this method are readily available. Adequate solution mixing (convection) is necessary to enhance mass transfer and shorten the reaction period; this can be achieved with a magnetic stir bar and bubbling an inert gas through the solution. However, use of industrial-scale batch cells is problematic as efficient mixing of the solution is difficult to ensure. As a result, flow-through reactors[124−128] have grown in popularly for use in large-scale reactions, where constant solution flow is a sufficient means of mass transfer.[124,129] In both batch and flow-through reactors, a divided or undivided cell may be used, as shown in Figure 2. As discussed below, divided and undivided cells each provide their own benefits and drawbacks; experimental considerations drive the decision to employ one over the other.

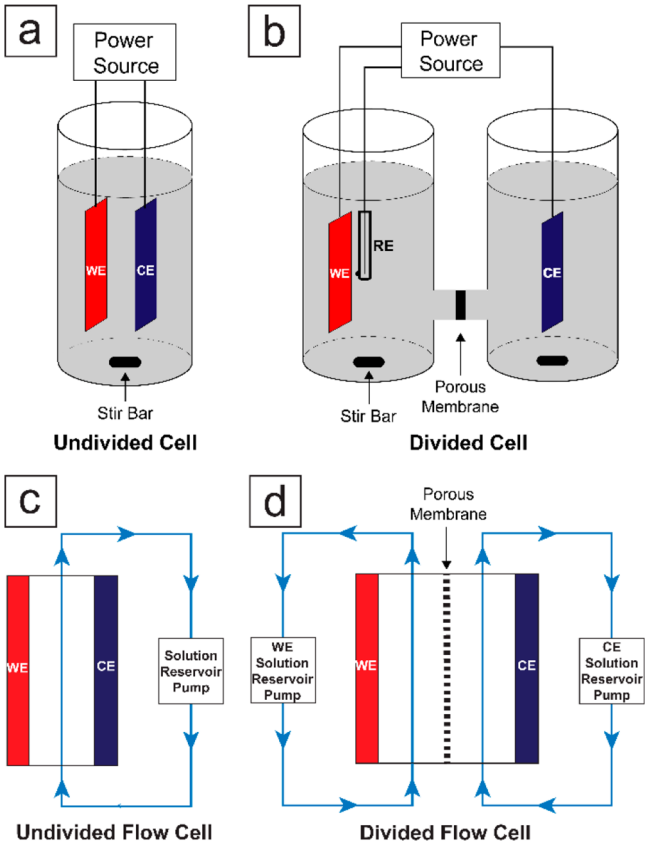

Figure 2. (a) Undivided batch electrochemical cell in a two-electrode configuration; (b) divided batch cell, shown in a three-electrode configuration with compartments separated by a membrane; (c) undivided flow electrochemical cell in a two-electrode configuration; (d) divided flow electrochemical cell in a two-electrode configuration.

Undivided electrochemical cells are favored as construction is relatively simple or unneeded (e.g., use of a glass vial). However, careful consideration must be given to ensure unwanted side reactions do not occur at the CE. Unsought processes include interference from products formed at the CE reacting with intermediates from the WE, formation of undesired products, or the reverse reaction of a reversible redox couple. When competitive side reactions arise and a sacrificial CE cannot be used, the cathode and anode can be housed in different compartments, separated by a porous material that allows current flow but obstructs content mixing.[130] Common separators in these divided cells include fritted glass and ion-exchange membranes; in some cases, a

https://doi.org/10.1021/acs.chemrev.1c00471
Chem. Rev. XXXX, XXX, XXX−XXX

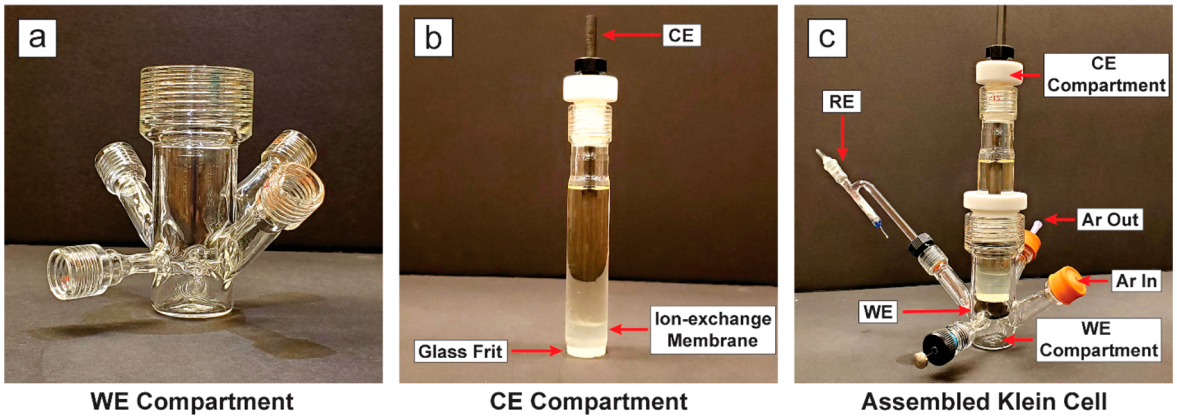

Figure 3. (a) WE and (b) CE compartments for electrolyses in a divided cell. (c) Assembled two-compartment electrolysis cell developed to maximize mass transfer of a solution through the WE, minimize ohmic drop through proper RE placement, and minimize overall cell resistance with fritted glass backed by an ion-exchange membrane.

combination of both is desirable. An example of a divided cell designed by Peters and co-workers[131] (Klein Cell, Figure 3) separates the two compartments with a fritted glass disk and ion-exchange membrane. For reactions in organic media, the membrane is made from methyl cellulose and the same electrolyte−solvent system used in the reaction. Alternatively, for reactions in aqueous media, agar is a suitable substitute for methyl cellulose.

Other considerations in cell design include electrode placement and orientation within the cell. In a two-electrode configuration, the relative sizes and positions of the WE and CE to each other are paramount to maintain efficiency. These electrodes should be of similar surface area such that the reaction rates at the cathode and anode are matched. Moreover, as mentioned previously, the WE and CE should be placed in close proximity but not too close as electric fields between electrodes can influence electrochemical reactions. In addition, if the electrode distance is too small, species of interest (e.g., electrogenerated catalysts) may be quenched at the CE. In contrast, for a three-electrode configuration, all points on the WE should be equidistant to the RE. This ensures a uniform potential across the WE. Placement of the CE should be close to the WE to minimize the overall cell resistance.[91,132] Finally, use of glassware with exceptionally small volumes may produce turbulent flow, causing irreproducible results—this is especially important in hydrodynamic voltammetry (section 3.1.3).

For many of the techniques to be discussed, the electrochemical cell must be placed within a Faraday cage,[133] which consists of a box made from a conductive material that shields ambient electrical noise from the electrochemical measurement of interest. This is particularly important for experiments that require precise measurements, pass low current (<1 μA), or utilize high frequencies (>1000 Hz). Faraday cages may be purchased commercially or homemade; in either case, for proper operation, the cage should be well grounded.

2.5. Methods of Electrosynthesis

Organic transformations can be achieved through constant-current electrolysis (CCE), constant-potential electrolysis (CPE), or alternating-current (pulse) electrolysis. Regardless of the method, transformation can occur at the WE or at both the WE and the CE simultaneously through paired electrolysis. Application of cathodic currents or potentials defines the WE as a cathode and the CE as an anode. Similarly, the opposite is true when applying anodic currents or potentials. Important considerations for each technique are considered in detail below.

2.5.1. Constant-Current and Constant-Potential Electrolysis. CCE typically employs a two-electrode configuration unless knowledge of the potential is required.[19,91,134] To achieve a desired current, a potential is applied to the WE, determined ultimately by the thermodynamics of electron transfer between the substrate and the electrode.[91] Initially, with excess substrate, the reaction is limited by electron-transfer kinetics; however, as substrate concentration decreases, the reaction becomes mass-transfer limited. The WE potential increases in magnitude, as necessary, to maintain the applied current. Proper selection of an electrolysis current is important as low currents result in sluggish electron-transfer rates, which leads to longer electrolysis times. However, high applied currents may generate undesirable side reactions (e.g., solvent breakdown). The latter may be prevented through addition of an overcharge protector, which provides a sacrificial oxidant/reductant to protect the substrate.[9] Electrolysis completion is indicated by a rapid shift in the WE potential as a result of total (or near total) substrate consumption.

In contrast to CCE, CPE requires a three-electrode configuration to ensure accurate potential measurement. When a potential is applied to the WE, a current response proportional to the concentration of substrate is measured. As substrate is consumed, current decays exponentially until a baseline value is reached. The potential selected is typically ∼120 mV more negative than the observed reduction potential—or more positive than the observed oxidation potential—in cyclic voltammetry (section 3.1.1) to ensure complete conversion of starting material.[91] In the case of substrates that exhibit complex electrochemistry (e.g., multiple peaks observed on a voltammogram), more accurate control of the applied potential may be desired to isolate the electrochemical reaction of interest.

Electroorganic synthesis is performed more frequently by means of CCE due to the simplicity and scalability of the technique. CPE suffers from longer reaction times and sophisticated cell geometries to ensure a uniform WE distance from the RE. However, an advantage of CPE over CCE involves ease in determination of the number of electrons (n) transferred for a specific process. Integration of the amperometric curve reveals the quantity of charge passed

https://doi.org/10.1021/acs.chemrev.1c00471
Chem. Rev. XXXX, XXX, XXX−XXX

(Q), expressed in Coulombs, which is directly related to *n* involved in the process. In addition, application of a constant potential allows product selectivity to be maintained with ease. For CCE, potential fluctuations can form undesired byproducts. To ensure selectivity, low applied currents must be utilized, which prevent dramatic potential changes until nearly all (~90%) of the starting material has been consumed.[19]

Selection between methods may be a matter of desired mechanistic information, materials available, or overall expense. Peterson et al.[135] described the utility of CCE over CPE for electrochemically controlled polymerization reactions. Whereas CPE resulted in uncontrolled polymerization and electrode passivation, selective control of cationic vinyl polymerization was achieved through TEMPO-mediated anodic CCE in a divided cell (Scheme 2). In this example,

Scheme 2. TEMPO-Mediated Anodic Polymerization Mechanism[a]

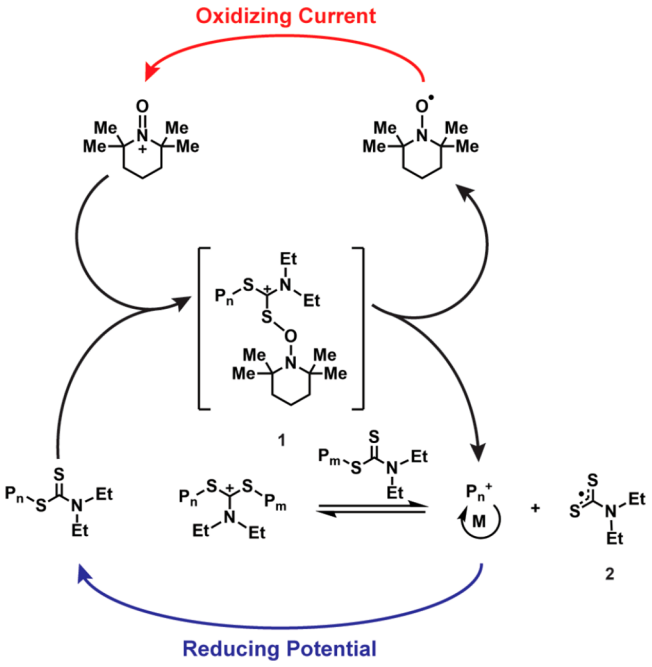

[a]Adapted with permission from ref 135. Copyright 2018 American Chemical Society.

polymerization was initiated through TEMPO oxidation, the product of which reacts with a dithiocarbamate chain-transfer agent to form intermediate **1**. Mesolytic cleavage of **1** regenerates TEMPO, produces dithiocarbamate intermediate **2**, and forms an oxocarbenium ion that participates in reversible addition−fragmentation chain transfer. Termination occurs through application of a cathodic current, which is proposed to reduce intermediate **2** to an anionic form and quench the cation responsible for chain propagation. In this case, CCE provided superior reaction control by allowing fluctuations in the WE potential in accordance with changing $TEMPO^+$ concentration.

2.5.2. Paired and Pulse Electrolysis. Aptly described by Hilt as the "holy grail of organic electrolysis", paired electrolysis is an exceptionally powerful electrosynthetic technique that maximizes the energy efficiency of the cell through reactions that occur at both the anode and the cathode.[115,136,137] Yan et al.[17] and Hilt et al.[115] provides in-depth descriptions of five common types of paired electrolysis methods as well as detailed examples of reactions carried out under each method. Likewise, Moeller and co-workers illustrate many organic transformations that can be carried out via paired electrosynthesis.[138−140] As shown in Figure 4, parallel paired electrolysis involves oxidation and reduction of two different substrates that occur simultaneously to afford two different products. Convergent paired electrolysis arises from the oxidation and reduction of two different substrates to produce two reactive intermediates, which combine to yield the desired product. Alternatively, divergent paired electrolysis involves a single substrate undergoing oxidation and reduction to afford two different products. Linear paired electrolysis[141] involves the oxidation and reduction of one substrate to produce the same compound. This special mode of paired electrolysis involves generation of strong oxidizing and reducing agents at the anode and cathode. In solution, these agents chemically oxidize and reduce the substrate to achieve the desired product.[142] In undivided cells, sequential reduction−oxidation results when substrate reduced at the cathode migrates to the anode, where oxidation affords a new product (or vice versa for sequential oxidation−reduction). Each method, illustrated in Figure 4a−e, has advantages and disadvantages; selection depends on the reaction of interest.

However, a major disadvantage of paired electrolysis is the mass-transfer-limited migration of substrates between electrodes. This issue is most apparent in sequential reduction−oxidation electrolysis, where formation of highly unstable, short-lived intermediates results in low reaction yields as intermediates undergo undesired side reactions. Alternating-current (pulse) electrolysis (Figure 4f) can overcome this deficiency by switching continuously between reductive and oxidative potentials at a single electrode before the substrate leaves the diffusion layer.[143] Rodrigo et al. illustrated this point remarkably through implementation of pulse electrolysis to trifluoromethylate a series of benzenes, furans, thiophenes, and pyrroles (Scheme 3).[143] Upon cathodic polarization of the electrode, triflyl chloride undergoes a one-electron reduction to $CF_3^{\bullet}$. Reaction between $CF_3^{\bullet}$ and **3a** or **3b** results in a highly unstable intermediate, as aromaticity is disrupted. Under sequential reduction−oxidation conditions, the lifetime of the intermediate is not long enough to allow migration from the cathode to the anode. However, through pulse electrolysis, positive polarization allows for immediate oxidation of this intermediate to form an allylic cation while still in the diffusion layer of the same electrode. Rapid deprotonation follows, which results in trifluoromethylated arene **4a** or **4b** and restoration of aromaticity.

In a similar fashion, Sattler et al.[144] synthesized various asymmetric disulfides (**9**) through combination of two symmetric disulfides (**5** and **6**). CCE resulted in a low (~50%) yield of **9**, as competitive polymerization passivates the electrode. This effect was even more apparent with longer electrolysis: conversion of **5** and **6** increased with time, while the yield of **9** decreased, indicative of detrimental polymerization. To prevent electrode passivation, pulse electrolysis was performed through application of +10 mA for 4 s, followed by a rest time of 1 s, then application of −10 mA for 4 s, followed by another 1 s rest time, and the cycle was repeated (Figure 5a). Negative electrode polarization results in S−S bond cleavage to form two thiolates (**7** and **8**). Under anodic conditions, the disulfide bond reforms (Figure 5b). This averts reaction between intermediates and unreduced substrate,

https://doi.org/10.1021/acs.chemrev.1c00471
Chem. Rev. XXXX, XXX, XXX−XXX

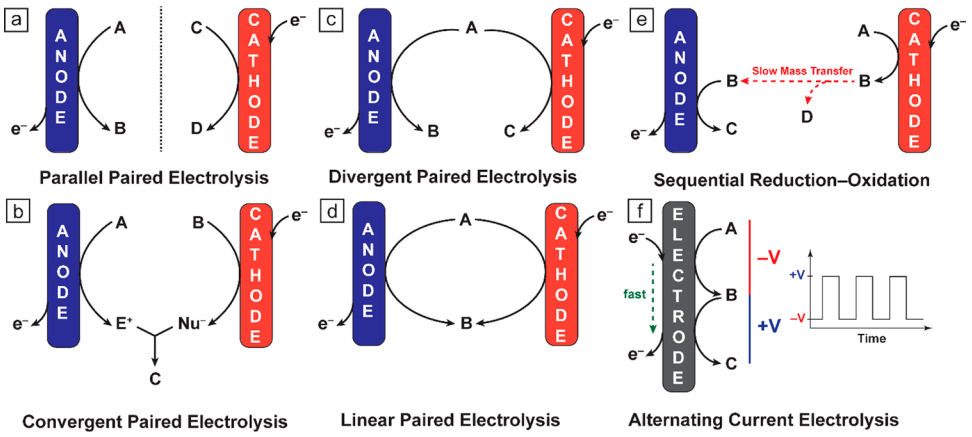

Figure 4. Various modes of paired electrosynthesis. (a) Parallel paired electrolysis; (b) convergent paired electrolysis; (c) divergent paired electrolysis; (d) linear paired electrolysis; (e) sequential reduction–oxidation; (f) alternating-current electrolysis. Panels a–d adapted with permission from ref 115. Copyright 2020 Wiley. Panels e and f adapted with permission from ref 143. Copyright 2020 American Chemical Society.

Scheme 3. Electrochemical Trifluoromethylation of Substituted Arenes by Means of Alternating-Current Electrolysis[a]

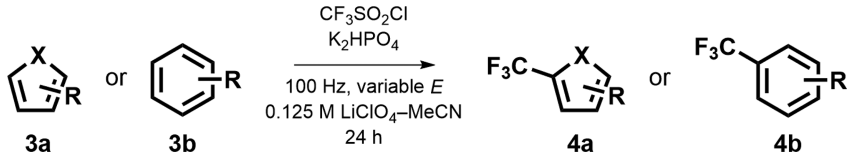

[a]Adapted with permission from ref 143. Copyright 2020 American Chemical Society.

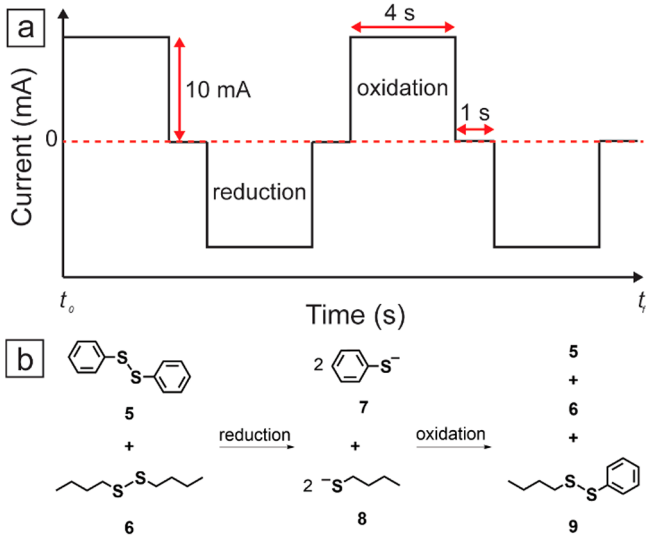

Figure 5. (a) Current response over time for alternating-current electrolysis of symmetric disulfides. (b) Sequential reduction–oxidation of 1,2-diphenyldisulfane and 1,2-dibutyldisulfane to 1-butyl-2-phenyldisulfane and the parent compounds. Bottom panel adapted with permission from ref 144. Copyright 2020 Wiley.

preventing uncontrolled polymerization. As a result, the percent yield of **9** was found to remain constant (ca. 60%) regardless of the electrolysis time.

2.5.3. Electron-Transfer and Follow-up Reactions. As evident throughout this section, selection of an electrolysis method is heavily dependent on the desired electrosynthetic reaction. These reactions can include both electron-transfer processes and secondary chemical reactions. Thus, a brief introduction to the myriad of steps possible in an electrosynthesis, which may influence method selection, is imperative.

Generation of a desired product is rarely a single-step process and often involves intermediates produced in subsequent electrochemical (E) and chemical (C) reactions. Detailed reaction mechanisms can provide the information necessary to optimize product yield and selectivity. However, proposing a detailed reaction mechanism first requires defining the order and nature of follow-up reactions (E, C, or both) as well as characterization of any intermediates formed.[145] As depicted in Figure 6, complete mechanistic analysis is not

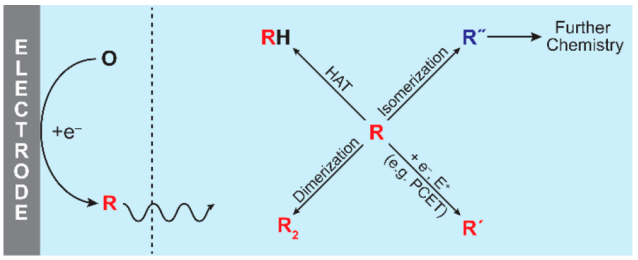

Figure 6. Direct one-electron reduction of **O** (top left) and mediated charge transfer (bottom left) to produce radical anion intermediate **R**. Depending on the reaction, **R** can afford various products as a result of competing chemical and electrochemical reactions ($\mathbf{R}_2$, **RH**, **R′**, and **R″**). Note "Further Chemistry" only occurs if products are unstable. HAT = hydrogen atom transfer; PCET = proton-coupled electron transfer.

trivial. Suppose the one-electron reduction of **O** yields radical anion species **R**. For simplicity, we assume that **R** behaves as a radical throughout this review; however, this species may also behave as an anion.[19] Through a subsequent EC step, **R** could accept a second electron to form the corresponding anion and then react further with electrophile $\mathbf{E}^+$ (e.g., H^+, CO_2) to form product **R′**.[146,147] Alternatively, through various C reactions, **R**

https://doi.org/10.1021/acs.chemrev.1c00471
Chem. Rev. XXXX, XXX, XXX–XXX

could dimerize to form $\mathbf{R}_2$,[148] abstract a hydrogen atom (typically from solvent) to form **RH**,[149,150] or isomerize to **R″**.[151,152] Further chemistry can also occur upon formation of unstable products. This simplified reaction scheme highlights only a few possible pathways that follow one-electron reduction of a substrate.

3. USE OF ANALYTICAL METHODS TO DETERMINE REACTION PATHWAYS AND CHARACTERIZE INTERMEDIATES

Various analytical methods are available to aid in proposing an accurate mechanism and detailed kinetic model. Often, a model is validated by a combination of electrochemical, spectroscopic, and chromatographic techniques. Furthermore, thermodynamic data, proposed through computational analysis, and results obtained through simulation provide confirmation of mechanisms. This section describes in situ and ex situ analytical methods that have been employed in electrosynthesis.

3.1. Electrochemical Methods

3.1.1. Cyclic Voltammetry. Cyclic voltammetry (CV) is one of the most utilized electrochemical methods and can provide a wealth of information for a given electrochemical process. A well-executed electrosynthesis begins with voltammetric analysis of relevant compounds. These studies determine the potential needed to drive an electrochemical reaction and appropriate potential windows for systems of interest. For in-depth analysis of CV, the reader is directed to a recent exposition from Elgrishi et al.[116] as well as several additional reports.[153−155]

The IUPAC convention for reporting a voltammogram plots potentials becoming more positive from left to right and oxidative currents positive. Alternatively, the polarographic (American) convention, plots potentials increasing right to left and cathodic potentials as positive. Under standard conditions, for a reversible, diffusion-controlled, electron-transfer process, the anodic and cathodic peak potentials are separated ideally by $57/n$ mV, where n is the number of electrons transferred.[156] The difference between the half-wave potential ($E_{1/2}$) and the half-peak potential ($E_{p/2}$) for the anodic or cathodic processes is $28.5/n$ mV. When reporting potentials, $E_{1/2}$ is more appropriate when the baseline is not well defined, whereas $E_{p/2}$ is appropriate when the peak potential is less certain due to peak broadening. Moreover, for a truly reversible, diffusion-controlled process at a planar electrode, oxidative and reductive peak currents are equal in magnitude and governed by the Randles−Ševčík equation (eq 1)

$$i_p = (2.69 \times 10^5) n^{3/2} A D^{1/2} \nu^{1/2} C \quad (1)$$

where A is the electrode surface (electroactive) area, D is the diffusion coefficient, ν is the scan rate, and C is the concentration of substrate in solution. Prior to analysis, peak currents must be defined accurately through baseline extrapolation. Equation 1 is typically employed to determine diffusion coefficients, as n can be estimated from peak separation and A, ν, and C are usually known. Alternatively, the electroactive area can be determined when a compound with known D, such as ferrocene, is analyzed. On the basis of the aforementioned relations, peak potentials are independent of the scan rate and the peak current is directly proportional to $\nu^{1/2}$ for completely reversible systems at slow to moderate scan rates. To ensure linearity, voltammograms are obtained at several scan rates.

Many electroorganic processes, such as bond breaking, are irreversible and a voltammetric peak is absent on the reverse scan. In this case, eq 1 must be modified

$$i_p = (2.99 \times 10^5) n(\alpha n_a)^{1/2} A D^{1/2} \nu^{1/2} C \quad (2)$$

where n_a is the number of electrons in the rate-limiting step and α is the transfer coefficient.[157] For electrosynthetic reactions, mechanisms often proceed through a combination of reversible and irreversible electron-transfer steps. For instance, Costentin et al.[158,159] and Bhugun et al.[160] investigated the catalytic efficiency of iron porphyrins toward CO_2 reduction in DMF at glassy carbon and mercury cathodes. Voltammograms of these porphyrins reveal three reversible redox couples corresponding to $Fe^{III}/Fe^{II}/Fe^{I}/Fe^{0}$ transitions in succession. In the presence of CO_2, the Fe^{I}/Fe^{0} redox couple becomes irreversible and the cathodic current increases. Similarly, Hickey et al.[161] studied the electrochemical properties of various monoligated Co^{II} complexes in the presence of benzyl bromide. Upon addition of the organic halide to a solution of [Co(II)(bpy)Br_2], the Co^{I}/Co^{II} oxidative wave disappears and the cathodic current increases as benzyl bromide concentration increases (Figure 7a). The absence of an anodic peak coupled with increased cathodic current indicates that electrogenerated catalyst reduces the substrate irreversibly and returns to the oxidized state. Comparably, the disappearance of the Co^{I}/Co^{II} anodic wave for the Co(II)-(pyrox)Br_2 complex (Figure 7b) is also apparent after addition of benzyl bromide, indicative of interaction between Co^{I} and benzyl bromide. However, an increase in cathodic current as a function of benzyl bromide concentration is not observed as Co^{II} is not regenerated following consumption of Co^{I} prior to the reverse scan.

Scan-rate studies are extremely informative in that detection of products from follow-up chemical reactions, determination of electron-transfer kinetics, and measurement of intermediate lifetimes are possible. Typically, CV is performed at scan rates between 0.02 and 5 V s^{-1}. Scan rates lower than 20 mV s^{-1} are discouraged to avoid unwanted concentration gradients. Scan rates faster than 5 V s^{-1} require ultramicroelectrodes to compensate for a large capacitive current, which overpowers the analytical signal. Consider an ECE mechanism (eqs 3−5), where C is reduced (eq 5) at a potential more negative than A (eq 3)[162]

$$A + e^- \rightleftharpoons B \quad (3)$$

$$B \xrightarrow{k_1} C \quad (4)$$

$$C + e^- \rightleftharpoons D \quad (5)$$

At low to moderate scan rates, two cathodic peaks should appear, the first irreversible as B is converted to C (eq 4) and the second reversible as D undergoes no other reactions (eq 5). If k_1 is sufficiently small, reversibility of the first step can be seen when the potential is swept faster than the chemical reaction occurs, allowing B to be oxidized. At these faster scan rates, the C/D redox couple is diminished or absent completely.

A common misconception exists that each voltammetric peak in a CV corresponds to the starting material gaining or losing an electron. In fact, reduction or oxidation of the parent compound often produces electrochemically active products

https://doi.org/10.1021/acs.chemrev.1c00471
Chem. Rev. XXXX, XXX, XXX−XXX

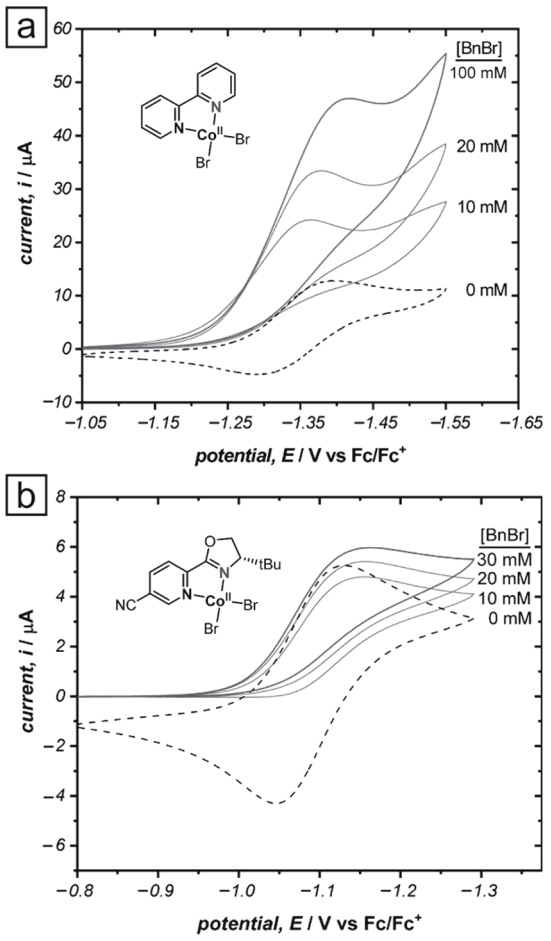

Figure 7. Cyclic voltammogram of the Co(II)/Co(I) couple of $CoBr_2$ ligated by (a) bipyridine or (b) substituted pyridyl oxazoline in the presence of increasing equivalents of benzyl bromide (BnBr). Experiments conducted with 1.0 mM $CoBr_2$ in the presence of 1.0 mM ligand at 100 mV s^{-1} in a 100 mM solution of $TBAPF_6$–MeCN. CVs are plotted in polarographic notation with positive currents corresponding to reduction. Reprinted with permission from ref 161. Copyright 2019 American Chemical Society.

through subsequent chemical reactions. Reduction or oxidation of these products might manifest themselves as subsequent voltammetric waves. A pertinent example from our group entails the electroreduction of the pesticide DDT at silver cathodes in oxygen-free 0.050 M $TMABF_4$–DMF.[163] Voltammograms collected show four cathodic peaks at −0.56, −1.26, −1.58, and −1.80 V vs Cd/Hg. CPE of 5 mM DDT at −0.71 V reveals that the parent molecule is reduced to DDD in a two-electron process (Figure 8). The carbanion intermediate generated is protonated by adventitious water. Alternatively, hydroxide (from water) can react with either DDT to form DDE or DDD to form DDMU. Each of these products is electrochemically active, and their reduction can be seen in subsequent cathodic peaks.

In the case of complex mechanisms, a many-electron process can also be present as a single voltammetric peak. As mentioned previously, the cathodic and anodic peak potentials are separated ideally by approximately $57/n$ mV for a truly reversible process. Thus, peak potentials from a voltammogram are informative to estimate the number of electrons transferred in each step. An excellent example of this can be seen through voltammograms of macromolecules **10** and **11**, as illustrated in Figure 9. At platinum cathodes in 0.2 M $TBAPF_6$–DCM, a single, reversible electron-transfer process at −1.15 V vs SCE is observed (Figure 9c).[164] Upon quantitative analysis, the redox wave of **10** was shown to correspond to a six-electron-transfer process to produce a hexacation species. Likewise, the redox wave of **11** corresponds to a four-electron process to produce a tetracation species.

Electron-transfer kinetics can be investigated by CV; however, analysis is quite arduous. Table 4 provides a list of kinetic parameters that can be determined by CV for a heterogeneous, one-electron process. Homogeneous electron-transfer and electrocatalytic reactions have been covered extensively[165−167] with notable contributions by Savéant and co-workers.[168−170] The interested reader is directed to thorough reviews of the field by Dempsey and co-workers[171,172] for rigorous treatment of homogeneous electron-transfer kinetics. Heterogeneous electron-transfer rate constants (k_s) and transfer coefficients (α) can be obtained through construction of a "trumpet plot" (Figure 10), which evaluates the peak potential (E_p) or $E_p - E_{1/2}$ as a function of log ν. Linear regression of the anodic and cathodic branches for $\Delta E_p/n > 200$ mV allows for k_s and α to be extracted by means of eqs 6–9.[154,157,173−178] To determine α, eq 6 is utilized when electron transfer is the rate-limiting step, whereas eq 7 is employed when α depends on the applied potential. For totally reversible electrochemical systems, k_s can be calculated by means of cathodic (eq 8) or anodic peaks (eq 9). In situations where $\Delta E_p/n < 200$ mV, alternative methods of trumpet plot analysis exist to obtain k_s. For an irreversible electrochemical reaction, k_s can be calculated with regard to either the peak current (eq 10) or the peak potential (eq 11). In each case, a more accurate value for n can be obtained voltammetrically by means of eqs 12 and 13 for reversible and irreversible reactions, respectively. To ensure all ensuing calculations are exact, n must be determined by at least two independent methods. Once electrochemical kinetics are well understood, rates of follow-up chemical reactions are more easily attainable. For example, for an irreversible chemical process preceded by a reversible electrochemical reaction (E_rC_i), the rate of C_i (k_c) can be measured through eq 14. Alternatively, for an E_iC_i reaction, the rate of C_i is identical with k_s.

Heterogeneous electron-transfer analysis of more complex systems is much more challenging. To this end, Savéant and co-workers developed convolutive potential-sweep voltammetry (CPSV)[180−185] as an effective tool to elucidate direct electrochemical reaction mechanisms. Other notable contributions include a comprehensive diagnostic tool developed by Shain et al.[154,186,187] and Nicholson et al.,[188,189] which allows for study of the overall electrochemical mechanism as well as reaction kinetics. For each reaction scheme, parameters such as peak current and peak separation vary with respect to scan rate. As a result, a series of voltammograms should be obtained to develop a relatively accurate model for the reaction mechanism.

3.1.2. Fast-Scan Voltammetry. A major drawback of voltammetry at millimeter-sized electrodes is the inability to measure lifetimes of short-lived (i.e., t < milliseconds) intermediates and exceptionally fast rate constants. Investigation of such species requires scan rates much faster than 100 V s^{-1}, which, as previously mentioned, leads to large capacitive currents that overpower the faradaic signal. In the 1980s, Wightman and colleagues overcame this issue through

https://doi.org/10.1021/acs.chemrev.1c00471
Chem. Rev. XXXX, XXX, XXX−XXX

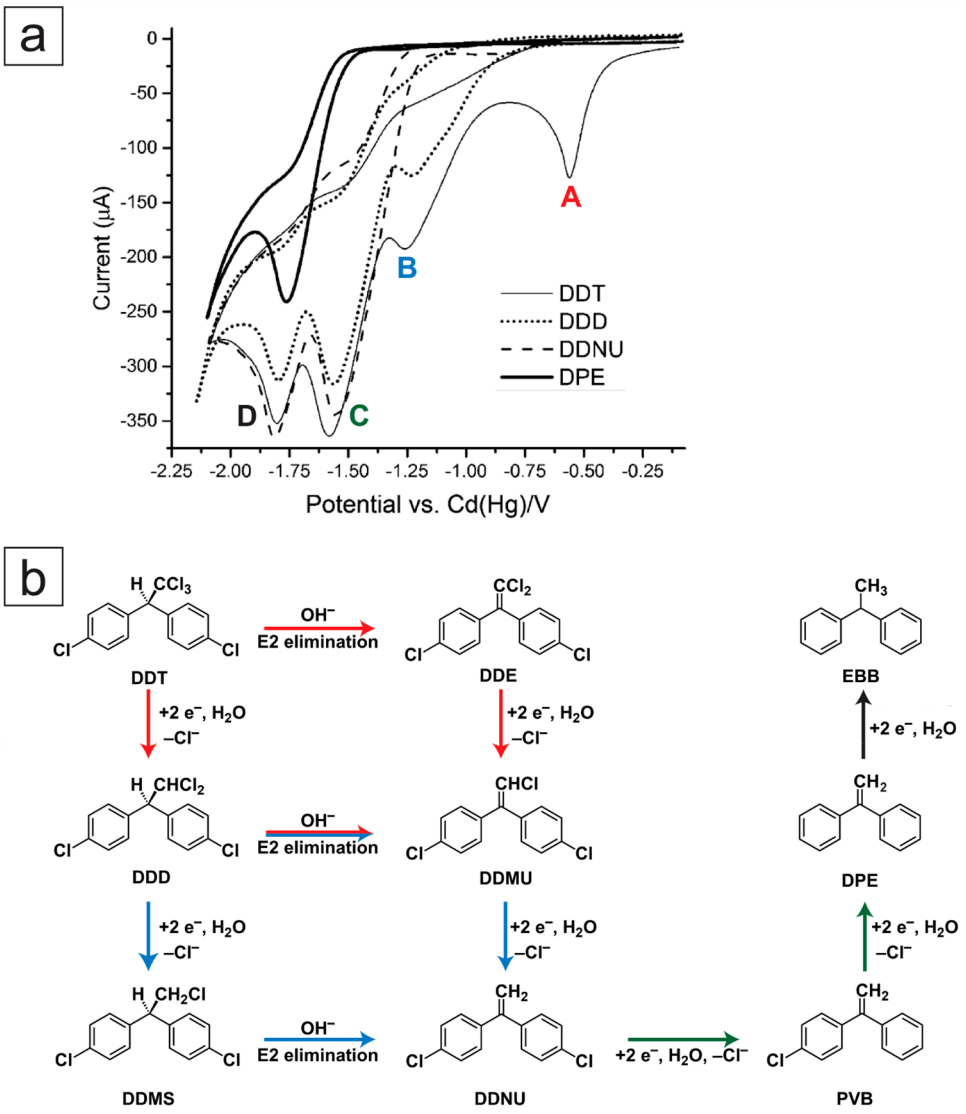

Figure 8. (a) Cyclic voltammograms at 100 mV s^{-1} for 5 mM DDT and associated degradation products at silver cathodes in 0.050 M $TMABF_4$–DMF. Potentials are reported against a Cd/Hg reference electrode. (b) Degradation route of DDT at silver cathodes in 0.050 M $TMABF_4$–DMF. DDD, DDE, and DDMU are electrochemically active. Each color-coded reaction pathway manifests in the corresponding voltammetric peak. Adapted with permission from ref 163. Copyright 2014 Elsevier.

fabrication of microelectrodes and ultramicroelectrodes (UMEs).[190,191] Although ohmic drop compensation and background correction (subtraction) are still necessary, UMEs result in minimized signal distortion for analysis at fast scan rates.[192−194] By definition, an UME has at least one dimension comparable to the diffusion layer thickness. Amemiya and co-workers recently simulated and experimentally investigated fast-scan voltammetry at nanogaps between two UMEs, which allows for electrochemical analysis without the need for background correction.[33,195] More recently, a convolution-based method was developed for subtraction of the differential capacitive contributions to the measured current.[193] This background correction method is especially important for in vivo measurements, in which environmental changes surrounding the electrode can occur. Exceptionally small volumes can also be probed, allowing for detection of small (micromolar) concentrations of electrochemically active species.[196] This has led to popularity in the bioanalytical community for detecting chemicals in the brain, such as dopamine.[197−199] Perhaps most appealing to the electrosynthetic chemist, microelectrodes work exceptionally well in highly resistive solvents (e.g., benzene) as less current is passed.[191]

In terms of electrosynthesis, UMEs are advantageous, particularly for mechanism elucidation and measurement of large rate constants. Andrieux et al. reported rate constants as large as 6.4×10^6 M^{-1} s^{-1}.[200] Schmittel et al. studied the mesolytic cleavage of 2,2-dimesitylenol ester derivatives (**12**) by means of CV and fast-scan CV (Scheme 4).[201] Voltammograms reveal an irreversible oxidative wave at 1.02 V vs Fc/Fc^+ in MeCN at 100 mV s^{-1}. Fast-scan CV was performed with a 25 μm Au UME to probe the reaction kinetics. As the scan rate increases from 100 to 5000 V s^{-1}, the oxidative wave becomes reversible and i_{pc}/i_{pa} approaches unity. This electron-transfer event corresponds to formation of a radical cation intermediate, which is followed by C−O bond cleavage, intramolecular cyclization, and a 1,2-methyl shift to form the corresponding 3-mesityl-4,6,7-trimethylbenzofuran derivative (**13**). Fast-scan CV allowed for rate constants of radical cation cleavage upward of 5000 s^{-1} to be measured.

https://doi.org/10.1021/acs.chemrev.1c00471
Chem. Rev. XXXX, XXX, XXX−XXX

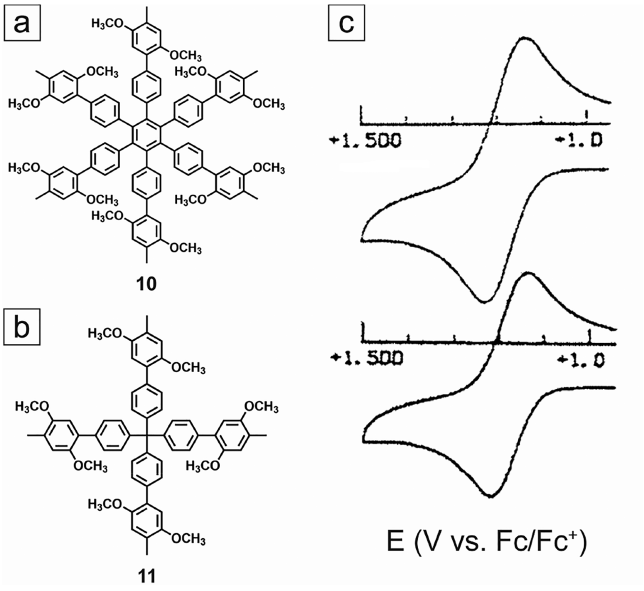

Figure 9. Macromolecule "electron sponges" containing (a) six electroactive aryl (2,5-dimethoxytolyl) groups (**10**) and (b) four electroactive aryl groups (**11**). Cyclic voltammogram for (c, top) 2 mM **10** and (c, bottom) 2 mM **11** in 0.2 M $TBAPF_6$–DCM at 200 mV s^{-1}. Formation of **10** hexacation and **11** tetracation was confirmed via quantitative analysis of each CV wave. Adapted with permission from ref 164. Copyright 2001 American Chemical Society.

Table 4. Relevant Equations for Kinetic Analysis of an Electrochemical Reaction with Heterogeneous Electron Transfer[a]

parameter	equation	
α	$-\frac{RT}{nF(\Delta E_p/\Delta \ln \nu)}$	(6)[154]
	$\frac{1.85RT}{nF(E_{p/2}-E_p)}$	(7)[154]
$k_s^{\text{reversible}}$	$E_{p,c} = E^0 - \frac{2.3RT}{\alpha nF}\log\left[\frac{\alpha nF\nu}{RTk_s}\right]$	(8)[173]
	$E_{p,a} = E^0 + \frac{2.3RT}{(1-\alpha)nF}\log\left[\frac{(1-\alpha)nF\nu}{RTk_s}\right]$	(9)[173]
$k_s^{\text{irreversible}}$	$i_p = 0.227nFAC_0^*k_s\exp\left[\left(\frac{-\alpha nF}{RT}\right)(E_p - E^0)\right]$	(10)[154]
	$E_p = E^0 - \frac{RT}{\alpha nF}\left[0.77 + \ln\left(\frac{\alpha nFD\nu}{RT}\right) - \ln k_s\right]$	(11)[154,157]
n	$E_{p/2} = E_{1/2} + 1.09\left(\frac{RT}{nF}\right)$	(12)[154]
	$i_p = 2.99\times10^5 n(\alpha n_\alpha)^{1/2}AD^{1/2}\nu^{1/2}C$	(13)[157]
k_c	$E_p = E_{1/2} - \frac{RT}{nF}\left[0.780 - \ln\sqrt{\frac{k_cRT}{nF\nu}}\right]$	(14)[154]

[a] R is the gas constant (8.314 J mol^{-1} K^{-1}); F is Faraday's constant (96485 C mol^{-1}); T is temperature (K); n is the number of electrons transferred per molecule; α is the transfer coefficient; ν is the potential sweep rate (V s^{-1}); A is the electrode surface area (m^2); D is the diffusion coefficient (cm^2 s^{-1}); k_s is the electron-transfer rate constant (cm s^{-1}); k_c is the rate constant of chemical reaction (M^{-1} s^{-1}).

In a similar fashion, Yang and Bard[202] investigated the mechanism of polyaniline (PANI) formation at Pt electrodes

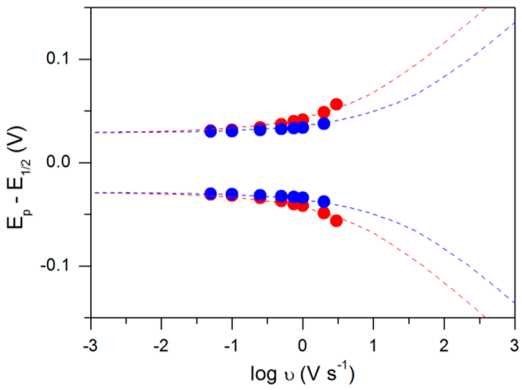

Figure 10. Generic trumpet plot employed to extract heterogeneous electron-transfer rate constants (k_s). Dashed lines represent the working function, and solid dots show experimental results; blue dots represent the Co(II/I) couple, and red dots represent the Co(III/II) couple. Reprinted with permission from ref 179. Copyright 2017 American Chemical Society.

Scheme 4. Mesolytic Cleavage of 2,2-Dimesitylenol[a] **Ester Derivatives**[b]

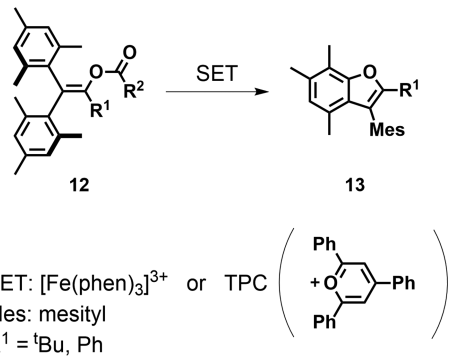

[a] mesityl = 2,4,6-trimethylphenyl [b] Adapted with permission from ref 201. Copyright 2001 American Chemical Society.

in aqueous 1 M H_2SO_4. Aniline undergoes a reversible one-electron oxidation to form a radical cation, for which the radical is located on the nitrogen or the *para* carbon. Two carbon radicals can dimerize to form benzidine or a carbon radical and a nitrogen radical dimerize to form *p*-amino-diphenylamine (ADPA). Both dimers can undergo another two-electron oxidation, incorporate another aniline, and polymerize further. To elucidate the initial polymerization steps, CV was performed at scan rates from 0.05 to 500 V s^{-1}. At each scan rate, 300 potential cycles were obtained; at slow scan rates, eight assignable peaks are present during the initial cycles. However, at 500 V s^{-1}, only one reversible redox couple is present during the initial cycles, which corresponds to the oxidation of ADPA. From these results, benzidine was determined to be a slower, minor intermediate, whereas polymerization proceeds predominantly through ADPA.

Microelectrodes and fast-scan CV have been utilized to detect intermediates with lifetimes on the order of microseconds.[203] Andrieux et al.[204] investigated the polymerization mechanism of various pyrroles and substituted pyrroles by means of fast-scan CV at Pt electrodes (5–17 μm) in 0.6 M $TEAClO_4$–MeCN. Cyclic voltammograms of each pyrrole at scan rates between 1.6 and 18 kV s^{-1} reveal partial or complete reversibility of the anodic wave at potentials positive of 1.00 V.

https://doi.org/10.1021/acs.chemrev.1c00471
Chem. Rev. XXXX, XXX, XXX–XXX

On the basis of these observations, polymerization proceeds through a radical cation intermediate with lifetimes ranging from 30 to 2000 μs dependent upon the substituent attached to the aromatic ring.

More recently, electrodes with nanometer dimensions (nanoelectrodes) have been constructed for advanced electrochemical experiments. Nanoelectrodes and nanoelectrode arrays[205] provide exceptionally low detection limits and improved measurement of fast rate constants.[206] While these electrodes show promise for enhancing knowledge of electrosynthetic mechanisms, their use in traditional electrosyntheses has not be widely explored.

3.1.3. Hydrodynamic Voltammetry. Many voltammetric experiments occur in the absence of forced convection, so that diffusion is the predominant mode of mass transfer. However, addition of external forces to a solution (e.g., stirring) can also be used to reveal important kinetic and mechanistic information about the system.[21] These hydrodynamic methods typically employ rotating disk electrodes (RDE) or rotating ring-disk electrodes (RRDE), as illustrated in Figure 11. A

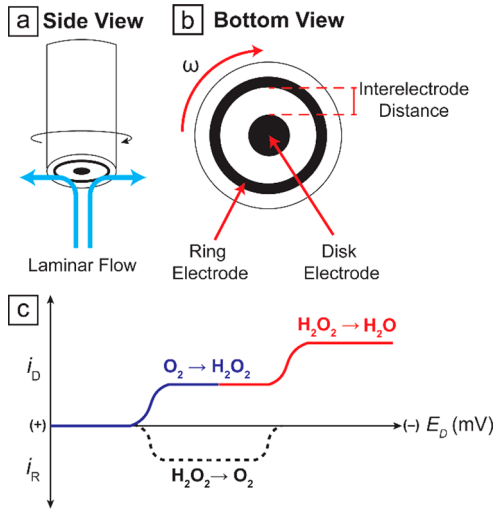

Figure 11. (a) Side view and (b) bottom view of a rotating ring-disk electrode (RRDE), including the laminar flow of the solution and angular velocity, ω. In the case of a rotating disk electrode (RDE), the ring is absent. (c) Disk (i_D) and ring current (i_R) observed for the oxygen reduction reaction.

RDE is a WE rotated at a set angular velocity (ω) such that the solution is moved to the central region of the disk and swept to the electrode edge. As the solution moves across the electrode, a laminar flow profile is created with well-defined mass-transport characteristics. The potential at the RDE (E_D) can be fixed or swept linearly as in CV. In the case of a RRDE, the solution first traverses the disk WE and is subsequently swept to the ring WE, held at potential E_R, and controlled independently of E_D. Analysis is made by measuring the current at the disk (i_D) and ring (i_R) as a function of disk potential.[207,208] Rotation of the WE allows for continuous replenishment of electroactive species at the electrode surface, which results in steady-state mass transfer, as described by the Levich equation

$$i_{l,c} = 0.620nFAD^{2/3}\omega^{1/2}\nu^{-1/6}C \quad (15)$$

where $i_{l,c}$ is the limiting current, ν is the hydrodynamic viscosity, and all other variables are as described previously. Use of a RRDE requires a bipotentiostat to control the potential at two WEs, referenced to a common RE.

In electrosynthesis, techniques involving a RDE (and, more specifically, RRDE) are exceptionally powerful for detection of intermediate species. The most studied example involves oxygen reduction,[209,210] which can occur as a two- or four-electron process in acidic media[211]

$$O_2(g) + 2H^+(aq) + 2e^- \rightleftharpoons H_2O_2(aq) \quad (16)$$

$$H_2O_2(aq) + 2H^+(aq) + 2e^- \rightarrow 2H_2O(aq) \quad (17)$$

$$O_2(g) + 4H^+(aq) + 4e^- \rightleftharpoons 2H_2O(aq) \quad (18)$$

Formation and consumption of the intermediate species, H_2O_2, can be monitored with the aid of a RRDE. As the disk potential is scanned cathodically, a current response is observed from the two-electron reduction of oxygen, as shown in Figure 11c. The potential at the ring electrode is held at a potential sufficient to reversibly oxidize H_2O_2, which generates a current at the ring. Currents at the disk and ring are related by the collection efficiency (N), which accounts for the specific geometric configurations of a given RRDE

$$N = \frac{-i_R}{i_D} \quad (19)$$

When the disk potential reaches the reduction potential of H_2O_2, a further increase in current is observed at the disk as a result of the two-electron reduction to water. However, the current at the ring decays to zero as H_2O_2 is no longer detected.

Amatore et al. extensively studied the mechanism of oxidative addition in Pd-catalyzed Heck and cross-coupling reactions by means of chronoamperometric RDE techniques.[212] Specifically, oxidative addition of $Pd(OAc)_2$ in the presence of triphenylphosphine was studied at RDEs in DMF. Formation of a tricoordinate Pd^0 complex was monitored by CV, where a reduction peak indicated formation of $Pd(OAc)_2(PPh_3)_2$. An oxidation peak was detected, which increased in magnitude at the expense of the reduction peak, suggesting spontaneous decomposition of the palladium complex to $Pd(PPh_3)_2(OAc)^-$. Chronoamperometry of $Pd(OAc)_2$ in the presence of PPh_3 was performed at a RDE polarized on the oxidative plateau of $Pd(PPh_3)_2(OAc)^-$. Complete conversion of $Pd(OAc)_2$ to the tricoordinate species was confirmed by a current plateau after 2 h. Upon addition of phenyl iodide, the current decays rapidly as the Pd^0 complex is consumed. However, the current increases again after 30 seconds as free iodide in solution becomes oxidized. The delay between the absence of Pd oxidation and the appearance of iodide oxidation suggests that a pentacoordinate Pd intermediate is formed in the oxidative addition process.

Hydrodynamic techniques can also be utilized to obtain kinetic information. Adamo et al. investigated the kinetics of Pd-catalyzed, oxidative homocoupling of biaryls through the reaction of arylboronic acid in the presence of molecular oxygen at Au RDEs.[213] In the absence of convection, $(\eta^2\text{-}O_2)Pd(PPh_3)_2$ exhibits an oxidation wave at 0.63 V vs SCE in 0.30 M $TBABF_4$–$CHCl_3$. The limiting current at a Au RDE, held at a potential of 0.70 vs SCE, was monitored over time as excess arylboronic acid was added to solution (Figure 12). A plot of $\ln(i_t/i_0)$, where i_t is the oxidation current after time t and i_0 is the initial oxidation current, against time showed that the peroxo complex reacts via first-order kinetics. This allowed

https://doi.org/10.1021/acs.chemrev.1c00471
Chem. Rev. XXXX, XXX, XXX−XXX

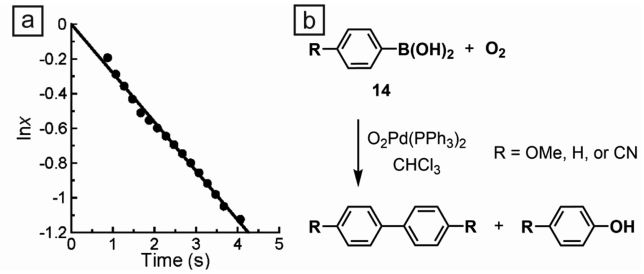

Figure 12. (a) Determination of the reaction kinetics for the homocoupling reaction, where $x = i_t/i_0$. Regression analysis of $\ln(x)$ over time shows the reaction follows first-order kinetics. (b) Palladium-catalyzed oxidative homocoupling of arylboronic acids in the presence of molecular oxygen to form biaryl species. Adapted with permission from ref 213. Copyright 2006 American Chemical Society.

for determination of the first-order rate constant (k_{obs}), which was found to be dependent on the concentration of arylboronic acid in solution. In the case of (4-methyoxyphenyl)boronic acid (**14**), plots of $\ln(k_{obs})$ against $\ln$ [**14**] and k_{obs} against [**14**]^2 reveal the reaction to be second order in arylboronic acid, requiring two molecules of starting material.

Alternatively, rate constants can be obtained by monitoring the change in $i_{l,c}$ as the rotation rate of the WE is increased. As suggested by eq 15, $i_{l,c}$ and the rotation rate are directly related; therefore, a plot of current vs $\omega^{1/2}$ should yield a linear response. However, deviations from this behavior are indicative of sluggish electron-transfer kinetics and manifest themselves as a plateau in the $i-\omega$ curve. In this case, a modification of eq 15 is necessary to produce the Koutecký–Levich equation (eq 20)

$$\frac{1}{i_D} = \frac{1}{i_K} + \frac{1}{i_{l,c}} = \frac{1}{i_K} + \frac{1}{0.620nFAD^{2/3}\omega^{1/2}\nu^{-1/6}C} \quad (20)$$

where i_K is the current that flows under kinetic limitations and all other variables retain previous meanings. With this, a plot of i^{-1} vs $\omega^{-1/2}$ results in a straight line with an intercept of i_K^{-1}. Once the kinetic-limited current is known, the rate constant (k) can be determined by the following relation

$$i_K = nFAj = nFAkC \quad (21)$$

Subsequently, k_s can be determined via eq 22

$$k = k_s \exp\left(\frac{-\alpha nF\eta}{RT}\right) \quad (22)$$

where j is the total flux at the electrode surface and η is the overpotential. Chen and Liu[214] utilized this method to investigate the kinetics of vanadium(V) reduction in water at a Au RRDE. The intrinsic rate constants of four vanadium(V) species, VO_2^+, $Na_xH_yV_{10}O_{28}^{(6-x-y)-}$, $H_xV_4O_{12+x}^{(4+x)-}$, and HVO_4^{2-}, were found to be 3.6×10^{-5}, 2.6×10^{-3}, 2.5×10^{-5}, and 3.1×10^{-6} cm s^{-1}, respectively. The comparatively large rate constant for the V_{10} species was attributed to both the oxygen atoms intertwined in the vanadium cage allowing facile electron transfer and the negligible V_{10} rearrangement in reduction.

Hydrodynamic voltammetry is not limited to techniques with rotating electrodes. Sonoelectrochemistry is a growing area of research that involves incorporation of acoustic fields (ultrasound) in electrochemical experiments. Banks et al., Marken et al., and Compton et al. have authored numerous fundamental publications and reviews on diffusion layer thinning, surface and mass transfer effects, and determination of k_s in sonovoltammetry.[215−219] Typical sonoelectrochemical cells contain the traditional WE, CE, and RE in addition to a sonic probe. Most frequently, the probe is at a "face-on" geometry with the WE, such that ultrasonic waves propagate directly toward the electrode surface. Cooling of the electrochemical cell is essential, as introduction of ultrasound results in solution heating. As with traditional hydrodynamic techniques, sonoelectrochemistry increases mass transport through convection. For comparison, a rotation rate of 200 Hz at a RDE would be necessary to obtain the same limiting current at a stationary electrode in the presence of 20 kHz ultrasound. The substantial increase in limiting current can be explained by the rearranged Levich equation

$$i_{l,c} = \frac{nFADC}{\delta} \quad (23)$$

where δ is the diffusion layer thickness and all other variables are as defined previously. In the case of rotating electrodes

$$\delta = 0.620D^{1/3}\omega^{-1/2}\nu^{1/6} \quad (24)$$

In the presence of ultrasound, the diffusion layer is remarkably thinner, which results in a larger limiting current. To quantify the effect of the sonication frequency on the diffusion layer thickness and determine δ, the system must be calibrated by means of known redox systems.[219]

Unlike classical hydrodynamic techniques, sonoelectrochemistry can alter reaction mechanisms as a result of transient cavitation introduced by ultrasound. A prominent example involves the reduction of fluorescein (**15**) at mercury-plated platinum electrodes in 0.1 M aqueous NaOH.[220] Under quiescent conditions, the reduction proceeds via a strictly electrochemical (E) mechanism, producing stable radical species **16** through a one-electron process. However, under insonation, n increases ($1 < n < 2$) and reduction shifts to a catalytic (EC') mechanism. Hydroxide radicals are produced from water sonolysis, which oxidizes **15** back to **16**, as shown in Scheme 5.

3.1.4. Pulse Voltammetry. Thus far, we have considered voltammetric techniques where the faradaic current (i_F) is easily distinguishable from the charging (capacitive) current (i_c). However, at low analyte concentration, i_F can be significantly smaller than i_c, leading to poor detection limits. In this context, pulse voltammetry can be employed to suppress the background current and extract the faradaic current. In pulse voltammetry, the current is sampled periodically as a series of potential pulses is applied. At each potential step, decay of the capacitive current allows measurement of the faradaic current with greater precision. Differential pulse voltammetry (DPV) and square wave voltammetry (SWV) are the most sensitive pulse techniques and have been employed extensively.[91] In DPV, a baseline potential is applied for a set amount of time; the potential is then stepped by a few hundreds of millivolts and held for a fixed time. The potential is then brought down to a value slightly higher than the original baseline, and the process is repeated,[221] which results in a staircase waveform (Figure 13a). The current is sampled just before the pulse, at time T′, and then again near the end of the pulse, at time T. Alternatively, in SWV, the potential is stepped by some value (ΔE_p) for approximately 2−3 ms and then stepped in the reverse direction to a value greater than ΔE_p, but opposite in sign, for an equal time. This process is

https://doi.org/10.1021/acs.chemrev.1c00471
Chem. Rev. XXXX, XXX, XXX−XXX

Scheme 5. Electrochemical Reduction and Chemical Oxidation of Fluorescein in the Presence of Ultrasound[a]

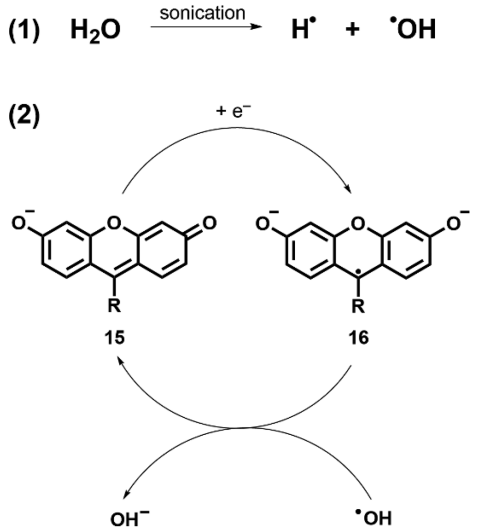

[a]Adapted with permission from ref 220. Copyright 1995 Royal Society of Chemistry.

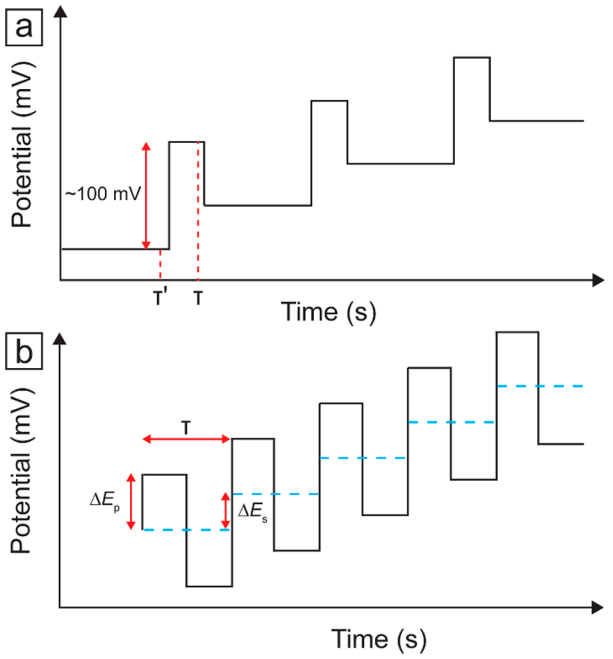

Figure 13. (a) Staircase waveform generated during differential pulse voltammetry. Current is sampled twice, at time T and T'. (b) Waveform generated during square wave voltammetry, where T is the total time of one cycle (about 5 ms), ΔE_s is the potential step height, and ΔE_p is the peak potential of the pulse.

repeated at constant frequency, but the amplitude is offset by a predetermined ΔE_s. The resulting waveform (Figure 13b) is a square wave superimposed on a staircase waveform with the amplitude of the square wave typically $50/n$ mV.[222] For both DPV and SWV, a voltammogram is obtained by subtracting the currents taken at each sampling time, which eliminates nonfaradaic currents.

DPV is commonly employed in the electrosynthetic community to improve the peak resolution for situations in which multiple cathodic or anodic peaks overlap in a standard CV. Roesel et al.[223] employed CCE to carry out electrocatalytic Newman−Kwart rearrangements on a variety of *O*-arylthiocarbamates (**17**, Scheme 6). CV of 25 *O*- and *S*-arylthiocarbamate derivatives was performed in 0.1 M $TBABF_4$−HFIP. For each *O*-aryl compound, two anodic peaks are observed: the first is at ca. 1.18 V vs $Ag/AgNO_3$, and the second is in the range from 1.39 to 1.59 V, dependent upon substituent identity. However, for each *S*-aryl compound, only one anodic peak is observed at ca. 1.44 V vs $Ag/AgNO_3$. From these voltammetric data, a Hammett plot was constructed to reveal the substituent influence on the oxidative behavior. However, for compounds with cyclohexadiene (*O*- and *S*-aryl derivative) and NO_2 (*O*-aryl derivative) substituents, poor anodic peak resolution inhibited calculation of $E_{p/2}$. To overcome this issue, DPV was utilized for all three substrates. Hammett-plot analysis for *O*- and *S*-arylthiocarbamate derivatives together with DFT calculations revealed that oxidation of the above-mentioned species produces a radical cation with charge localized on the thiocarbamoyl group. However, resonance delocalization allows for charge movement to the sulfur group. Subsequently, intramolecular electrophilic aromatic substitution follows, producing **18** radical cation with the charge centered on the aromatic ring. Finally, reduction of the cation produces the final product.

CV and DPV have helped in unraveling the oxidation mechanism of silyl enol ethers to produce the corresponding seven-membered ring (Scheme 7).[224] CCE of (*S*)-((3-(3-(furan-3-yl)propyl)cyclopent-1-en-1-yl)oxy)trimethylsilane (**19**) was found to require almost double the current expected

Scheme 7. Electrocyclization of Silyl Enol Ethers to Form a Seven-Membered Ring at a Carbon Anode in the Presence of 2,6-Lutidine[a]

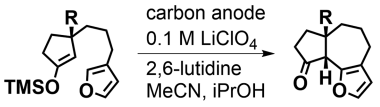

19 R = H
20 R = CH_3

[a]Adapted with permission from ref 224. Copyright 2005 American Chemical Society.

Scheme 6. Electrocatalyzed Newman−Kwart Rearrangement of *O*-Arylthiocarbamates to *S*-Arylthiocarbamate[a]

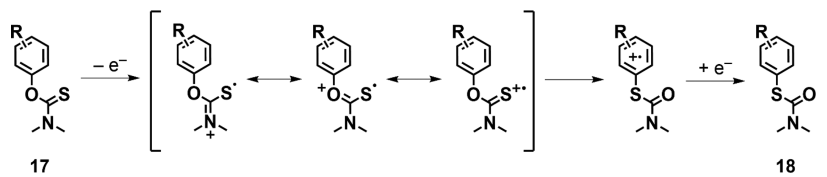

[a]Adapted with permission from ref 223. Copyright 2020 American Chemical Society.

https://doi.org/10.1021/acs.chemrev.1c00471
Chem. Rev. XXXX, XXX, XXX−XXX

for annulation of the corresponding methyl derivative (**20**). To unravel the role of the substituent, CV and DPV were carried out on both enol ethers in TBAPF$_6$−MeCN. Voltammograms for **19** and **20** reveal oxidation potentials of 0.81 and 0.70 vs Fc/Fc$^+$, respectively. The methyl group present in **20** was found to lead to a *gem*-dialkyl effect that enhances the rate of cyclization on the time scale of electron transfer. In contrast, the effect is absent in **19** since R = H rather than methyl. Consequently, subsequent electron transfer to the electrogenerated radical cation intermediate affords unwanted follow-up reactions, such as polymerization, resulting in larger charge consumption.

SWV was utilized to determine the ligation state of Co^{II} complexes when mixing 1.0 mM CoBr$_2$ with various amounts of ligand.[225] As shown in Figure 14a, two distinct redox species are observed depending on the amount of ligand added. Upon addition of 0.5 mM ligand, one distinct peak is observed at −1.43 V vs Fc/Fc$^+$; a second peak (ca. −1.34 V) appears after addition of 2.0 mM ligand and becomes predominant after 2.5 mM ligand is added. This allowed the fraction of the ligation state to be plotted against ligand equivalents added, which revealed the relative amounts of mono- and bisligated Co^{II} (Figure 14b).[161] For each SWV experiment, the cathodic peak was normalized with respect to the amount of ligand. This same procedure was employed to aid in understanding of the oxidative addition mechanism between Co^I complexes containing pyridine-oxazoline (pyrox) bidentate ligands (**21**) and aryl bromides (**22**) (Scheme 8).[226] Oxidative addition rate constants were measured by CV at various scan rates to determine the amount of Co^I consumed.

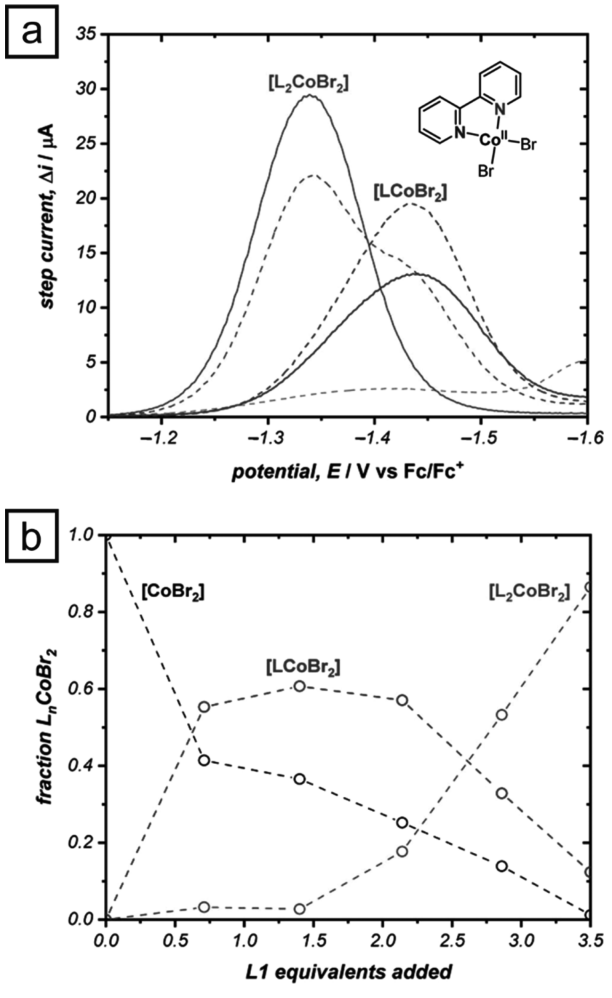

Figure 14. (a) Square wave voltammograms of 1.0 mM CoBr$_2$ in the presence of 0.0, 0.5, 1.5, 2.0, and 2.5 mM 2,2-bipyridine in a 100 mM solution of TBAPF$_6$−MeCN. (b) Voltammetric titration of CoBr$_2$ in the presence of 2,2-bipyridine resulting from square wave voltammograms. Voltammograms were performed with a 3 mm boron-doped diamond working electrode at 50 Hz under an Ar atmosphere at 25 °C. Panels a and b reprinted with permission from ref 161. Copyright American Chemical Society 2019.

Scheme 8. Oxidative Addition of Co^I Pyrox Complexes with Benzylic Bromides[a]

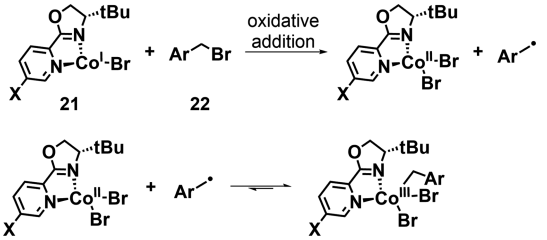

[a]Adapted with permission from ref 226. Copyright 2019 American Chemical Society.

Tennyson et al.[227] applied pulse voltammetric techniques as a means to deconvolute unresolved redox waves. A series of *N*-heterocyclic carbenes containing Ni, Pd, and Pt centers was investigated for use in redox-switchable catalysis. Voltammograms of each bis(1,3-dimesityl-4,9-dioxo-2,3,4,9-tetrahydro-1*H*-naphtho[2,3-*d*]imidazol-2-yl)metal(IV) chloride complex in 0.1 M TBAPF$_6$−DCM at a Au WE exhibit broad reduction peaks at ca. −0.80 V vs SCE (Figure 15a, 15c, and 15e). Subsequent voltammograms obtained by means of DPV reveal that these broad cathodic peaks correspond to two separate one-electron reductions, each corresponding to one quinone moiety in the molecule (Figure 15b, 15d, and 15f). Gas chromatography analysis over 24 h revealed that catalysis is halted upon reduction of the quinone moieties but can be reestablished through subsequent oxidation.

3.1.5. Thin-Layer Voltammetry. Kinetic information on an electrosynthetic process can be obtained also through the use of exceptionally small cell volumes. The solution is confined between the WE and another surface (e.g., the electrochemical cell wall or another electrode), such that a thin layer, smaller in thickness than the diffusion layer (<50 μm), is formed. The most common applications of thin layers are steady-state amperometry and linear sweep or cyclic voltammetry. In the former case, the thin layer is housed in a small space between two electrodes. Reduction of a species at the cathode is followed quickly by oxidation at the anode and vice versa as a result of the exceptionally small distance the species must travel. This generates a steady-state current, which allows for determination of common kinetic parameters such as α and k_s. Recently, a number of methods have been employed for the construction of thin-layer electrochemical cells.[228−230] In these devices, an amplified current is produced by repeated reduction and oxidation of analyte molecules. For instance, voltammetry of 2,5-diferrocenylthiophene and 2,3,4-triferrocenylthiophene in a nanochannel device enabled calculation of the kinetic parameters from steady-state

https://doi.org/10.1021/acs.chemrev.1c00471
Chem. Rev. XXXX, XXX, XXX−XXX

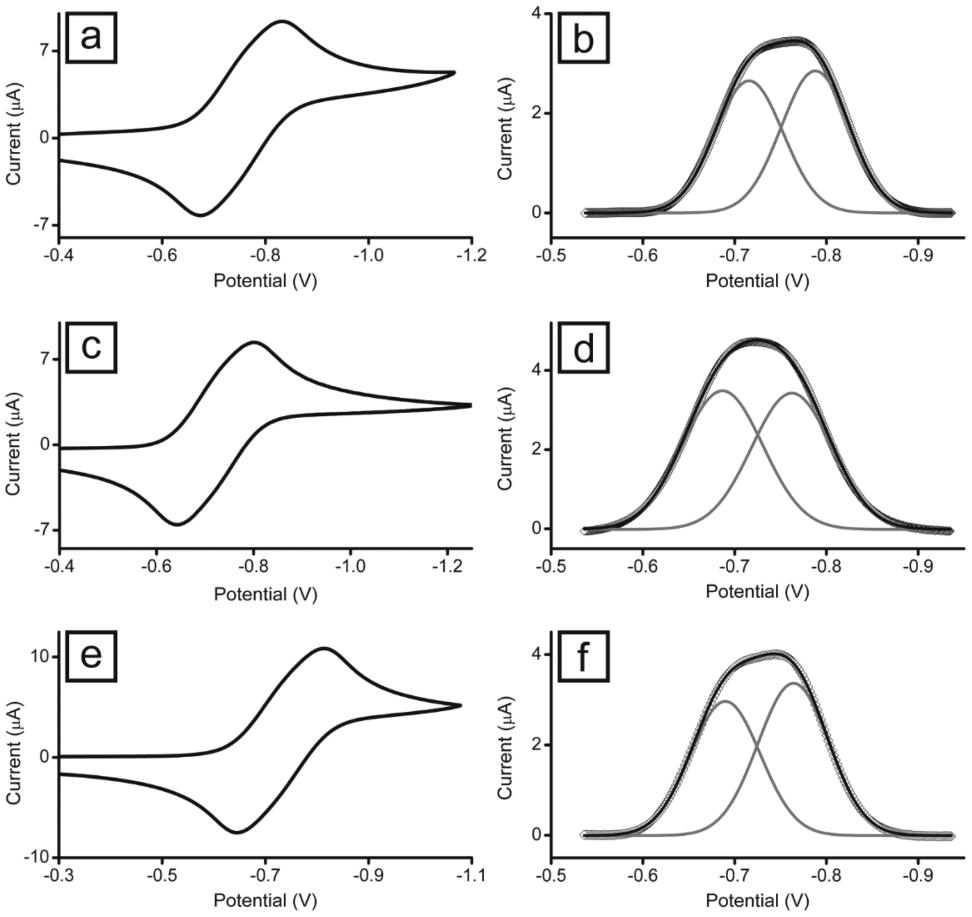

Figure 15. Cyclic and differential pulse voltammograms of Ni-centered (a, b), Pd-centered (c, d), and Pt-centered (e, f) *N*-heterocyclic carbenes in 0.1 M $TBAPF_6$–DCM. DPV peaks are shown as open circles; deconvoluted and fitted peaks are shown as gray and black solid traces. Reprinted with permission from ref 227. Copyright 2010 American Chemical Society.

currents.[231] Alternatively, thin-layer conditions can be achieved with a scanning electrochemical microscope (section 3.4).[232] Pathirathna et al.[195] achieved quasi-steady-state currents in cyclic voltammograms collected at a double-barrel carbon nanogap electrode at scan rates of up to 100 V s^{-1}. The generator electrode potential was swept in the negative direction to reduce $Ru(NH_3)_6^{3+}$ to $Ru(NH_3)_6^{2+}$, which was subsequently reoxidized back to $Ru(NH_3)_6^{3+}$ at the collector electrode. The ability to collect kinetic information at such high scan rates was made possible by the 1 nm spacing between the electrodes.

An interesting application of thin-layer electrochemistry involves the study of interfaces between two immiscible electrolyte solutions (ITIES). Initial studies were pioneered by Gavach and Guastalla[233−236] and then expanded upon by Koryta[237−239] as well as Girault and Schiffrin.[240−243] When analyzing an ITIES, a single WE is coated with a thin layer of organic solvent containing the species of interest and then immersed in an aqueous solution containing a redox mediator. The organic layer prevents diffusion of the mediator to the electrode surface to participate in electron transfer. Reduced (or oxidized) species at the electrode surface diffuse to the aqueous−organic interface, where interaction with the mediator results in chemical reoxidation (or rereduction), producing a semisteady state. Similar to hydrodynamic voltammetry, the observed current is measured as a function of mediator concentration, wherein a plot of i_{obs}^{-1} vs $[analyte]^{-1}$ allows for determination of k_s from the slope of the line.

3.2. Spectroscopic Methods

Electrochemical methods are sufficient to detect and measure the lifetime of many electrogenerated intermediates. However, structural information on transient species is still required to determine accurate and detailed mechanisms. Such information can be deduced via application of spectroscopic techniques. In this context, simultaneous exploitation of electrochemical and spectroscopic studies can prove tremendously beneficial owing to a class of techniques broadly referred to as spectroelectrochemistry (SEC). Numerous books and reviews have described the breadth of approaches to SEC.[244−249] In this section, we focus on ultraviolet−visible (UV−vis), infrared (IR), Raman, nuclear magnetic resonance (NMR), and electron paramagnetic resonance (EPR) spectroscopies coupled to electrochemical methods for mechanistic studies of electroorganic reactions.

3.2.1. Ultraviolet−Visible Spectroscopy. UV−vis SEC is the most common in situ SEC method, largely due to instrumentation availability and easy setup.[245] Measurements are collected via transmission or reflectance mode, as illustrated in Figure 16.[250] In transmission UV−vis SEC, light passes perpendicular (Figure 16a) or parallel (Figure 16b) to the WE and solution. Commonly, minigrids or optically transparent electrodes (OTEs) are employed as the WEs. Alternatively, reflectance mode is achieved when light reflects

https://doi.org/10.1021/acs.chemrev.1c00471
Chem. Rev. XXXX, XXX, XXX−XXX

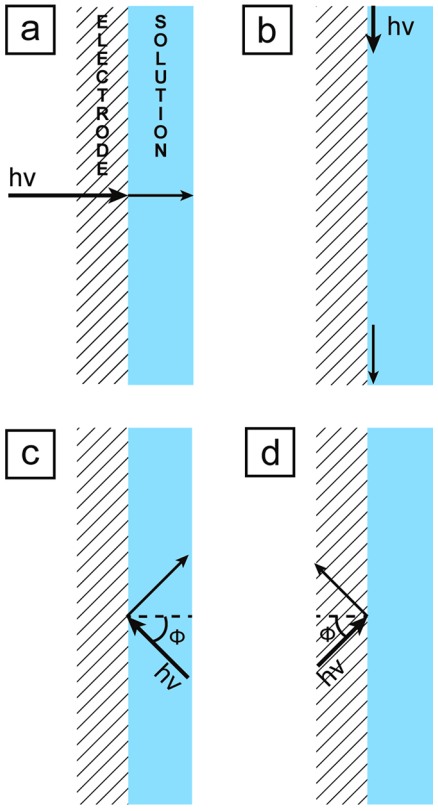

Figure 16. Common optical configurations for spectroelectrochemical cells showing the path of incident light (thick line) and detected light (thin line) in transmission mode (a) normal and (b) parallel to the electrode or (c) internal and (d) external reflectance modes. Adapted with permission from ref 250. Copyright 2018 Elsevier.

off an electrode surface.[251] In internal reflectance, light passes through the solution, reflects off a metal or opaque WE, and passes back through the solution (Figure 16c).[32] In contrast, external reflectance is achieved when light shines through the back side of an OTE and reflects upon contact with the electrode (Figure 16d).[252] In addition to a single (specular) reflection, multiple reflections can occur as is the case for attenuated total reflectance (ATR),[251] which allows for increased sensitivity. Investigation of species at a distance of 100 nm away from the electrode is possible due to the existence of an evanescent standing wave in solution near the electrode.[250,253−255]

In the simplest design, an UV−vis SEC cell can be constructed with modifications to a standard cuvette by addition of a WE, CE, and RE with the WE placed in the optical path. More complex cells that take advantage of solution flow and thin-layer SEC have also been designed. Compton and co-workers[256] constructed an optically transparent thin-layer SEC cell (Figure 17) that employs a gold-mesh minigrid WE with a QRE and CE placed up- and downstream, respectively.

In the context of electrosynthesis, UV−vis SEC has been employed to provide mechanistic and kinetic information.[257−262] Yogendra et al. investigated the electrochemically induced ring opening and closing of the cyclotri(phosphonio)-methanide dication **23** to phosphanylcarbodiphosphorane **24** (Scheme 9).[257] On the cathodic sweep, consumption of **23** and production of **24** is observed, whereas on the reverse sweep, the opposite is seen. Multiple consecutive scans coupled with

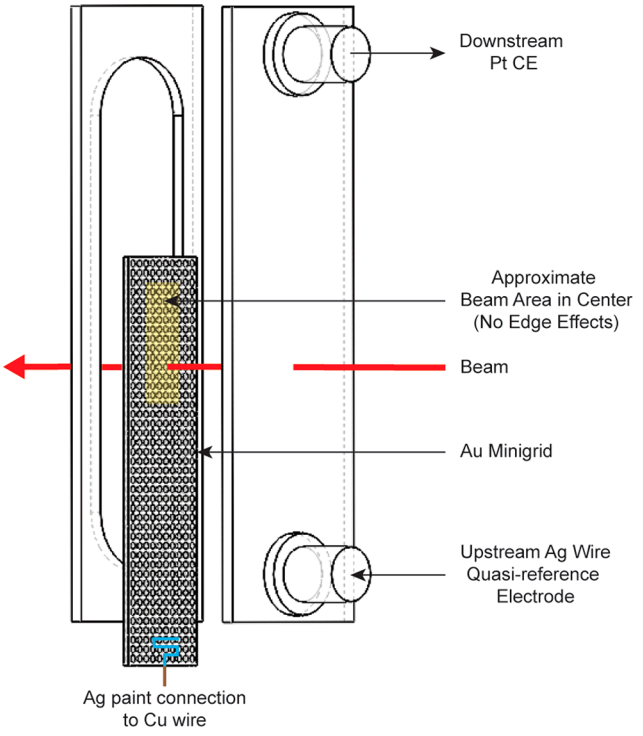

Figure 17. Optically transparent, flow-through thin-film UV−vis spectroelectrochemical cell. Adapted with permission from ref 256. Copyright 1989 American Chemical Society.

Scheme 9. Electrochemically Induced Ring Opening and Closing of the Cyclotri(phosphonio)methanide Dication[a]

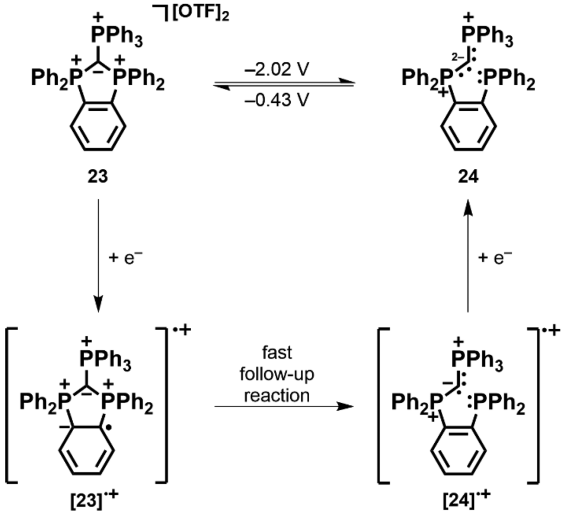

[a]Adapted with permission from ref 257. Copyright 2017 American Chemical Society.

in situ UV−vis provide evidence for an overall reversible ring-opening−closing process. A reversible ECE pathway was proposed, wherein a one-electron reduction is followed by P−C bond cleavage. Subsequently, a second one-electron reduction affords **24**.

Zhang et al.[263] utilized UV−vis SEC to study the electropolymerization of metal-centered pyridine complexes containing *N*-phenyl carbazole and vinyl moieties. The initial monomer was anchored by a phosphite group to an indium−tin oxide (ITO) WE. As illustrated in Figure 18a, application of

https://doi.org/10.1021/acs.chemrev.1c00471
Chem. Rev. XXXX, XXX, XXX−XXX

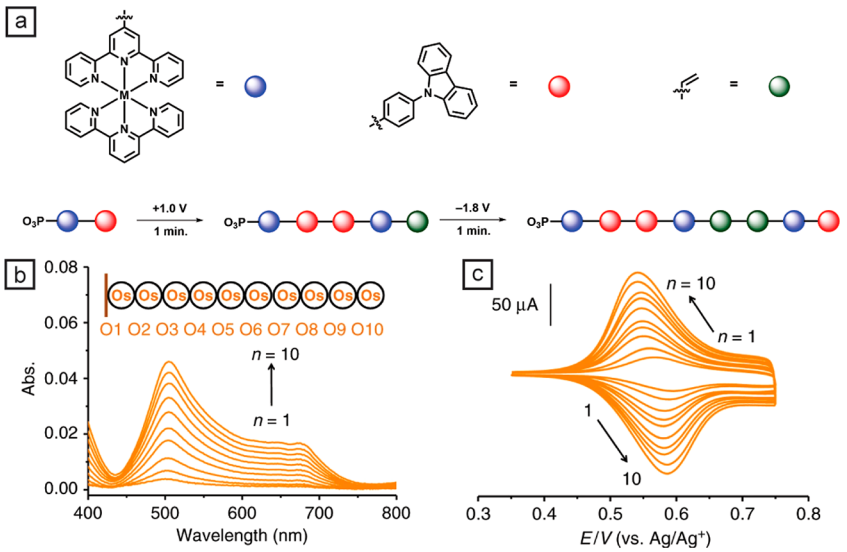

Figure 18. (a) Electropolymerization of metal-centered pyridine complexes through oxidative *N*-phenyl carbazole coupling and reductive vinyl coupling. (b, c) Real-time UV−vis spectra and cyclic voltammograms obtained between anodic and cathodic potential sweeps of an Os-centered pyridine complex. Panels b and c are reprinted with permission from ref 263. Copyright Nature 2020.

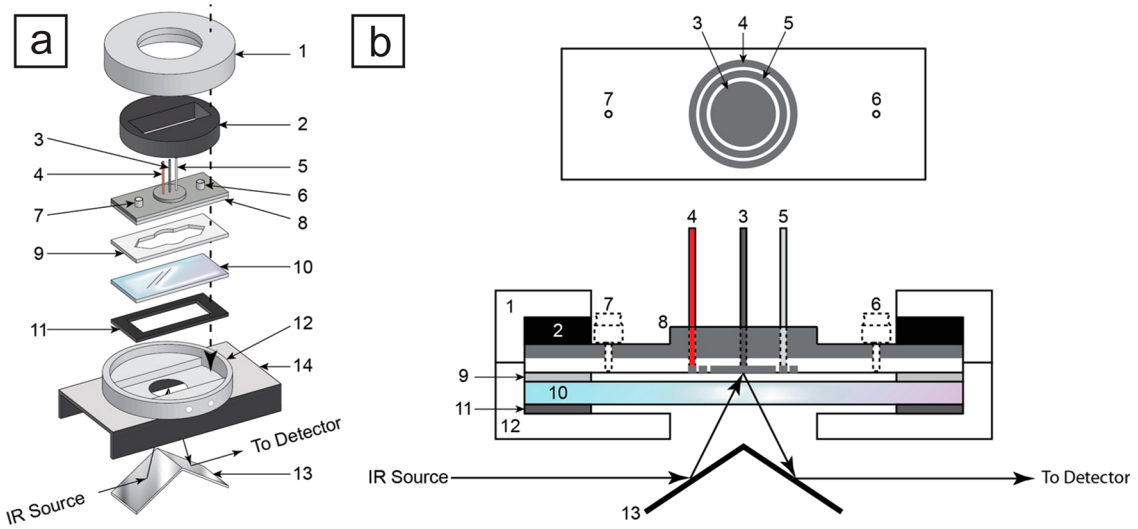

Figure 19. Disassembled view of the reflectance IR SEC developed by Kubiak and co-workers: (1) tightening brass cap (threaded inside); (2) brass ring required to tighten the cell; (3) WE; (4) auxiliary/CE; (5) pseudo-RE; (6, 7) injection ports; (8) cell body, top part aluminum, lower part Teflon (all three electrodes and both filling ports are press fitted into the cell body, so that they can be replaced if needed); (9) Teflon spacer; (10) CaF_2 window; (11) rubber gasket; (12) hollow brass cell body with threaded inlet and outlet ports (Swagelock) for connection to a circulating bath; (13) mirrors; (14) two-mirror reflectance accessory (Thermo-SpectraTech FT-30; not shown in cross-sectional view). Reprinted with permission from ref 283. Copyright 2014 American Chemical Society.

a positive potential results in oxidative coupling of *N*-phenyl carbazole, leading to addition of another metal−pyridine complex. Similarly, when the potential is switched cathodically, reductive vinyl coupling results in addition of another monomer. Cyclic voltammograms at the redox potential of the metal center combined with real-time UV−vis spectra were obtained to monitor the course of the reaction (Figure 18b and 18c). Absorbance and voltammetric current increase linearly as a function of polymer chain length. This method was expanded further to pyridine complexes with various metal centers.

UV−vis SEC is primarily utilized for determination of kinetic parameters such as the overall order of an electrochemical reaction, the rate of radical disappearance, and the stability of electrogenerated intermediates. However, UV−vis SEC does not provide comprehensive structural information, and electroisomerization cannot be distinguished by means of this technique.

3.2.2. Infrared and Near-Infrared Spectroscopy. Infrared spectroelectrochemistry (IR SEC) is a powerful technique frequently employed to probe the structures and orientations of adsorbed species, detect formation of new species, and monitor degradation of starting materials. Moreover, this technique has been utilized to investigate the bonding of electrogenerated intermediates to the electrode, determine charge states in redox reactions,[264−266] and measure the rate of fast electron transfer in mixed-valence compounds.[264,267−276]

As with UV−vis spectroscopy, IR SEC can be performed in transmission or reflectance mode; each method requires different cell designs. For transmission studies, electrochemical reactions are investigated by monitoring changes in the

https://doi.org/10.1021/acs.chemrev.1c00471
Chem. Rev. XXXX, XXX, XXX−XXX

radiation intensity as light passes through the cell. Almost all transmission IR SEC cells are modified from the original design developed by Petek et al.[277] To minimize solvent absorption and electrode interference, thin-layer cells are commonly used with similar electrode compositions and orientations to those in UV−vis studies.[278,279] Alternatively, reflectance mode is advantageous due to decreased light obstruction. However, this setup is more complicated as extra mirrors are required to focus light off the electrode and to the detector. To this end, Kubiak developed a popular cell for reflectance IR SEC studies (Figure 19). Moreover, BioLogic, Pike Technologies, Metrohm, and Specac, to name a few, have commercially available cells for IR SEC. Detailed analysis of IR SEC modes, principles, and cell construction are provided elsewhere.[250,280−282]

Potential-sweep methods, particularly cyclic voltabsorptometry (CVA) and derivative cyclic voltabsorptometry (DCVA), are popular for IR SEC.[284] For each method, absorbance is recorded while the WE potential is swept at 20 mV s^{-1} or slower. A narrow window of wavenumbers is monitored for optimal speed and data resolution. For CVA, absorbance is monitored as a function of time (or applied potential), while in DCVA, the absorbance differential is plotted against potential. In addition, a 3D graph is generated that includes absorbance, wavenumber, and time. Tian et al.[285] performed CVA and DCVA to investigate 1,8-dihydroxy-9,10-anthracenedione (Q) reduction via IR SEC. Reduction of Q affords dimers π−Q_2, which rearranges to form σ−Q_2; however, previous electrochemical studies did not provide a detailed pathway for their formation and interconversion. An irreversible reduction peak is observed at ca. −1.0 V vs Fc/Fc^+ on the first voltammetric cycle of Q in MeCN (Figure 20a, black trace). However, the second cycle shows a quasi-reversible peak at −1.0 V and an irreversible oxidation peak at 0.12 V (Figure 20a, red trace). Through subsequent analysis, reduction at −1.0 V was determined to be a one-electron process to form $Q^{\bullet-}$, which dimerizes to form π−$Q_2^{\bullet-}$ and then rearranges to form σ−$Q_2^{\bullet-}$. Further reduction of σ−$Q_2^{\bullet-}$ yields dianion and tetraanion species. In situ FT-IR SEC, CVA, and DCVA (Figures 20b, 20c, and 20d, respectively) were utilized to confirm the reaction mechanism shown in Figure 20e.

In comparison to other SEC methods, in situ IR has been utilized most frequently for analysis of electroorganic reactions as this technique provides direct structural information and reaction kinetics. However, due to intense water absorbance, IR SEC is limited to use of select dry, aprotic, organic solvents with appropriate solvent windows.

3.2.3. Raman Spectroscopy. Similar to IR, Raman spectroscopy provides information from molecular vibrations.[286] This technique operates on the basis of inelastic (Raman) scattering, which results in wavelength shifts that correspond to molecular vibration frequency.[244] While Raman spectroscopy provides unique structural information, only a small percentage of light is inelastically scattered, which results in a weak signal. Variations of Raman spectroscopy, such as surface-enhanced Raman spectroscopy (SERS), correct for this issue through signal amplification caused by electromagnetic interaction of incident Raman light with metal surfaces.[287−289] Fleischmann et al.[290] first observed this phenomenon in studies of pyridine at Ag electrodes, illustrating the possible applications of Raman SEC at metal electrodes. Figure 21a shows the original stationary-electrode cell designed by Fleischmann et al.[290] for Raman SEC.

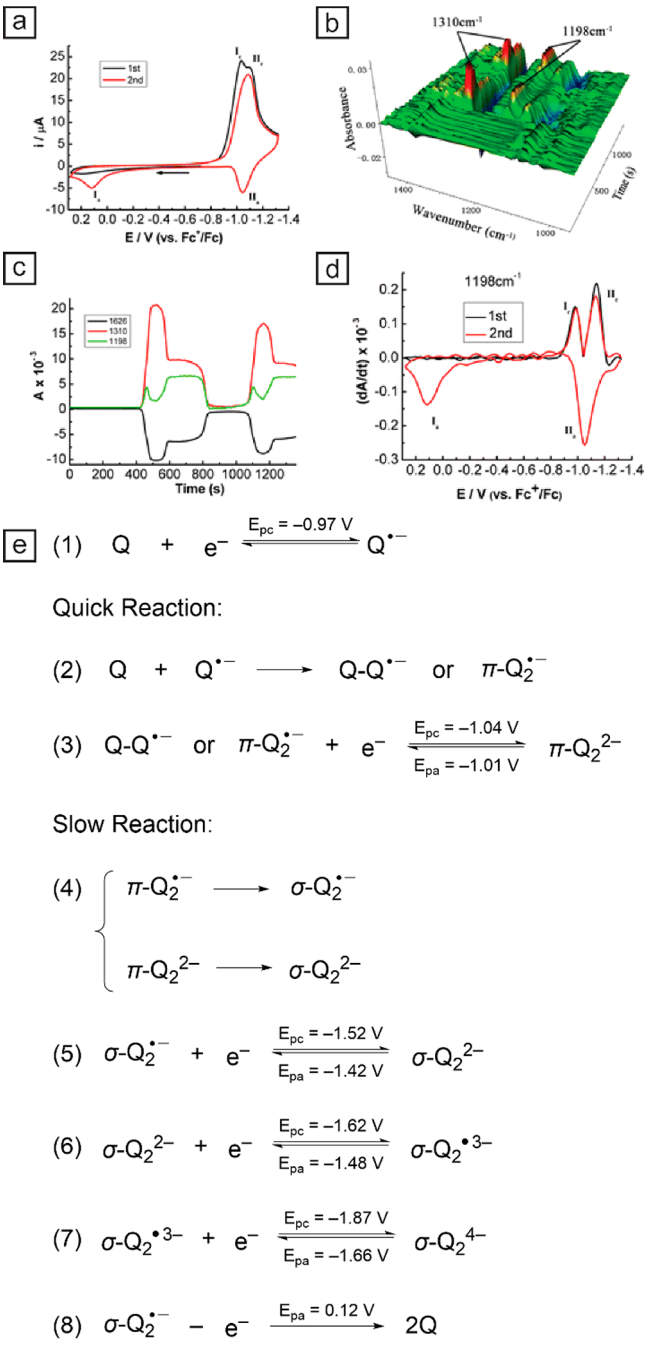

Figure 20. (a) Cyclic voltammogram, (b) corresponding 3D spectra of FT-IR SEC, (c) cyclic voltabsorptometry, and (d) derivative cyclic voltabsorptometry of 10 mM 1,8-dihydroxy-9,10-anthracenedione (Q) in MeCN containing TBAP (0.2 M). (e) Proposed reaction mechanism for Q reduction. FT-IR SEC studies were conducted in a thin-layer cell, and potential was scanned at 5 mV s^{-1} in the range from 0.28 to −1.32 V. To make the DCVA data readily comparable to CV, the second reduction and first oxidation in the DCVA data were multiplied by −1. Reprinted with permission from ref 285. Copyright 2013 American Chemical Society.

Modern in situ Raman SEC is achieved with the aid of a confocal microscope coupled to an electrochemical cell with common designs implementing a stationary electrode. However, many redox molecules are prone to photodegradation, which can be minimized through the use of moving (or rotating) electrodes or flow-through cells.[244,291,292]

https://doi.org/10.1021/acs.chemrev.1c00471
Chem. Rev. XXXX, XXX, XXX−XXX

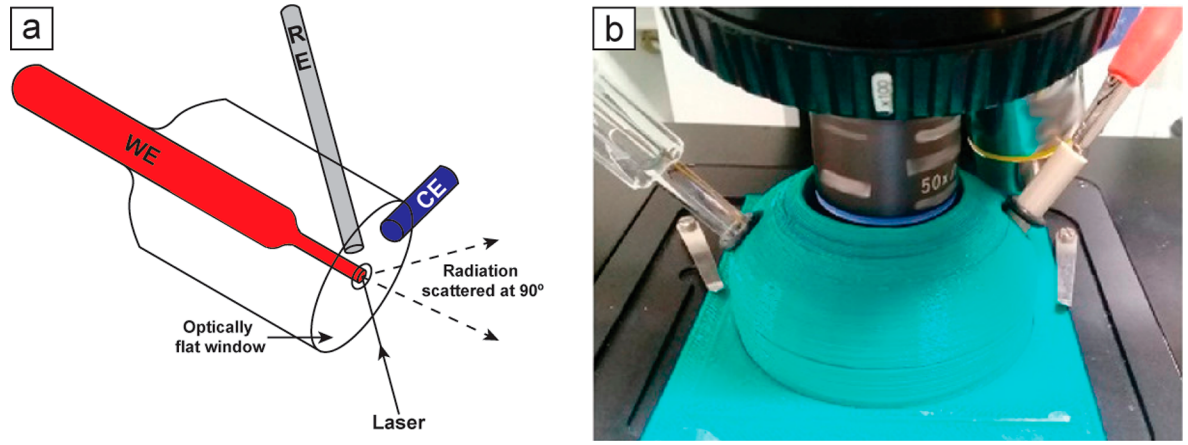

Figure 21. (a) Original Raman SEC cell set up designed by Fleischmann. Adapted with permission from ref 290. Copyright 1974 Elsevier. (b) Three-dimensional-printed cell coupled to a Raman spectrometer. Compartments on the side house the RE and CE. Reprinted with permission from ref 293. Copyright 2019 American Chemical Society.

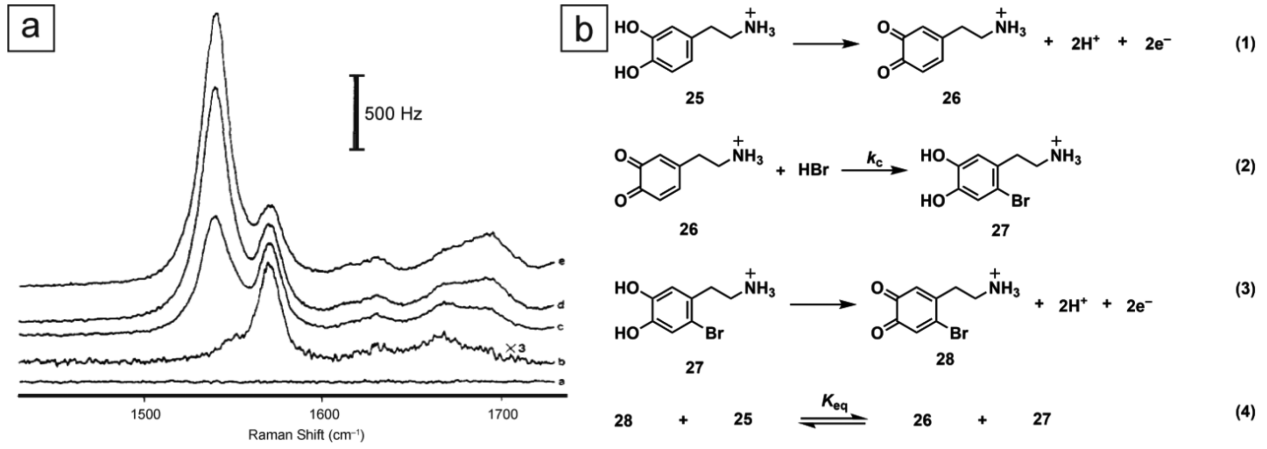

Figure 22. (a) Raman spectra for oxidation of dopamine (**25**) in the presence of 1 M HBr. Spectral lines were collected at 0 (curve a), 0−50 (curve b), 100−150 (curve c), 200−250 (curve d), and 400−450 ms (curve e) after potential step from 0 to 0.85 V vs Ag/AgCl. Reprinted with permission from ref 296. Copyright 1988 American Chemical Society. (b) Proposed mechanism for oxidation of dopamine in the presence of 1 M HBr. Reprinted with permission from ref 295. Copyright 1987 American Chemical Society.

A recent report by Bonacin and co-workers developed a 3D-printed SEC cell for in situ Raman measurements (Figure 21b).[293] The low production cost (<USD 2) together with the short manufacturing time (3.5 h) make this novel cell exceptionally appealing.

As with IR SEC, Raman SEC allows for analysis of structural changes in molecules near or at the electrode surface. In addition, Raman spectroscopy is nondestructive, and commercial instrumentation is readily available.[294] Furthermore, this technique offers (1) high spectral resolution, which allows for selective monitoring of various compounds, (2) high temporal resolution as the acquisition time is similar to or faster than reactions at the electrode, and (3) high sensitivity capable of detecting small analyte amounts.[295] As a result, Raman SEC is ideal to monitor intermediates and elucidate reaction mechanisms. McCreery and co-workers[296] utilized this technique to investigate dopamine (**25**) oxidation in the presence of HBr (Figure 22). Initially, no peaks are present between 1300 and 1800 cm^{-1} as dopamine does not have a strong Raman signal (Figure 22a, curve a). As the potential is stepped to 0.85 V vs Ag/AgCl, dopamine oxidation produces dopamine *o*-quinone (**26**) with Raman peaks at 1572 and 1672 cm^{-1}. With additional time, the 1572 cm^{-1} band decreases and a new band at 1540 cm^{-1} (Figure 22a, curves b−e) appears, indicating that **26** is unstable. Though less prominent, changes in the 1600−1750 cm^{-1} region suggest formation of an intermediate and a stable product. On the basis of spectral analysis, a mechanism for **25** oxidation in the presence of HBr was proposed (Figure 22b).[296]

Surface adsorption effects can also prove beneficial for mechanistic analysis. Wang et al.[297] employed in situ SERS SEC coupled with density-functional theory (DFT) to further understand the catalytic role of Ag electrodes in carbon−halogen bond reduction. Key intermediate species (such as a benzyl anion−Ag adduct) were identified, which aided in mechanism validation. Similarly, Itoh and McCreery investigated the chemisorption phenomenon of azobenzene[298] and nitroazobenzene[299] monolayers on a carbon electrode surface. These studies are particularly remarkable as a Raman signal was still detected despite the lack of signal enhancement at carbon. Despite these advantages, Raman SEC has not yet been widely employed for mechanistic elucidation of organic electrosyntheses, primarily due to the inherently low signal-to-noise ratio.

3.2.4. Nuclear Magnetic Resonance Spectroscopy. Early studies involving nuclear magnetic resonance spectroe-

https://doi.org/10.1021/acs.chemrev.1c00471
Chem. Rev. XXXX, XXX, XXX−XXX

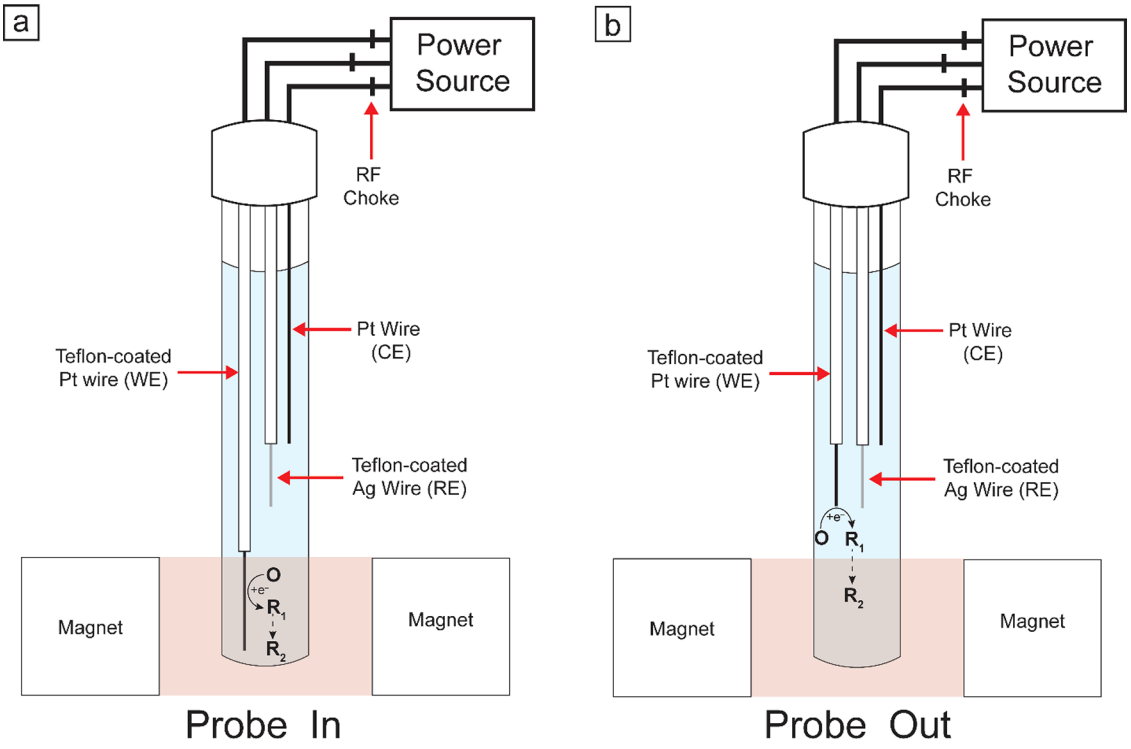

Figure 23. Schematic of the NMR SEC cell for the (a) probe-in method with the WE inside the magnetic field and (b) probe-out method with the WE outside of the magnetic field.

lectrochemistry (NMR SEC) incorporated a three-electrode assembly into a 5 mm NMR tube to monitor electrolysis with ^{1}H NMR spectroscopy.[300] Since then, NMR SEC has undergone significant and rapid growth in various aspects including cell design and suitable NMR methods. NMR SEC is most typically employed in bulk electrolysis methods and CV; each presents advantages and disadvantages.[301] For example, CV is relatively fast compared to NMR; thus, slow scan rates (<20 mV s^{-1}) must be utilized. However, despite these difficulties, the relatively nondestructive nature of CV compared to electrolytic methods allows various analyses to be performed in one experimental setup.

NMR SEC studies are usually performed in a three-electrode configuration with the CE and QRE placed outside the magnetic-field region to enhance field homogeneity.[302] On the basis of the WE position with respect to the magnetic field, NMR SEC analyses are divided into two categories (Figure 23). "Probe-in" methods employ a WE located inside the NMR-active region, which allows for detection of small concentrations of electrogenerated intermediates. However, the WE must consist of a nonmagnetic material with proper shape and dimensions to minimize magnetic field disturbances.[303] Some electrodes well suited for probe-in analysis include semiconductors (fluorine-doped tin oxide or boron-doped electrodes), special carbon fibers,[304] or thin Au films symmetrically deposited inside a glass tube.[305] Alternatively, "probe-out" methods employ a WE positioned outside the magnetic region, which affords a homogeneous magnetic field and NMR spectra with narrow, well-resolved peaks.[304] Moreover, because the WE is located outside the magnetic field, the WE can be constructed from a vast range of materials. However, since the active region is spatially separate from the WE, unstable electrogenerated products can degrade prior to migration into the effective magnetic region. Thus, probe-out methods can suffer from elevated detection limits.

Possible interactions between the magnetic field and the cell connection wires must be considered in NMR SEC cell design. Use of wires with internal shields and RF chokes may be necessary to preserve the electrochemical signal quality and minimize magnetic field interference.[306] Moreover, strategies for efficient solution mixing must be addressed as mechanical mixing is not possible. In the absence of convection, mass transport becomes diffusion controlled, which results in long electrolysis times. However, convection can be achieved via the magnetohydrodynamic force, where the interaction between the electric and the magnetic fields present during NMR SEC results in effective solution stirring.[307−309]

Typically, multiple ^{1}H or ^{13}C NMR spectra, obtained at various time points throughout electrolysis, are necessary to gain a better understanding of the reaction pathway. Although these analyses are limited to stable intermediates, as each scan lasts a few seconds, improvements in cell design have enabled advanced methods of analysis. For instance, NMR SEC with 2D NMR provides information about the carbon and hydrogen nuclei simultaneously, which decreases the time required to obtain spectra. Ultrafast 2D NMR SEC was utilized to monitor the electroreduction of 9-chloroanthracene (**29**, Figure 24) in a 95:5 MeCN/water mixture containing 0.1 M $TBAPF_6$.[310] Two-electron reduction of **29** affords anthracene (**30**), which oxidizes to form intermediate **31** and then reacts with water to form intermediate **32**. Subsequently, **32** can dimerize to form **33**, or oxidize and deprotonate to form **34**. Neither **31** nor **32** is detected with NMR spectroscopy due to the paramagnetic nature of these compounds.

While NMR SEC can measure diamagnetic intermediates with lifetimes of a few seconds, detection of exceptionally short-lived (microseconds to milliseconds) intermediates

https://doi.org/10.1021/acs.chemrev.1c00471
Chem. Rev. XXXX, XXX, XXX−XXX

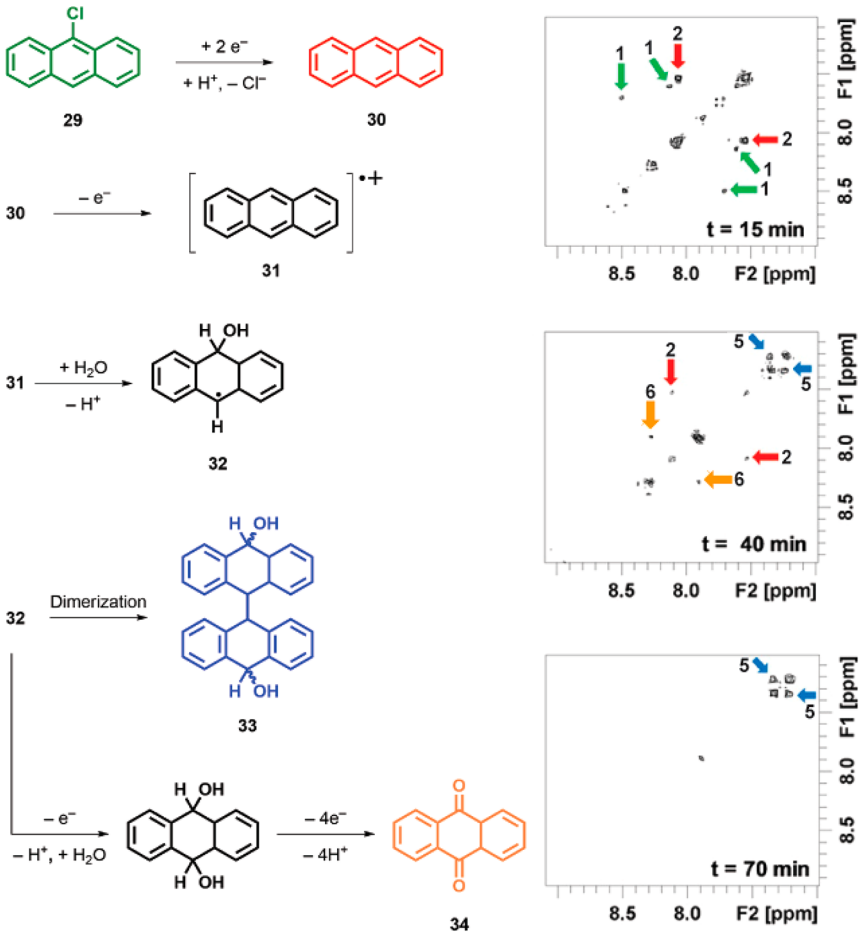

Figure 24. Ultrafast COSY-NMR analysis of 9-chloroanthracene (**29**) reduction in MeCN-d_3/D_2O 95:5 (v/v)−$TBAPF_6$ (0.1 M). NMR SEC cell was constructed inside a 5 mm NMR tube with carbon fiber as the WE, carbon fiber as the CE, and Pd wire as the QRE. NMR spectra were obtained every 3 min, and reaction mechanism was elucidated with respect to the formation and disappearance of certain peaks. Compounds **29**, **30**, **33**, and **34** were detected with NMR spectroscopy, and intermediates **31** and **32** were assumed to form with regard to electrochemical evidence. Adapted with permission from ref 310. Copyright 2014 American Chemical Society.

requires faster, multidimensional, NMR methods. In addition, electrolysis often involves production of free radicals, which cannot be detected by NMR. Some developments have been made to facilitate free-radical detection;[311] however, EPR SEC is a more suitable technique. Finally, intricate cell design and the high cost of deuterated solvents provide further limitations.

3.2.5. Electron Paramagnetic Resonance Spectroscopy. EPR spectroscopy utilizes the interaction of electromagnetic radiation and organic species when placed in a magnetic field for detection of free radicals and paramagnetic compounds.[312−316] Microwave radiation is focused and shown onto a paramagnetic sample, and the absorbance is measured.[312,316,317] Because the energy of the incident photon is low, EPR bypasses most electronic states for a molecule and probes only the ground state (or close electronic states).[316] In the case of molecules with heteroatoms, further splitting of the EPR spectrum results from nuclei cycling through their spin states.[317] Detection of short-lived intermediates is accomplished by in situ electron paramagnetic resonance spectroelectrochemistry (EPR SEC), similar in practice to probe-in NMR SEC. A silica tube (∼1 mm i.d.) serves as the electrochemical cell with only the WE and solution exposed to radiation when placed in the resonant cavity.[318−320] Alternatively, for longer-lived intermediates, ex situ EPR can be utilized, which results in a homogeneous solution and eliminates positioning effects from anisotropic samples.[313] In each method, a sufficiently high concentration (∼10^{-6} M) of radicals must be generated to obtain an EPR spectrum.[317]

Mirífico et al.[321] investigated the electroreduction mechanism of isatin (**35**, ISH) in 0.1 M $NaClO_4$−DMF at a vitreous carbon electrode in the presence of CH_3I (Scheme 10). Through a one-electron process, **35** is reduced to **35**$^{\bullet-}$, which can react with either CH_3I to afford NMI (**37**) or **35** to afford ISH^- (**35**$^-$) and $ISH_2^{\bullet}$(**36**). The latter pathway was confirmed via electrolysis of **35** in the absence of CH_3I. Disappearance of the **35**$^{\bullet-}$ signal over time was observed by ex situ EPR analysis. Together with formation of dimeric species **38**, this was taken as evidence that a chemical step occurs during electrolysis to form **37** and **38**. Dimer oxidation, followed by reaction with a superoxide anion, forms a molozonide species (**39**), which converts to an ozonide (**40**). Hydrolysis of intermediate **40** forms **37** and **41**.

Oftentimes, radical lifetimes are so short that not even in situ EPR can detect these species. In such cases, a spin trap is added—producing a spin adduct—which is less reactive and maintains a sufficiently high concentration of radicals. While this technique can confirm the presence of a radical, most structural information is lost as the spin adduct is formed.[317] Mo and co-workers[322] employed this method to elucidate a reduction mechanism for aryl diazonium salts in the presence

https://doi.org/10.1021/acs.chemrev.1c00471
Chem. Rev. XXXX, XXX, XXX−XXX

Scheme 10. Proposed Mechanism for the Synthesis of NMI and NMIA[a]

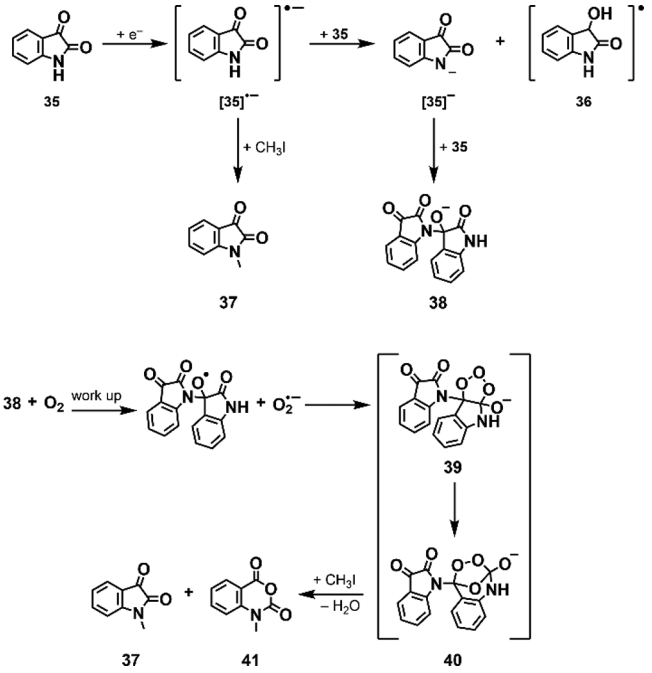

[a]Adapted with permission from ref 321. Copyright 2019 American Chemical Society.

of a halogen source at Pt electrodes. No radicals were observed upon in situ EPR SEC analysis; as a result, *N*-benzylidene-*tert*-butylamine *N*-oxide (PBN) was added as a spin-trap agent, which reacted with the radical intermediate to form an EPR-detectable adduct. This confirmed the presence of an aryl radical, which abstracts a halogen from the halogen source to form the corresponding aryl halide.

Quantitation by means of EPR[323] is typically performed by (1) comparing the signal with a suitable internal standard such as TEMPOL,[324] (2) monitoring the relative signal over time,[324,325] (3) comparing the relative ratios of two EPR-active species,[324,326] or (4) standard addition.[327] In each case, double integration of the output signal is required to obtain the area under the absorbance curve. Tamski et al.[324] described a detailed methodology for quantification of electrochemical-EPR where accuracy within 3% was achieved in the micromolar to millimolar range. While possible, quantitation via EPR is uncommon due to the transient lifetimes and exceptionally low concentrations of radicals. Chromatography is better suited for higher precision and accuracy.[317]

A major drawback involving EPR SEC is the noninnocence of conventional electrodes, such as graphene, which are EPR active. To overcome this obstacle, other diamagnetic materials, such as W, can serve as suitable replacements. Moreover, these experiments should be performed at room temperature, although free-radical detection is more convenient under low-temperature conditions (solid-state EPR). Finally, high-dielectric solvents attenuate the signal from EPR-active species, which can limit solvent choice.

3.3. Chromatographic Techniques

Elucidation of electrochemical mechanisms often requires separation, identification, and quantitation of the products. Liquid chromatography (LC) and gas chromatography (GC) are analytical techniques employed for mixture analysis. Generally, LC is implemented for analysis of macromolecules or thermally liable compounds, whereas GC is employed for analysis of volatile compounds. For effective separation, care must be taken in selection of the column (length, stationary phase composition), mobile phase (for LC), and temperature program (for GC). Optimization of the parameters is beyond the scope of this review; however, the interested reader can find more on the history, theory, and method development of LC and GC in the literature.[328−331]

Identification of compounds is often achieved by coupling a mass spectrometer to a chromatography column. In *Modern Practice of Gas Chromatography* (4th ed.), Grob[328] described IR and MS as exceptional techniques for identifying unknowns. However, MS is the superior technique in part due to existing MS libraries of known compounds.[328,332−334] Unfortunately, MS libraries for LC-MS (or tandem MS) are far more limited than what is used in GC-MS. This is largely due to significant disparity in electrospray ionization (ESI) and atmospheric-pressure chemical ionization (APCI) spectra depending on instrument designs and experimental parameters (e.g., ionization and collision energy).[335] These challenges have been minimized as most published LC-MS libraries include mass spectra acquired through more than one collision energy.[336] Nonetheless, when analyzing a mixture, products should be separated and individually characterized.

LC-MS and GC-MS are powerful analytical tools for the qualitative and quantitative analyses of mixtures. General methods for quantitative analysis include calibration curves, addition of an internal standard, and area normalization. Calibration curves are less common in chromatography as detector response changes over time and thus requires "checks" or calibrations. Alternatively, the method of internal standards presents a more robust option. For accurate quantitation, an appropriate internal standard should be electroinactive, commercially available, and have a similar molecular structure, weight, and polarity as the analytes. Peters and co-workers[337] demonstrated the need for a suitable internal standard in the quantitation of highly volatile hydrocarbons. An internal standard with similar properties to the analyte allowed for solution-phase and gas-phase quantitation to determine the overall product formation. Other groups[129,338,339] reported relative product yields via area normalization by analyzing the relative abundance of compounds. This is a simpler procedure that does not involve extensive preparation of standards or addition of extra compounds. However, this method does not account for products that may not appear on the chromatogram. Furthermore, differences in ionization and partition efficiencies may lead to systematic error.

3.3.1. Liquid Chromatography. Recent reviews explore applications of electrochemistry-coupled mass spectrometry (EC-MS) with some attention to EC-LC-MS.[340,341] As mentioned previously, LC is a versatile technique that can be combined with electrochemistry for the analysis of small organic molecules,[342−347] nucleic acids,[348−350] peptides and proteins,[351−354] pharmaceutical compounds,[355−359] and agrochemicals.[360−362] However, this list is not comprehensive and only illustrates the wealth of research articles on applications of EC-LC.

Online analysis is a remarkable application of EC-MS, enhanced by incorporation of LC. Recent publications by Mekonnen et al.[360,363] exemplify the use of online EC-LC, and others have modified such setups to analyze solutions via MS

https://doi.org/10.1021/acs.chemrev.1c00471
Chem. Rev. XXXX, XXX, XXX−XXX

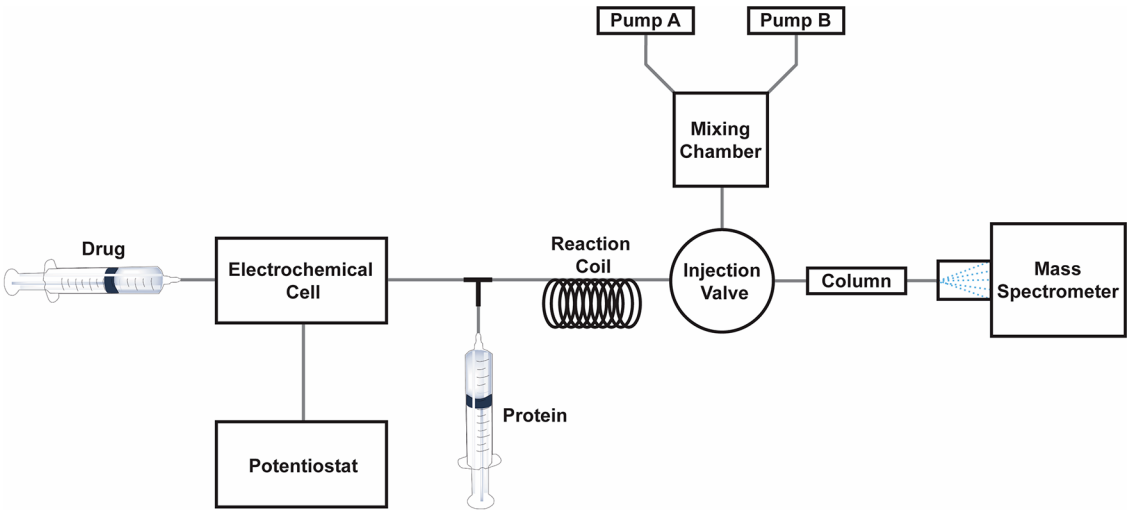

Figure 25. General setup of EC-LC-MS (ESI). Adapted with permission from ref 364. Copyright 2008 American Chemical Society.

Scheme 11. Partial Mechanism for the Reduction of Phthalide[a]

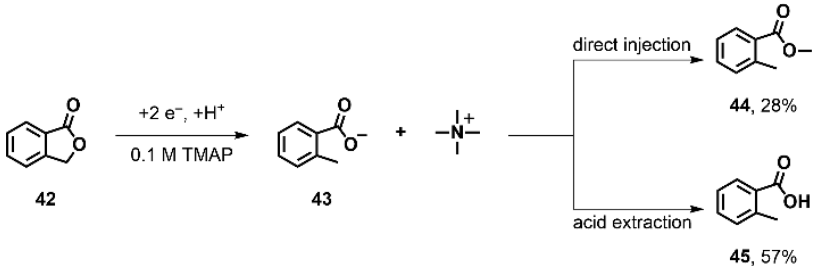

[a]Adapted with permission from ref 369. Copyright 2013 Elsevier.

and LCMS.[364] The configuration presented in Figure 25 takes advantage of flow electrochemistry for online analysis through LC-MS (ESI). In this case, a drug of interest was injected into the EC cell and oxidized before reacting chemically with a protein to form a drug−protein adduct prior to LC-MS analysis.[364] For solely electrochemical reactions, a second injection port and reaction mixing system are not needed. In a similar fashion, Santi et al.[365] employed 2D-HPLC for optimization of enantioselective electrochemical oxidation of *N*-arylcarbonylated L-proline to enantiomerically enriched methoxylated amides. Implementation of online 2D-HPLC allowed for efficient assessment of charge impact, anode material, temperature, flow rate, and substrate concentration on the reaction outcome. Despite the benefits associated with online EC-LC, a major drawback is the inability to detect short-lived, unstable intermediates. In this case, direct EC-MS analysis is more suitable and will be discussed further in section 3.3.3.

3.3.2. Gas Chromatography. GC is preferred for analysis of gases and volatile compounds. For online-GC analysis, a gastight cell must be used with an outlet connected to the GC injection port. Yeo and co-workers[366] utilized this method to investigate the performance of a modified Cu WE for the selective reduction of CO_2 to ethane. Online-GC analysis was performed at a 10 min sampling rate with a dual detector for monitoring H_2 (thermal conductivity detector or TCD), hydrocarbons (flame ionization detector or FID), and CO (FID). Cu_2O-derived Cu, together with $PdCl_2$ added to the electrolyte, was shown to have the best electrocatalytic performance, as evidenced by the higher yields of ethane. In a similar fashion, Liu and co-workers[367] analyzed the efficacy of crystal defects on Cu nanoneedle electrodes toward the reduction of CO_2. Electrolyses were performed for 3 h, and online-GC analysis (30 min sampling) was employed to detect H_2, CO, CH_4, and C_2H_4. Oxidatively treated Cu nanoneedles displayed superior performance compared to annealed Cu nanoneedles for the reduction of CO_2, as shown through increased formation of C_2H_4.

For offline-GC analysis, sample preparation becomes important. de Koning and co-workers described many modern methods of sample preparation for GC analysis.[368] Typically, a simple liquid−liquid extraction is sufficient for postelectrolysis analysis. For instance, Pasciak et. al[369] studied the reduction of phthalide (Scheme 11, **42**) in 0.1 M tetramethylammonium perchlorate (TMAP)−DMF as well as 0.1 M tetrabutylammonium perchlorate (TBAP)−DMF. Reduction proceeds via a mixture of one- and two-electron-transfer processes to produce 2-methylbenzoate (**43**). Analysis of the catholyte via GC and GC-MS through direct injection leads to formation of 2-methylbenzoate ester (**44**). However, when the catholyte is partitioned between diethyl ether and 10% aqueous HCl, 2-methylbenzoic acid (**45**) is detected. **43** and tetraalkylammonium cation were determined to chemically react at high temperatures (~200 °C) in the injector port to form **44**. This interference led to inaccurately low yields. In TMAP−DMF, the apparent yield of **43**, through detection of **44**, was 28% upon analysis by direct injection. However, the yield of **43**, via detection of **45**, was 57% when a liquid−liquid extraction was performed prior to analysis. Analogously, in TBAP−DMF,

https://doi.org/10.1021/acs.chemrev.1c00471
Chem. Rev. XXXX, XXX, XXX−XXX

product distributions revealed 42% of *n*-butyl 2-methylbenzoate and 84% **45**.

3.3.3. Mass Spectrometry. As discussed before, mass spectrometers aid in structural elucidation. While often paired with chromatographic techniques, MS can be used standalone for reaction monitoring and rapid product identification. Wang et al.[370] investigated the electrochemical [3 + 2] annulation of *N*-cyclopropyl-3,5-dimethylaniline (**46**) with styrene in MeCN containing lithium triflate (Figure 26a). At a carbon anode

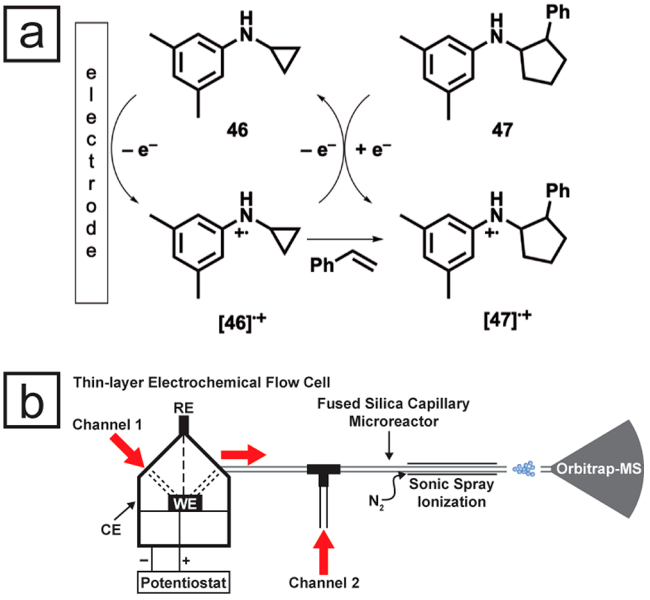

Figure 26. (a) [3 + 2] annulation of *N*-cyclopropyl-3,5-dimethylaniline (**46**) at carbon cathodes in MeCN. (b) Home-built electrochemistry-mass spectrometry (EC-MS) instrument by Chen and coworkers. Adapted with permission from ref 370 Copyright 2021 Royal Society of Chemistry.

biased to 3.0 V vs Ag/AgCl, **46** undergoes a one-electron oxidation to a radical cation. This intermediate reacts with styrene to form the 3,5-dimethyl-*N*-(2-phenylcyclopentyl)-aniline radical cation (**47**$^{\bullet+}$), which gains an electron from **46** resulting in a chain reaction. Species **46**$^{\bullet+}$ and [**47** + H]$^+$ were detected by means of sonic spray ionization (SSI)-MS operated in tandem with the electrochemical reaction (Figure 26b). In a similar fashion, Ye et al.[371] studied the Au-catalyzed oxidative dimerization of terminal alkynes at a RVC anode in MeCN. Under a constant current of 5 mA, a terminal alkyne attaches to the Au center of the catalyst, which then undergoes a two-electron Au^I/Au^{III} oxidation. Through transmetalation, a second terminal alkyne attaches to form a Au^{III} complex, which was verified by means of nanoelectrospray ionization (nESI)-MS. Reductive elimination then occurs, producing the homo- or heterodiyne product.

MS is also employed to analyze unstable reaction intermediates with short (from milliseconds to seconds) lifetimes. Online-MS was employed to study electrochemical processes as early as 1971.[244,341,372−377] Notably, Wolter and Heitbaum developed differential electrochemical mass spectrometry (DEMS), where an electrochemical cell is connected to a high-vacuum system that leads to a mass spectrometer.[378] For an in-depth description of state-of-the-art cells, the reader is directed toward exemplary publications.[244,376] A hydrophobic membrane is placed between the cell and the vacuum system, which allows volatile compounds and dissolved gases to reach the mass spectrometer. Electron impact (EI) is applied to gaseous analytes before reaching the detector, which results in more accurate quantitation, simpler fragmentation patterns, and fast response rates (<0.1 s). Typical applications of DEMS include mechanistic analysis of small molecule oxidation (i.e., fuel cell related studies), CO_2 reduction, hydrogen evolution, and reduction or oxidation of nitrogenated species.[341,376,377,379] For instance, Clark et al.[380] employed DEMS to monitor CO_2 reduction products directly at the surface of a Cu cathode coated with a hydrophobic membrane. Acetaldehyde was confirmed to be an intermediate in CO_2 reduction and a precursor to ethanol. While this review emphasizes applications of DEMS, the technique is restricted to analysis of volatile compounds and has limited commercial availability.

Alternatively, semi- and nonvolatile compounds can be analyzed in a thin-layer flow cell via online EC-MS (ESI). Thin-layer flow cells allow for lower supporting electrolyte concentrations, which minimizes ion interference in MS. Hoffman et al. utilized online EC-MS to monitor products formed in sulfadiazine oxidation and propose a mechanism.[374] Potential sweep combined with selected ion monitoring at a predetermined m/z revealed the potential at which intermediates and products were formed. High-resolution and collision-induced dissociation (CID) mass spectra were

Scheme 12. Reduction of Halo-Organic Compounds via (a) One-Electron or (b) Two-Electron Transfer

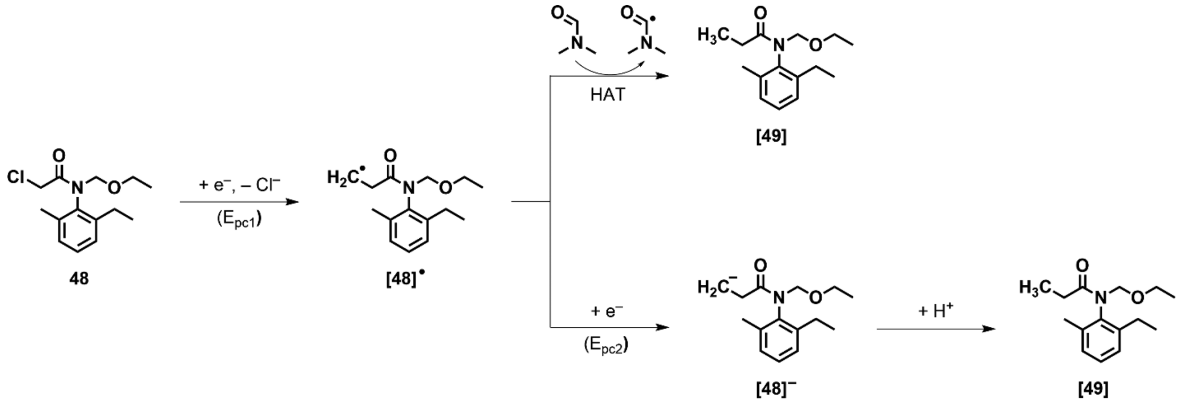

[a]Adapted with permission from ref 382. Copyright 2020 The Electrochemical Society.

https://doi.org/10.1021/acs.chemrev.1c00471
Chem. Rev. XXXX, XXX, XXX−XXX

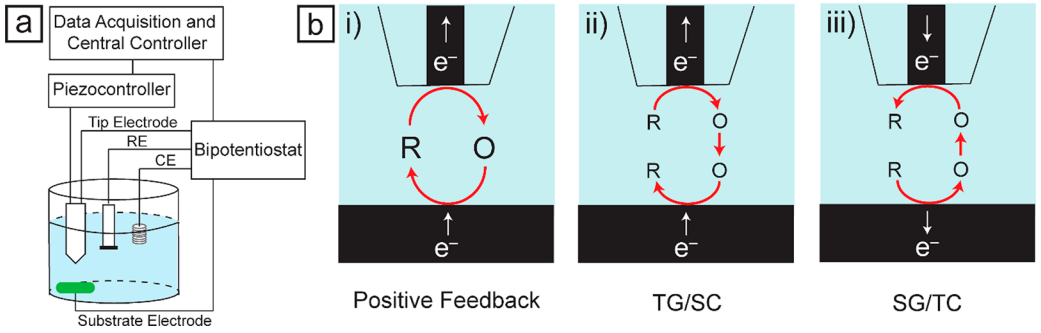

Figure 27. (a) Schematic of the SECM instrumentation and (b) various experiment modes including (i) feedback mode, (ii) tip generator/substrate collector mode (TG/SC), and (iii) substrate generator/tip collector mode (SG/TC).

collected to identify compound masses and structures with high accuracy.

In addition to structural elucidation, MS can aid in mechanistic analysis through isotope labeling. For example, reduction of halo-organic compounds proceeds via a one- or two-electron transfer. Following an initial one-electron transfer, a radical intermediate is formed. This intermediate can then abstract a hydrogen atom or undergo radical coupling to form a dimer. In the case of an overall two-electron process, a second electron is transferred to the radical intermediate, forming a subsequent carbanion intermediate, which can then react with a suitable electrophile. Both radical and carbanion intermediates can be detected through incorporation of a deuterium ($D^{\bullet}$) or deuteron (D^{+}).[381−383] A pertinent example from the Peters' group involves electroreduction of acetochlor (**48**) in DMF, as illustrated in Scheme 12.[382] Reduction in the presence of a $D^{\bullet}$ (DMF-d_7) and D^{+} (D_2O and HFIP−OD) source was conducted to validate possible pathways. Significant D^{+} incorporation was observed when a D^{+} source was employed, but no $D^{\bullet}$ incorporation was seen in the presence of DMF-d_7. In this context, the mechanism was proposed to occur through pathway b. An initial one-electron transfer to **48** generates radical intermediate **48**$^{\bullet}$, which accepts a second electron to form carbanion intermediate (**48**$^{-}$). Proton abstraction results in the final product, deschloroacetochlor (**49**).

3.4. Scanning Electrochemical Microscopy

Electron-transfer rates and intermediate lifetimes can also be measured by means of scanning electrochemical microscopy (SECM). Engstrom et al.[384] first reported SECM with a carbon fiber microelectrode and glassy carbon macroelectrode to determine product concentration profiles, map electrochemical activity, and detect short-lived intermediates. Afterward, Bard and co-workers expanded upon this technique in the late 1980s,[385,386] and the field continues to grow immensely.[387] SECM instrumentation and important experiment modes are depicted in Figure 27.[388] Two microelectrodes (tip and substrate) are placed in close proximity to one another (typically from 50 nm to 5 μm), and the potential of each electrode is independently controlled.[388] The position of these electrodes can be finely tuned across the x, y, and z directions with the aid of a micromanipulator and piezoelectric scanners. Most SECM studies are performed in dc mode; however, a few studies employ AC-SECM for surface interrogation.[389] Among the various DC-SECM experiments, feedback and generator/collector (G/C) modes are more widely utilized for kinetic studies.[390]

3.4.1. Feedback Mode. First reported by Wipf et al.,[391] feedback mode has been employed in various electrochemical studies, such as surface mapping and kinetic analysis. When the tip is positioned infinitely far from the substrate (i.e., $d \geq 10a$, where a represents the radius of the tip electrode), a steady-state current (i_{ss}) is achieved. As the tip electrode advances toward the substrate electrode, the tip current (i_T) is measured and plotted as a function of distance to construct an approach curve, from which electrosynthetic kinetic parameters can be determined. Zhou and co-workers[392] investigated the electrohydrodimerization of dimethyl fumarate (DF) and fumaronitrile (FN) in 0.1 M $TBABF_4$−DMF via SECM feedback mode. Each of these compounds undergoes a one-electron reduction followed by coupling of radical anions. Analysis via feedback-mode SECM revealed that dimerization is a second-order process with rate constants of 160 and 1.9×10^5 M^{-1} s^{-1} for DF and FN, respectively.

3.4.2. Generator-Collector (G/C) Modes. G/C experiments can be performed in tip generator/substrate collector (TG/SC) or substrate generator/tip collector (SG/TC) mode with application of a constant potential or potential sweep. In either condition, electrogenerated species formed at the generator diffuse toward the collector where detection occurs. Under constant potential, the generator and collector are biased at two different potentials and the electrode currents are measured as a function of time. However, the potential applied must be chosen carefully so the current produced at both electrodes is diffusion limited. Early studies by Bard and co-workers[393] utilized this mode of SECM to investigate the electropolymerization of aniline at a Pt substrate electrode separated from a W tip by a thin film of Nafion. The distance between the electrodes was maintained by a constant feedback current of 1 nA. Scanning electron microscopy (SEM) images of the Pt substrate reveal a unique pattern of polyaniline deposited on the surface of the electrode.

An alternative experiment involves fast potential sweep of either the tip or the substrate, which allows for detection of a range of electrogenerated species. This also allows for a more facile approach for kinetic studies. Changes in sweep rate directly impact the generation rate of transient species, which allows for correlation between the generation rate and the collected population. This information can be employed further to develop a time-dependent kinetic model. An important factor in kinetic analysis with SECM in G/C mode is the distance between the collector and the generator. For extremely short-lived species or rapid chemical reactions, d must be minimized so a high concentration of electrogenerated species can be detected at the collector. Cao et al.[394] employed

https://doi.org/10.1021/acs.chemrev.1c00471
Chem. Rev. XXXX, XXX, XXX−XXX

SECM in nanogaps (i.e., d < 300 nm) to study the kinetics of rapid electrochemical reactions. Electrooxidation of *N,N*-dimethylaniline (DMA) was studied with SECM in TG/SC mode at Pt UMEs in 0.25 M $TBAPF_6$–MeCN.[395] One-electron oxidation of DMA produces a radical cation ($DMA^{\bullet+}$) that promptly dimerizes to afford *N,N,N,N*-tetramethylbenzidiene (TMB, Figure 28a). Previous studies with either FSCV

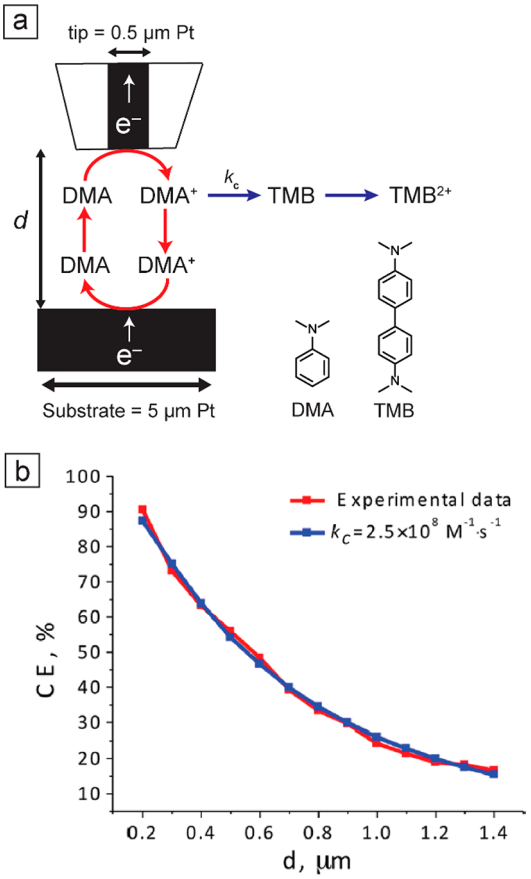

Figure 28. SECM in TG/SC mode was employed to study irreversible electrodimerization of DMA in 0.25 M $TBAPF_6$–MeCN. (a) DMA electrooxidation at the tip electrode (Pt, a = 0.5 μm) affords the corresponding radical cation. Portion of $DMA^{\bullet+}$ promptly dimerizes to afford TMB (blue arrows), while unreacted radical cation arrives at the substrate electrode (red arrow) made of Pt (a = 5 μm) where they are detected. (b) Experimental collection efficiency (CE%) vs d for the DMA oxidation was fitted to the theoretical results obtained from COMSOL simulations. With regard to the closeness of the simulated and experimental results, the dimerization rate constant was estimated to be 2.5 × 10^8 M^{-1} s^{-1}. Panel b is reprinted with permission from ref 394. Copyright American Chemical Society 2014.

or RRDE did not yield accurate dimerization rate constants or provide approximate lifetimes of $DMA^{\bullet+}$.[395] The collection efficiency (CE, %) was plotted as a function of tip–substrate distance, which varied from 200 nm to 1.4 μm (Figure 28b, red line). A theoretical model (Figure 28b, blue line) was then fitted to the experimental data. The dimerization rate constant and the lifetime of $DMA^{\bullet+}$ were estimated to be 2.5 × 10^8 M^{-1} s^{-1} and 10 μs, respectively.[394]

The tip distance and scan rate can also be varied to structurally influence the electrogenerated products. Heinze and co-workers[396] studied thiophene polymerization on a MnO_2-coated glass surface with a 10 μm Pt tip. Nitrite oxidation at the tip produces protons, which are involved in the oxidation of thiophene to a radical cation by MnO_2 at the substrate. Dimerization occurs through radical–radical coupling, and the process is repeated to form higher order polymers. These polymers are not soluble in the aqueous media and thus deposit onto the substrate over time. It was found that variation of the tip distance and scan rate could alter the dimensions of the polymer, as illustrated in Figure 29.

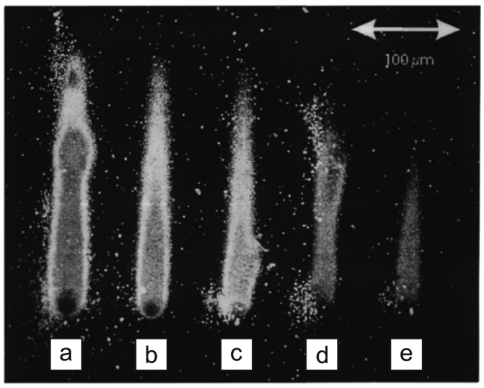

Figure 29. Electropolymerization of thiophene (20 mM) at a MnO_2-coated glass substrate under a constant current of 20 nA. Ten micrometer Pt tip was initially 5 μm from the substrate and then gradually moved away to 26 μm at a slope of 0.07. Tip scan rates were (a) 0.6, (b) 0.8, (c) 1.0, (d) 1.2, and (e) 1.4 μm s^{-1}. Reprinted with permission from ref 396. Copyright 2001 American Chemical Society.

SECM in surface-interrogation mode (SI-SECM) can be utilized to study inner-sphere electron transfer coupled with homogeneous chemical reactions.[397,398] In SI-SECM, the substrate electrode is biased with a potential profile composed of a short dc pulse with known magnitude and open-circuit value. This results in adsorption of a minute amount of electrogenerated species onto the substrate electrode. The tip potential adjusts to a known bias value with a short delay (t_{delay}) from the end of the dc pulse, which leads to formation of the active form of a redox mediator. Species adsorbed at the substrate can then react with the active mediator. The tip current is proportional to the concentration of electrogenerated species adsorbed onto the substrate. Incredibly rapid reactions, on the order of 0.5–10 μs, can be probed by fast switching techniques and shrinking t_{delay} to microseconds.[399] Simple redox reactions, such as oxygen reduction on Au and Pt surfaces, have been studied by this method.[400] While analysis of more complex reactions appears feasible, this method has seldom been employed for mechanistic elucidation in electrosynthesis.

An important application of SECM is investigation of ion transfer between two immiscible electrolyte solutions (ITIES), as introduced in section 3.1.5.[401] In this context, SECM has been used predominantly to study complexation constants[402] and fast electron-transfer processes across two solvent systems.[403] Moreover, ITIES can be employed as an effective tool to deconvolute an electrosynthetic reaction by increasing the lifetimes of highly unstable intermediates. The reactivity of these species can be controlled through transfer to a secondary solvent wherein possible side reactions (e.g., HAT and PCET) are minimized. As with SI-SECM, ITIES has only been used to analyze simple electrochemical reactions that involve one-

https://doi.org/10.1021/acs.chemrev.1c00471
Chem. Rev. XXXX, XXX, XXX–XXX

electron-transfer processes coupled with a chemical reaction (i.e., one electron, one substrate), and no reports toward more complex electrosyntheses are known.[404−407]

3.5. Computational Methods

Simulations were implemented in organic electrochemistry as early as 1948 in an effort to understand reaction mechanisms, kinetics, and thermodynamics.[73,408] Traditionally, simulations follow the same procedure: (1) physicochemical modeling to describe processes that occur at the WE surface, in the diffusion layer, and in bulk solution, (2) mathematical modeling to describe the system with set initial and boundary conditions, (3) implementation of algorithms to minimize complex mathematical models to tractable solutions, and (4) solution verification in which the results are compared to experimental data to determine simulation validity.[73] While simulations were originally programmed de novo, modern approaches utilize packaged software to simplify approaches to electrochemical computation and lower the barrier to entry. What follows is a discussion of common simulation methods for organic electrochemistry.

3.5.1. Density Functional Theory. Since the introduction of DFT by Kohn and Hohenberg in 1964,[409] different methods have been developed to better facilitate calculations.[410] In terms of electrosynthesis, DFT calculations have been applied commonly to predict redox potentials and reaction intermediates. This is useful for screening structures to find an optimal redox mediator or when analyzing reaction mechanisms.[411] While other methods (e.g., Hartree−Fock, Møller−Plesset perturbation theory, configuration interaction) involve molecular wave function computation, DFT calculates the total electron density and does not require a wave function.[412] More in-depth information on the fundamentals of DFT can be found in other publications.[409,411,413−415]

As mentioned previously, DFT is typically implemented for potential estimation and prediction of reaction intermediates. Traditionally, standard reduction potentials are computed as a combination of electron affinity and enthalpy of solvation and then referenced to the SHE with addition of an experimental constant.[416] Zuman[417] employed the Hammett formalism to relate half-wave potentials to substituent effects on a variety of substituted aromatics. However, this method suffers from the narrow class of compounds that can be studied.[418] To address this issue, Hicks et al. calculated the electron affinities for various compounds with low-level computational methods followed by increasingly rigorous methods.[416] Due to computational cost, DFT is often used in combination with faster, low-level methods to ease calculations. Any errors or approximations made during the early stages of computation are eventually canceled out by higher level calculations. Electron affinities for 29 monosubstituted chalcones were computed via increasingly complex quantum mechanical (QM) methods.[416] Initial calculations by AM1 and PM3 semiempirical methods were followed by ab initio HF/3-21G and HF/6-31G* methods. Finally, DFT with the B3LYP hybrid functional with a 3-21G or 6-31G* basis set was executed. Full geometry optimization was performed at every step, which provided a means to construct a correlation between each molecule and the reduction potential. This correlation aided in E_{pc} prediction of 71 additional polysubstituted chalcones with a standard deviation of 22 mV (Figure 30). Electron affinities were then correlated to reduction potentials for 100 chalcones by the ab initio DFT

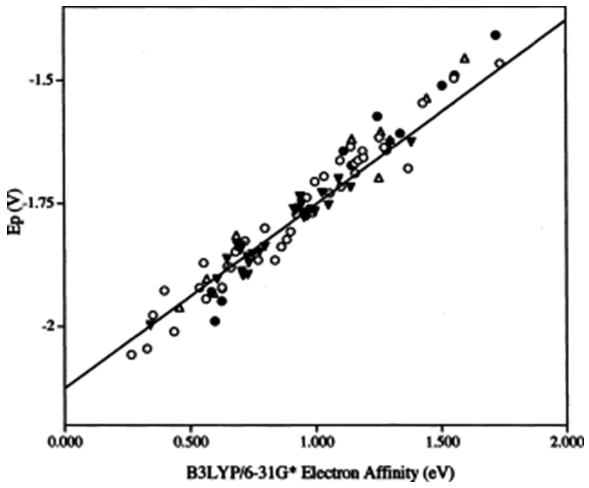

Figure 30. Plot of experimental reduction potentials vs DFT B3LYP/6-31*G electron affinities for substituted chalcones superimposed on the correlation line for 29 monosubstituted chalcones: (▼) monosubstituted chalcones; (○) disubstituted chalcones; (●) trisubstituted chalcones; (△) tetrasubstituted chalcones. Reprinted with permission from ref 416. Copyright 2004 Elsevier.

B3LYP/6-31G* method. While this study accurately predicted potentials for a large number of compounds, similar studies have been performed to predict redox potentials for smaller data sets (typically < 25 compounds).[411,419,420]

Another application of DFT involves the prediction of reaction intermediates, which is particularly important for discernment between concerted and stepwise electron transfer. Alligrant et al.[421] determined the effects of acidity and hydrogen bonding on PCET of quinones and hydroquinones in MeCN through DFT combined with voltammetry and ^{1}H NMR. Geometry optimization and vibrational-frequency analysis in MeCN was treated by means of an implicit-solvent model. DFT B3LYP was performed with 6-31*, 6-31+G*, and 6-31G** basis sets to calculate ΔG and pK_a values for intermediate species and determine a reaction pathway. It was found that hydroquinone oxidation in the presence of amines occurs by a stepwise CECE mechanism, whereas reduction of 1,4-quinone in the presence of Brønsted acids proceeds via an ECEC mechanism.[421]

3.5.2. Numerical Simulations. Simulation of the electrochemical results offers a reliable method to calculate unknown reaction parameters and confirm proposed reaction schemes. As shown in Figure 31a, a simple CV for the one-electron reduction of **O** to **R** includes three regions. Region 1 (Schottky region) illustrates the double-layer capacitance, whereas Regions 2 and 3 represent faradaic processes.[91] Currents in the latter two regions are limited by electron-transfer kinetics and mass transfer due to diffusion, respectively. Accurate current determination for regions 2 and 3 necessitates Fick's laws of diffusion to be solved with high accuracy to create a concentration profile for species **O** and **R** in the double layer (Figure 31b). To this end, finite difference methods (FDM) and finite element methods (FEM) are typically employed.[422,423]

Finite Difference Method. FDMs provide a simple yet accurate numerical approach for spatial and temporal discretization of highly symmetrical continuous domains with two or fewer dimensions. In principle, FDM uses a Taylor series expansion to divide a given space into units of known

https://doi.org/10.1021/acs.chemrev.1c00471
Chem. Rev. XXXX, XXX, XXX−XXX

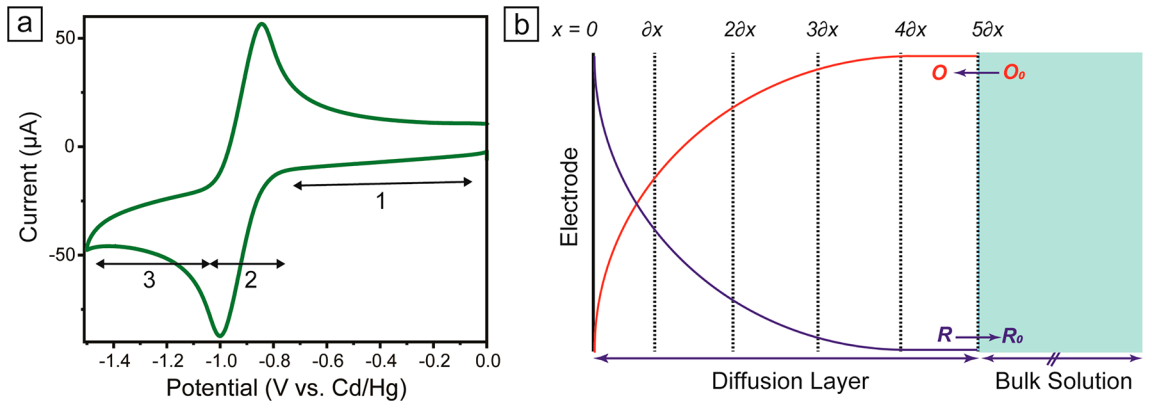

Figure 31. (a) Cyclic voltammogram for the one-electron reduction of **O** to **R**. (b) Concentration profiles of species **O** and **R** in the diffusion layer.

length.[424] With this approach, partial differential equations in a given space transform into a series of linear algebraic equations, known as finite difference equations, which can be solved via matrix methods. This approach is especially desirable in terms of computational cost, as even personal computers can solve vast matrices with ease.

From the long list of FDM variants developed to solve electrochemical systems, fast implicit finite difference (FIFD) has received considerable attention. Developed by Rudolph, this method became the basic principle of DigiSim and other software.[425−428] FIFD allows for any combination of electrochemical and chemical reactions to be studied with simulation of various forms of mass transport possible. Recently, Gamry developed DigiElch for processing and simulating electrochemical results on the basis of FIFD.

Digital simulation has been utilized extensively to confirm electrosynthetic mechanisms.[429,430] Batchelor-McAuley and Compton described the theory for analysis of cyclic voltammograms simulated with the aid of DigiSim.[431] One example explores the pH-dependent two-electron, two-proton reduction of anthraquinones (AQ, Scheme 13). Experimental and

Scheme 13. Generalized Square Scheme for the Anthraquinone $2H^+$, $2e^-$ Redox System[a]

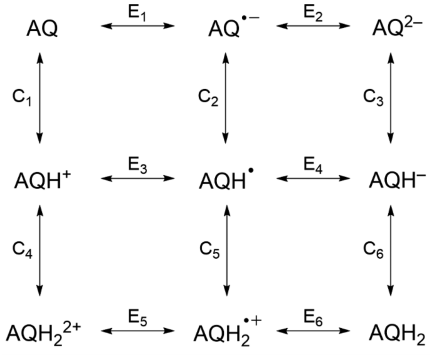

[a]Adapted with permission from ref 432. Copyright 2010 American Chemical Society.

simulated cyclic voltammograms for anthraquinone-2,6-disulfonate (Figure 32a and 32b) and anthraquinone-2-sulfonate (Figure 32c and 32d) were obtained for pH 1−13. Simulated cyclic voltammograms depict a change in peak height, peak separation, and wave shape as the pH changes, which are also reflected in the experimental results. It was determined that reduction of anthraquinones occurs via an EE process to form AQ^{2-} at pH 13 (Scheme 13, E_1E_2) and an EECC process to form AQH_2 at pH 10 (Scheme 13, $E_1E_2C_3C_6$). Between pH 4 and 7, reduction proceeds through an ECEC mechanism (Scheme 13, $E_1C_2E_4C_6$) and at pH 1 by a CECE process (Scheme 13, $C_1E_3C_5E_6$), both of which lead to formation of AQH_2.[432]

Finite Element Method. FEM is preferred for cases involving a lower degree of symmetry or complicated reaction schemes. This method is particularly useful for scanning probe techniques or electrochemical studies at microarray electrodes.[433] The mathematical theory of FEM and FDM is similar; however, FEM applies free quadrangles or triangles to carry out discretization. Thus, FEM offers higher flexibility toward discretization, allowing more complex geometries to be solved.[434] Detailed discussions pertinent to the mathematical basis of FEM can be found elsewhere.[435]

Numerous platforms, including COMSOL, MATLAB, and FIDAP, have been developed to perform finite-element analysis.[436] However, COMSOL has received more attention from the electrochemical community due to greater flexibility, advanced predefined modules, and higher reliability compared to other platforms. Amemiya and co-workers employed SECM to study rapid electron transfer of 7,7,8,8-tetracyanoquinodimethane (TCNQ).[437] Voltammograms for feedback and SG/TC modes were simulated with COMSOL to determine mass transport, thermodynamic, and kinetic parameters. Computational simulations combined with experimental results indicated diffusion rates of 1.6×10^{-5} and 2.0×10^{-5} cm^2 s^{-1} for $TCNQ^{\bullet-}$ and TCNQ, respectively. The electron-transfer rate constant was determined to be 7 cm s^{-1}.

Finally, we would like to stress that researchers are not limited in simulation software choice. With regard to the system of interest, appropriate numerical simulations can be executed with proper selection of computer software or programming language, such as MATLAB and Python for home-built FEM and FDM simulations, respectively. Regardless, reaction mechanisms must be studied thoroughly, and relevant kinetic and thermodynamic parameters must be determined as accurately as possible.

4. FUTURE DIRECTIONS AND CONCLUSIONS

At the writing of this review, electrosynthesis continues to grow rapidly in popularity, which warrants an in-depth analysis of ways to understand electroorganic reaction mechanisms. This review has explored the many techniques available to

https://doi.org/10.1021/acs.chemrev.1c00471
Chem. Rev. XXXX, XXX, XXX−XXX

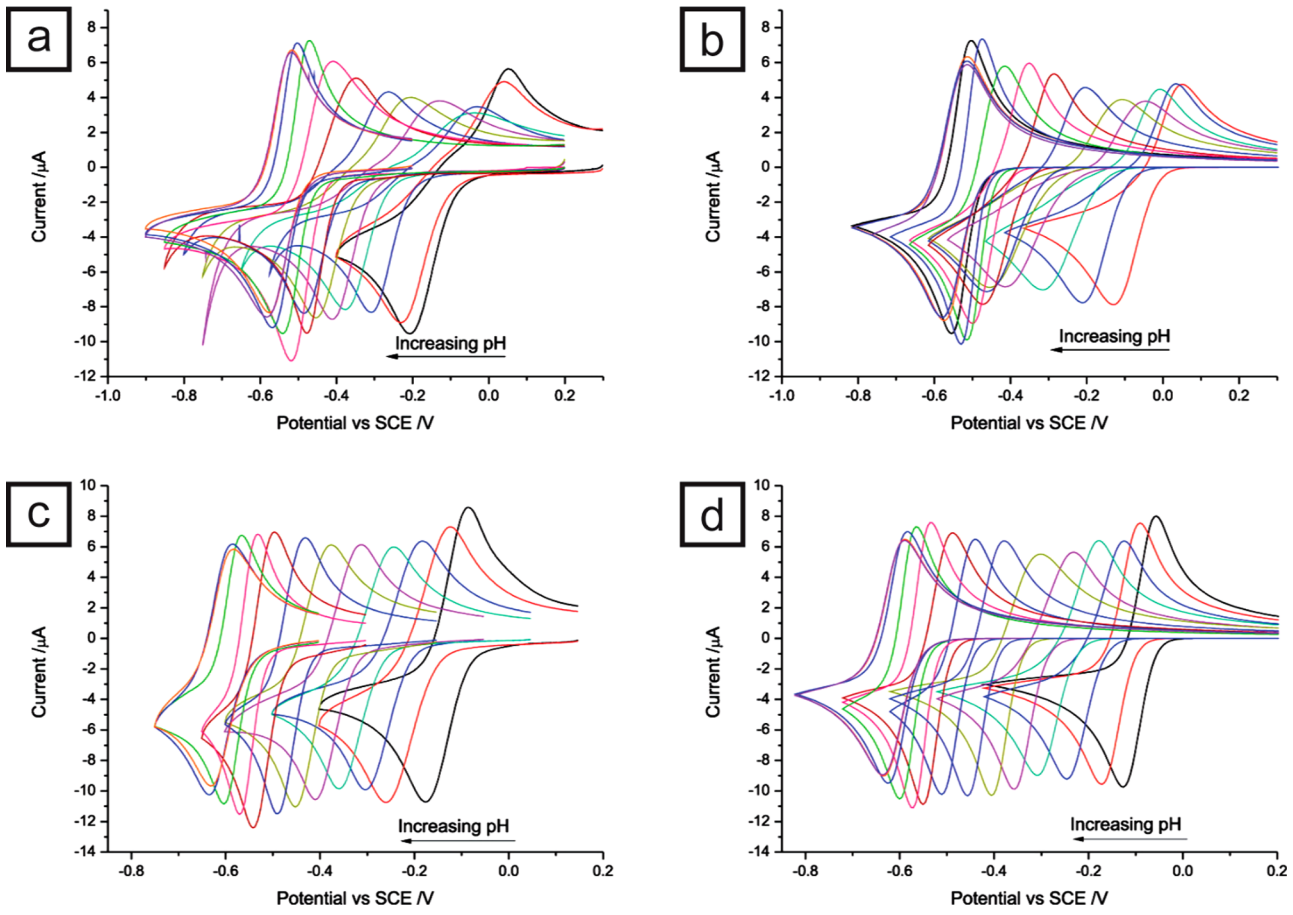

Figure 32. Overlaid cyclic voltammograms for (a, b) 1 mM anthraquinone-2,6-disulfonate and (c, d) 1 mM anthraquinone-2-sulfonate over the full pH range 1−13. (a, c) Experimental and (b, d) simulated results are plotted separately. Reprinted with permission from ref 432. Copyright 2010 American Chemical Society.

identify and quantitate electrosynthetic intermediates and products and thereby construct accurate and detailed mechanisms. Table 5 contains a detailed compilation of the advantages and limitations of each technique described. While each of these methods can provide unique information about the system of interest, oftentimes it is worth employing more than one technique to verify the reaction mechanism. With constantly improving electronics, development of faster, more sensitive instruments will allow detection of intermediates with lifetimes much shorter than nanoseconds and accurate quantitation of species in the nanomolar or even picomolar range. To conclude this discussion, recent advancements of the aforementioned techniques are discussed briefly.

Synthetic methods and analysis tools for electrosynthesis continue to grow rapidly. Recently, pulse and paired electrolysis have been employed more frequently, as these methods allow for replacement of multistep reactions with a one-pot scheme. However, the present pulse electrolysis methods employ symmetrical pulses with millisecond durations. Owing to advances in electronics, use of asymmetric ac or dc pulses with variable amplitudes is possible in addition to pulse times as fast as 1 ns. With this, exceptionally short-lived intermediates can be generated and detected at a desirable rate. However, the capacitance of the double layer must be considered for short pulse times.

In situ multi-SEC is a field capable of benefiting the electrosynthetic community but has not been explored in detail. A recent review described the combined application of different in situ SEC methods, such as EPR, NMR, Raman, and IR.[240] While development of setups that allow for multi-SEC methods is not trivial, there are some that are worth mentioning. Remarkably, Petr et al. developed a cell setup for simultaneous UV−vis−EPR SEC.[438] Similarly, Colina and co-workers created a setup that allows for simultaneous UV−vis and Raman SEC experiments.[439] Construction of multi-SEC setups allows for a larger number of complex electrochemical processes to be investigated as different spectroscopic techniques often provide complementary information about a system. In addition to these tandem methods, higher resolution techniques (from microseconds to femtoseconds) can be extremely beneficial, particularly for reactions involving formation of radicals. In addition, in situ NMR spectroelectrochemistry can provide valuable information regarding accurate reaction dynamics. While the present methods offer 2D NMR analysis with a time domain of milliseconds, faster, multidimensional in situ spectroelectrochemical studies will offer a great contribution to understanding accurate reaction dynamics.

As discussed, scanning probe techniques have been used to study electrosynthetic reactions. In particular, SECM has enabled complex electroorganic reactions to be studied with ease. In a few instances, scanning electrochemical cell microscopy (SECCM) has also been used to measure the lifetimes of short-lived intermediates, analyze various reaction pathways, and estimate the reduction potentials of various electrogenerated intermediates. Electrochemical and ion-trans-

https://doi.org/10.1021/acs.chemrev.1c00471
Chem. Rev. XXXX, XXX, XXX−XXX

Table 5. Advantages and Limitations of Analytical Techniques To Understand Electrosynthetic Mechanisms

Technique		Advantages and Limitations
Electrochemical Methods	CV	• simple and most popular technique for determination of electrochemical activity of analyte including redox potentials, reversibility, and kinetic information • inability to detect short-lived intermediates
	FSCV	• can use highly resistive solvents (UMEs); detection of intermediates with lifetimes on the order of microseconds; able to measure exceptionally large rate constants (as fast as 10^6) • requires ultramicroelectrodes
	Hydrodynamic Voltammetry	• detection of intermediates; measurement of rate constants; thinner diffusion layer • cell design/dimensions critical
	Pulse Voltammetry	• can suppress background current and extract faradaic current, improve detection limits, improve resolution • longer data acquisition time compared to CV
	Thin-Layer Voltammetry	• good for determining kinetics parameters such as α and k_s; can obtain voltammetry at fast scan rates • intricate cell design
Spectroscopic Methods	UV-vis	• simple cell design; good kinetics investigations • lacks structural information
	IR	• provides structural information • water is a major interferant
	Raman	• complimentary to IR; provides structural information • low signal-to-noise ratios
	NMR	• provides structural information • high cost of deuterated solvents; can only detect stable intermediates (lifetime of a few seconds); cannot detect free radicals
	EPR	• can detect radicals • large concentration of radicals (~10^{-6} M) is necessary to generate spectrum • conventional electrodes cannot be utilized • high dielectric solvents can attenuate signal
Chromatographic Techniques	LC	• suitable for analysis of small and large organic compounds • inability to detect short-lived, unstable intermediates
	GC	• advantageous for gaseous and volatile compounds • requires gas-tight cell; not suitable for thermally labile compounds
	MS	• good for reaction monitoring and rapid product identification; aids in structural elucidation, detection of stable intermediates (lifetime > milliseconds); good for mechanistic analysis aided by isotope labeling • instruments are costly; analysis can be convoluted when not combined with chromatography
Microscopy	SECM	• good for surface mapping and kinetic analysis; detection of unstable intermediates (lifetime 0.5–10 μs) • can require more complex/custom instrumentation • construction of small-scale electrodes can be nontrivial
Computational Methods	DFT	• predicts reaction potentials and intermediates; does not require a wavefunction • calculations are dependent on accurate experimental results; inaccurate results lead to imprecise models
	Numerical Methods	• simulate various forms of mass transport; simulate any combination of electrochemical and chemical reactions; simulate CVs • modelling 3D geometries and more complex forms of mass transfer is computationally expensive, decreases accuracy and increases simulation time

fer measurements can be conducted in tandem with SECCM, allowing for more challenging studies to be performed. For example, the kinetics of fast, heterogeneous electron transfer and the interplay between surface topography and charge-transfer rate have been conducted via SECCM.[440] Although similar studies have been reported,[441,442] SECCM has not been utilized in the analysis of electroorganic mechanisms to our knowledge. The lack of activity in this field and the capacity of SECCM to resolve challenging electrochemical studies create significant opportunities for future studies.

AUTHOR INFORMATION

Corresponding Author

R. Daniel Little − *Department of Chemistry, University of California Santa Barbara, Santa Barbara, California 93106, United States;* orcid.org/0000-0001-5836-3814; Email: little@chem.ucsb.edu

Authors

Eric C. R. McKenzie − *Department of Chemistry, Indiana University, Bloomington, Indiana 47405, United States*

Seyyedamirhossein Hosseini − *Department of Chemistry, University of Utah, Salt Lake City, Utah 84112, United States*

Ana G. Couto Petro − *Department of Chemistry, Indiana University, Bloomington, Indiana 47405, United States*

Kelly K. Rudman − *Department of Chemistry, Indiana University, Bloomington, Indiana 47405, United States*

Benjamin H. R. Gerroll − *Department of Chemistry, Indiana University, Bloomington, Indiana 47405, United States*

Mohammad S. Mubarak − *Department of Chemistry, The University of Jordan, Amman 11942, Jordan;* orcid.org/0000-0002-9782-0835

https://doi.org/10.1021/acs.chemrev.1c00471
Chem. Rev. XXXX, XXX, XXX−XXX

Lane A. Baker − *Department of Chemistry, Indiana University, Bloomington, Indiana 47405, United States;* orcid.org/0000-0001-5127-507X

Complete contact information is available at: https://pubs.acs.org/10.1021/acs.chemrev.1c00471

Author Contributions

[§]E.C.R.M. and S.H.: First authors

Notes

The authors declare no competing financial interest.

Biographies

Eric C. R. McKenzie is a Ph.D. candidate in the Jacobson research group at Indiana University. He received his B.S. degree in Chemistry and B.A. degree in Modern European History from the University of North Carolina at Chapel Hill in 2016. His undergraduate research involved construction of dye-sensitized photoelectrochemical cells in the laboratory of Professor Thomas J. Meyer. His present research involves mechanistic organic electrochemistry with focus on catalytic reduction of halogenated phenols.

Seyyedamirhossein Hosseini is a postdoctoral research fellow at the Center for Synthetic Organic Electrochemistry (CSOE) at the University of Utah. He received his Ph.D. degree in Analytical Chemistry at Indiana University under the tutelage of Professor Dennis G. Peters. His research in Professor Henry White's research group is focused on electrosynthesis of small molecules and use of analytical and electroanalytical methods to define the elementary steps of a reaction cycle during an electrosynthetic reaction.

Ana G. Couto Petro earned her B.S. degree in Chemistry at University of Indianapolis in 2016. She recently completed her Ph.D. degree in Analytical Chemistry at Indiana University (2021). Her doctoral studies focused on the electrochemistry of halophenylacetamides to elucidate a reduction mechanism for this class of compounds which aids in the development of remediation strategies, particularly of chlorophenylacetamide herbicides.

Kelly K. Rudman is a Ph.D. candidate in the Skrabalak research group at Indiana University. She received her B.Sc. degree in Chemistry with a specialization in Material Science from the University of Virginia in 2017 and conducted research for Gary Koenig and Charles W. Machan. Her present research focuses on the electrosynthesis of metallic nanoparticles.

Benjamin H. R. Gerroll is a Ph.D. candidate in the Baker research group at Indiana University. He received with his B.S. degree in Biology in 2012 from Indiana University. Afterward, he worked in the Peters research group before beginning his graduate studies in 2015. In the Peters research group, his research involves mechanistic organic electrochemistry with an emphasis on cathodic remediation of persistent organic pollutants. Presently, his research is centered on mechanistic electrochemistry with a focus on heterogeneous and homogeneous catalysis.

Mohammad S. Mubarak received his B.Sc. and M.Sc. degrees in Chemistry from the University of Jordan in 1976 and 1978, respectively, and obtained his Ph.D. degree from Indiana University, Bloomington, in 1982. He did postdoctoral work at the University of Oklahoma between October 1982 and August 1983. He currently holds the rank of Professor at the University of Jordan and Adjunct Professor of Chemistry at Indiana University. His research focuses on electrochemistry, synthetic organic chemistry (especially the synthesis of compounds with expected biological activity), medicinal chemistry, and drug design and discovery.

Lane A. Baker is a Professor of Chemistry at Indiana University and presently holds a James F. Jackson Chair. He received his B.S. degree in Chemistry from Missouri State University and his Ph.D. degree in chemistry at Texas A&M University, followed by postdoctoral appointments at the Naval Research Laboratory and the University of Florida. He has been at Indiana University since 2006, where his group has focused on the development of instruments and applications related to nanoscale electrochemistry.

R. Daniel Little (Dan) received his B.S. degree in Chemistry and Mathematics from the University of Wisconsin, Superior, and Ph.D. degree in Chemistry from the University of Wisconsin under the tutelage of Howard Zimmerman. He carried out postdoctoral studies with Jerome Berson at Yale. He currently holds the position of Distinguished Research Professor at the University of California, Santa Barbara (UCSB).

ACKNOWLEDGMENTS

This review is dedicated to the memory of our beloved colleague, mentor, and friend, Professor Dennis G. Peters. The authors acknowledge Krista M. Kulesa for helpful guidance and insight on inorganic electrochemistry. Support from the Department of Chemistry at Indiana University and the National Science Foundation (CHE-1808133) are also acknowledged. In addition, the authors are exceptionally grateful to the profound research that has been described in this review.

REFERENCES

(1) Minteer, S. D.; Baran, P. Electrifying Synthesis: Recent Advances in the Methods, Materials, and Techniques for Organic Electrosynthesis. *Acc. Chem. Res.* **2020**, *53*, 545−546.
(2) Buriez, O. The Strong Potential of Organic and Molecular Electrochemistry. *Curr. Opin. Electrochem.* **2020**, *24*, A1−A3.
(3) Francke, R.; Little, R. D.; Inagi, S. Organic Electrosynthesis. *ChemElectroChem* **2019**, *6*, 4065−4066.
(4) Schäfer, H. J. Contributions of Organic Electrosynthesis to Green Chemistry. *C. R. Chim.* **2011**, *14*, 745−765.
(5) Frontana-Uribe, B. A.; Little, R. D.; Ibanez, J. G.; Palma, A.; Vasquez-Medrano, R. Organic Electrosynthesis: A Promising Green Methodology in Organic Chemistry. *Green Chem.* **2010**, *12*, 2099−2119.
(6) Yoshida, J.-I.; Suga, S.; Suzuki, S.; Kinomura, N.; Yamamoto, A.; Fujiwara, K. Direct Oxidative Carbon-Carbon Bond Formation Using the "Cation Pool" Method. 1. Generation of Iminium Cation Pools and Their Reaction with Carbon Nucleophiles. *J. Am. Chem. Soc.* **1999**, *121*, 9546−9549.
(7) Kirste, A.; Elsler, B.; Schnakenburg, G.; Waldvogel, S. R. Efficient Anodic and Direct Phenol-Arene C,C Cross-Coupling: The Benign Role of Water or Methanol. *J. Am. Chem. Soc.* **2012**, *134*, 3571−3576.
(8) Hu, P.; Peters, B. K.; Malapit, C. A.; Vantourout, J. C.; Wang, P.; Li, J.; Mele, L.; Echeverria, P.-G.; Minteer, S. D.; Baran, P. S. Electroreductive Olefin−Ketone Coupling. *J. Am. Chem. Soc.* **2020**, *142*, 20979−20986.
(9) Truesdell, B. L.; Hamby, T. B.; Sevov, C. S. General $C(sp^2)$−$C(sp^3)$ Cross-Electrophile Coupling Reactions Enabled by Overcharge Protection of Homogeneous Electrocatalysts. *J. Am. Chem. Soc.* **2020**, *142*, 5884−5893.
(10) Sauermann, N.; Meyer, T. H.; Qiu, Y.; Ackermann, L. Electrocatalytic C−H Activation. *ACS Catal.* **2018**, *8*, 7086−7103.
(11) Ackermann, L. Metalla-Electrocatalyzed C−H Activation by Earth-Abundant 3d Metals and Beyond. *Acc. Chem. Res.* **2020**, *53*, 84−104.
(12) Sauermann, N.; Meyer, T. H.; Tian, C.; Ackermann, L. Electrochemical Cobalt-Catalyzed C−H Oxygenation at Room Temperature. *J. Am. Chem. Soc.* **2017**, *139*, 18452−18455.

(13) Jiao, K.-J.; Xing, Y.-K.; Yang, Q.-L.; Qiu, H.; Mei, T.-S. Site-Selective C−H Functionalization via Synergistic Use of Electrochemistry and Transition Metal Catalysis. *Acc. Chem. Res.* **2020**, *53*, 300−310.
(14) Kang, L.-S.; Luo, M.-H.; Lam, C. M.; Hu, L.-M.; Little, R. D.; Zeng, C.-C. Electrochemical C−H Functionalization and Subsequent C−S and C−N Bond Formation: Paired Electrosynthesis of 3−Amino−2−Thiocyanato−α, β−Unsaturated Carbonyl Derivatives Mediated by Bromide Ions. *Green Chem.* **2016**, *18*, 3767−3774.
(15) Yamamoto, K.; Kuriyama, M.; Onomura, O. Anodic Oxidation for the Stereoselective Synthesis of Heterocycles. *Acc. Chem. Res.* **2020**, *53*, 105−120.
(16) Jiang, Y.; Xu, K.; Zeng, C. Use of Electrochemistry in the Synthesis of Heterocyclic Structures. *Chem. Rev.* **2018**, *118*, 4485−4540.
(17) Yan, M.; Kawamata, Y.; Baran, P. S. Synthetic Organic Electrochemical Methods Since 2000: On the Verge of a Renaissance. *Chem. Rev.* **2017**, *117*, 13230−13319.
(18) Shatskiy, A.; Lundberg, H.; Kärkäs, M. D. Organic Electrosynthesis: Applications in Complex Molecule Synthesis. *ChemElectroChem* **2019**, *6*, 4067−4092.
(19) Moeller, K. D. Using Physical Organic Chemistry to Shape the Course of Electrochemical Reactions. *Chem. Rev.* **2018**, *118*, 4817−4833.
(20) Pollok, D.; Waldvogel, S. R. Electro-Organic Synthesis−A 21st Century Technique. *Chem. Sci.* **2020**, *11*, 12386−12400.
(21) Sandford, C.; Edwards, M. A.; Klunder, K. J.; Hickey, D. P.; Li, M.; Barman, K.; Sigman, M. S.; White, H. S.; Minteer, S. D. A Synthetic Chemist's Guide to Electroanalytical Tools for Studying Reaction Mechanisms. *Chem. Sci.* **2019**, *10*, 6404−6422.
(22) Costentin, C.; Savéant, J.-M. Concepts and Tools for Mechanism and Selectivity Analysis in Synthetic Organic Electrochemistry. *Proc. Natl. Acad. Sci. U. S. A.* **2019**, *116*, 11147−11152.
(23) Nguyen, B. H.; Perkins, R. J.; Smith, J. A.; Moeller, K. D. Photovoltaic-Driven Electrosynthesis and Efforts Toward More Sustainable Oxidation Reactions. *Beilstein J. Org. Chem.* **2015**, *11*, 280−287.
(24) Lohrengel, M. Galvanostat; Potentiostat. In *Encyclopedia of Applied Electrochemistry*; Kreysa, G., Ota, K.-i., Savinell, R. F., Eds.; Springer: New York, 2014; pp 925−927, 1697−1702.
(25) McKubre, M. C.; MacDonald, D. D. Electronic Instrumentation for Electrochemical Studies. In *Comprehensive Treatise of Electrochemistry*; White, R. E., Bockris, J. O'M., Conway, B. E., Yeager, E., Eds.; Plenum: New York, 1984; Vol. *8*, pp 1−98.
(26) Colburn, A. W.; Levey, K. J.; O'Hare, D.; Macpherson, J. V. Lifting the Lid on the Potentiostat: A Beginner's Guide to Understanding Electrochemical Circuitry and Practical Operation. *Phys. Chem. Chem. Phys.* **2021**, *23*, 8100−8117.
(27) Glasscott, M. W.; Verber, M. D.; Hall, J. R.; Pendergast, A. D.; McKinney, C. J.; Dick, J. E. SweepStat: A Build-It-Yourself, Two-Electrode Potentiostat for Macroelectrode and Ultramicroelectrode Studies. *J. Chem. Educ.* **2020**, *97*, 265−270.
(28) Gopinath, A. V.; Russell, D. An Inexpensive Field-Portable Programmable Potentiostat. *Chem. Educ.* **2006**, *11*, 23−28.
(29) Meloni, G. N. Building a Microcontroller Based Potentiostat: A Inexpensive and Versatile Platform for Teaching Electrochemistry and Instrumentation. *J. Chem. Educ.* **2016**, *93*, 1320−1322.
(30) Couper, A. M.; Pletcher, D.; Walsh, F. C. Electrode Materials for Electrosynthesis. *Chem. Rev.* **1990**, *90*, 837−865.
(31) Heard, D. M.; Lennox, A. J. J. Electrode Materials in Modern Organic Electrochemistry. *Angew. Chem., Int. Ed.* **2020**, *59*, 18866−18884.
(32) *Laboratory Techniques in Electroanaytical. Chemistry.*, 2nd ed.; Kissinger, P. T.; Heineman, W. R., Eds.; Marcel Dekker, Inc.: New York, 1996.
(33) Pathirathna, P.; Balla, R. J.; Amemiya, S. Simulation of Fast-Scan Nanogap Voltammetry at Double-Cylinder Ultramicroelectrodes. *J. Electrochem. Soc.* **2018**, *165*, G3026−G3032.
(34) Andrieux, C. P.; Garreau, D.; Hapiot, P.; Pinson, J.; Savéant, J.-M. Fast Sweep Cyclic Voltammetry at Ultra-Microelectrodes: Evaluation of the Method for Fast Electron-Transfer Kinetic Measurements. *J. Electroanal. Chem. Interfacial Electrochem.* **1988**, *243*, 321−335.
(35) Wipf, D. O.; Kristensen, E. W.; Deakin, M. R.; Wightman, R. M. Fast-Scan Cyclic Voltammetry as a Method to Measure Rapid Heterogeneous Electron-Transfer Kinetics. *Anal. Chem.* **1988**, *60*, 306−310.
(36) Wipf, D. O.; Wightman, R. M. Submicrosecond Measurements with Cyclic Voltammetry. *Anal. Chem.* **1988**, *60*, 2460−2464.
(37) Tomiyasu, H.; Shikata, H.; Takao, K.; Asanuma, N.; Taruta, S.; Park, Y.-Y. An Aqueous Electrolyte of the Widest Potential Window and Its Superior Capability for Capacitors. *Sci. Rep.* **2017**, *7*, 45048.
(38) Coustan, L.; Bélanger, D. Electrochemical Activity of Platinum, Gold and Glassy Carbon Electrodes in Water-in-Salt Electrolyte. *J. Electroanal. Chem.* **2019**, *854*, 113538.
(39) Coustan, L.; Shul, G.; Bélanger, D. Electrochemical Behavior of Platinum, Gold and Glassy Carbon Electrodes in Water-in-Salt Electrolyte. *Electrochem. Commun.* **2017**, *77*, 89−92.
(40) *Electroanalytical Methods:Guide to Experiments and Applications*, 2nd ed.; Scholz, F., Ed.; Springer: New York, 2010.
(41) Cowlard, F. C.; Lewis, J. C. Vitreous carbon—A New Form of Carbon. *J. Mater. Sci.* **1967**, *2*, 507−512.
(42) Friedrich, J. M.; Ponce-de-León, C.; Reade, G. W.; Walsh, F. C. Reticulated Vitreous Carbon as an Electrode Material. *J. Electroanal. Chem.* **2004**, *561*, 203−217.
(43) Wang, J. Reticulated Vitreous Carbon—A New Versatile Electrode Material. *Electrochim. Acta* **1981**, *26*, 1721−1726.
(44) Carta, R.; Palmas, S.; Polcaro, A.; Tola, G. Behaviour of a Carbon Felt Flow by Electrodes Part I: Mass Transfer Characteristics. *J. Appl. Electrochem.* **1991**, *21*, 793−798.
(45) Oren, Y.; Soffer, A. Graphite Felt as an Efficient Porous Electrode for Impurity Removal and Recovery of Metals. *Electrochim. Acta* **1983**, *28*, 1649−1654.
(46) Lim, Y.; Chu, J. H.; Lee, D. H.; Kwon, S.-Y.; Shin, H. Increase in Graphitization and Electrical Conductivity of Glassy Carbon Nanowires by Rapid Thermal Annealing. *J. Alloys Compd.* **2017**, *702*, 465−471.
(47) Velický, M.; Toth, P. S.; Woods, C. R.; Novoselov, K. S.; Dryfe, R. A. Electrochemistry of the Basal Plane versus Edge Plane of Graphite Revisited. *J. Phys. Chem. C* **2019**, *123*, 11677−11685.
(48) Kinoshita, K. *Carbon: Electrochemical and Physicochemical Properties*; Wiley: New York, 1988.
(49) Martínez-Huitle, C. A.; Waldvogel, S. R. Trends of Organic Electrosynthesis by Using Boron-Doped Diamond Electrodes. In *Novel Aspects of Diamond From Growth to Applications*; Yang, N., Ed.; Springer: Cham, Switzerland, 2019; pp 173−197.
(50) Lips, S.; Waldvogel, S. R. Use of Boron-Doped Diamond Electrodes in Electro-Organic Synthesis. *ChemElectroChem* **2019**, *6*, 1649−1660.
(51) Cobb, S. J.; Ayres, Z. J.; Macpherson, J. V. Boron Doped Diamond: A Designer Electrode Material for the Twenty-First Century. *Annu. Rev. Anal. Chem.* **2018**, *11*, 463−484.
(52) Muzyka, K.; Sun, J.; Fereja, T. H.; Lan, Y.; Zhang, W.; Xu, G. Boron-Doped Diamond: Current Progress and Challenges in View of Electroanalytical Applications. *Anal. Methods* **2019**, *11*, 397−414.
(53) Ullah, M.; Ahmed, E.; Hussain, F.; Rana, A. M.; Raza, R. Electrical Conductivity Enhancement by Boron-Doping in Diamond Using First Principle Calculations. *Appl. Surf. Sci.* **2015**, *334*, 40−44.
(54) Yang, N.; Yu, S.; Macpherson, J. V.; Einaga, Y.; Zhao, H.; Zhao, G.; Swain, G. M.; Jiang, X. Conductive Diamond: Synthesis, Properties, and Electrochemical Applications. *Chem. Soc. Rev.* **2019**, *48*, 157−204.
(55) Yang, N.; Hees, J.; Nebel, C. E. Diamond Ultamicro- and Nano-electrode Arrays. In *Novel Aspects of Diamond*; Yang, N., Ed. Springer: Cham, Switzerland, 2015; pp 273−293.
(56) Katsuki, N.; Takahashi, E.; Toyoda, M.; Kurosu, T.; Iida, M.; Wakita, S.; Nishiki, Y.; Shimamune, T. Water Electrolysis Using

https://doi.org/10.1021/acs.chemrev.1c00471
Chem. Rev. XXXX, XXX, XXX−XXX

Diamond Thin-Film Electrodes. *J. Electrochem. Soc.* **1998**, *145*, 2358−2362.
(57) Martin, H. B.; Argoitia, A.; Landau, U.; Anderson, A. B.; Angus, J. C. Hydrogen and Oxygen Evolution on Boron-Doped Diamond Electrodes. *J. Electrochem. Soc.* **1996**, *143*, L133−L136.
(58) Santana, M. H. P.; De Faria, L. A.; Boodts, J. F. C. Electrochemical Characterisation and Oxygen Evolution at a Heavily Boron Doped Diamond Electrode. *Electrochim. Acta* **2005**, *50*, 2017−2027.
(59) Turygin, V. V.; Tomilov, A. P. Possible Trends in the Development of Applied Electrochemical Synthesis of Organic Compounds (Review). *Russ. J. Electrochem.* **2015**, *51*, 999−1020.
(60) Yi, Y.; Weinberg, G.; Prenzel, M.; Greiner, M.; Heumann, S.; Becker, S.; Schlögl, R. Electrochemical Corrosion of a Glassy Carbon Electrode. *Catal. Today* **2017**, *295*, 32−40.
(61) McCreery, R. L. Advanced Carbon Electrode Materials for Molecular Electrochemistry. *Chem. Rev.* **2008**, *108*, 2646−2687.
(62) Swain, G. Solid Electrode Materials. In *Handbook of Electrochemistry*; Zoski, C. G., Ed. Elsevier: Oxford, U.K., 2006; pp 111−153.
(63) Stamenkovic, V. R.; Mun, B. S.; Arenz, M.; Mayrhofer, K. J. J.; Lucas, C. A.; Wang, G.; Ross, P. N.; Markovic, N. M. Trends in Electrocatalysis on Extended and Nanoscale Pt-Bimetallic Alloy Surfaces. *Nat. Mater.* **2007**, *6*, 241−247.
(64) Karthik, P. E.; Alessandri, I.; Sengeni, A. Review—A Review on Electrodes Used in Electroorganic Synthesis and the Significance of Coupled Electrocatalytic Reactions. *J. Electrochem. Soc.* **2020**, *167*, 125503.
(65) Lamy, C. Electrocatalytic Oxidation of Organic Compounds on Noble Metals in Aqueous Solution. *Electrochim. Acta* **1984**, *29*, 1581−1588.
(66) Barek, J.; Zima, J. Eighty Years of Polarography − History and Future. *Electroanalysis* **2003**, *15*, 467−472.
(67) Kyriacou, D. *Modern Electroorganic Chemistry*; Springer: Berlin, Germany, 1994.
(68) Batanero, B.; Pérez, M. J.; Barba, F. Electrosynthesis of 3-Chloro-4-Substituted Coumarins. *J. Electroanal. Chem.* **1999**, *469*, 201−205.
(69) Claus, H.; Schäfer, H. J. 3,3-Dichlorotetrahydrofurans by Reductive Addition of 3-Bromo 1,1,1-Trichloroalkanes to Carbonyl Compounds. *Tetrahedron Lett.* **1985**, *26*, 4899−4902.
(70) Anderson, J. D.; Baizer, M. M.; Petrovich, J. P. Electrolytic Reductive Coupling. XIII. Intramolecular Reductive Coupling. Electrohydrocyclization. *J. Org. Chem.* **1966**, *31*, 3890−3897.
(71) Little, R. D.; Fox, D. P.; Van Hijfte, L.; Dannecker, R.; Sowell, G.; Wolin, R. L.; Moens, L.; Baizer, M. M. Electroreductive Cyclization. Ketones and Aldehydes Tethered to α,β-Unsaturated Esters (Nitriles). Fundamental Investigations. *J. Org. Chem.* **1988**, *53*, 2287−2294.
(72) Rabjohn, N.; Flasch, G. W., Jr. Kolbe Electrosynthesis of Alkanes with Multiple Quaternary Carbon Atoms. *J. Org. Chem.* **1981**, *46*, 4082−4083.
(73) *Organic Electrochemistry: Revised and Expanded*, 5th ed.; Hammerich, O., Speiser, B., Eds.; CRC Press: Boca Raton, FL, 2015.
(74) Borrill, A. J.; Reily, N. E.; Macpherson, J. V. Addressing the Practicalities of Anodic Stripping Voltammetry for Heavy Metal Detection: A Tutorial Review. *Analyst* **2019**, *144*, 6834−6849.
(75) Economou, A.; Fielden, P. R. Applications, Potentialities and Limitations of Adsorptive Stripping Analysis on Mercury Film Electrodes. *TrAC, Trends Anal. Chem.* **1997**, *16*, 286−292.
(76) Ariño, C.; Serrano, N.; Díaz-Cruz, J. M.; Esteban, M. Voltammetric Determination of Metal Ions Beyond Mercury Electrodes. A Review. *Anal. Chim. Acta* **2017**, *990*, 11−53.
(77) Mikkelsen, Ø.; Schrøder, K. H. Amalgam Electrodes for Electroanalysis. *Electroanalysis* **2003**, *15*, 679−687.
(78) Isse, A. A.; Falciola, L.; Mussini, P. R.; Gennaro, A. Relevance of Electron Transfer Mechanism in Electrocatalysis: The Reduction of Organic Halides at Silver Electrodes. *Chem. Commun.* **2006**, 344−346.
(79) Shain, I.; Perone, S. P. Application of Stripping Analysis to the Determination of Iodide with Silver Microelectrodes. *Anal. Chem.* **1961**, *33*, 325−329.
(80) Murray, R. W. Chemically Modified Electrodes for Electrocatalysis. *Philos. Trans. R. Soc. A* **1981**, *302*, 253−265.
(81) Murray, R. W. Chemically Modified Electrodes. *Acc. Chem. Res.* **1980**, *13*, 135−141.
(82) Ata, M. S.; Poon, R.; Syed, A. M.; Milne, J.; Zhitomirsky, I. New Developments in Non-Covalent Surface Modification, Dispersion and Electrophoretic Deposition of Carbon Nanotubes. *Carbon* **2018**, *130*, 584−598.
(83) Murray, R. W. Chemically Modified Electrodes. In *Electroanalytical Chemistry*; Bard, A. J., Ed.; Marcel Dekker: New York, 1984; Vol. *13*.
(84) Snell, K. D.; Keenan, A. G. Surface Modified Electrodes. *Chem. Soc. Rev.* **1979**, *8*, 259−282.
(85) Zen, J.-M.; Senthil Kumar, A.; Tsai, D.-M. Recent Updates of Chemically Modified Electrodes in Analytical Chemistry. *Electroanalysis* **2003**, *15*, 1073−1087.
(86) Gütz, C.; Selt, M.; Bänziger, M.; Bucher, C.; Römelt, C.; Hecken, N.; Gallou, F.; Galvão, T. R.; Waldvogel, S. R. A Novel Cathode Material for Cathodic Dehalogenation of 1,1-Dibromo Cyclopropane Derivatives. *Chem. Eur. J.* **2015**, *21*, 13878−13882.
(87) Murray, R. W.; Ewing, A. G.; Durst, R. A. Chemically Modified Electrodes Molecular Design for Electroanalysis. *Anal. Chem.* **1987**, *59*, 379A−390A.
(88) Das, A.; Stahl, S. S. Noncovalent Immobilization of Molecular Electrocatalysts for Chemical Synthesis: Efficient Electrochemical Alcohol Oxidation with a Pyrene−TEMPO Conjugate. *Angew. Chem., Int. Ed.* **2017**, *56*, 8892−8897.
(89) Wattanakit, C. Chiral Metals as Electrodes. *Curr. Opin. Electrochem.* **2018**, *7*, 54−60.
(90) Ghosh, M.; Shinde, V. S.; Rueping, M. A Review of Asymmetric Synthetic Organic Electrochemistry and Electrocatalysis: Concepts, Applications, Recent Developments and Future Directions. *Beilstein J. Org. Chem.* **2019**, *15*, 2710−2746.
(91) Bard, A. J.; Faulkner, L. F. *Electrochemical Methods: Fundamentals and Applications*, 2nd ed.; Wiley, 2001.
(92) Dincan, E.; Sibille, S.; Perichon, J.; Moingeon, M.-O.; Chaussard, J. Electrosynthesis of Ketones from Organic Halides and Anhydrides. *Tetrahedron Lett.* **1986**, *27*, 4175−4176.
(93) Saboureau, C.; Troupel, M.; Périchon, J. Organic electrosynthesis with a sacrificial anode. Chemical reductive degradation of the solvent N,N−dimethyl formamide. *J. Appl. Electrochem.* **1990**, *20*, 97−101.
(94) Sibille, S.; d'Incan, E.; Leport, L.; Périchon, J. Electrosynthesis of Alcohols from Organic Halides and Ketones or Aldehydes. *Tetrahedron Lett.* **1986**, *27*, 3129−3132.
(95) Sock, O.; Troupel, M.; Périchon, J. Electrosynthesis of Carboxylic Acids from Organic Halides and Carbon Dioxide. *Tetrahedron Lett.* **1985**, *26*, 1509−1512.
(96) Shimakoshi, H.; Luo, Z.; Inaba, T.; Hisaeda, Y. Electrolysis of Trichloromethylated Organic Compounds Under Aerobic Conditions Catalyzed by the B_{12} Model Complex for Ester and Amide Formation. *Dalton Trans.* **2016**, *45*, 10173−10180.
(97) Chaussard, J.; Folest, J.-C.; Nedelec, J.-Y.; Périchon, J.; Sibille, S.; Troupel, M. Use of Sacrificial Anodes in Electrochemical Functionalization of Organic Halides. *Synthesis* **1990**, *1990*, 369−381.
(98) Ishifune, M.; Yamashita, H.; Kera, Y.; Yamashita, N.; Hirata, K.; Murase, H.; Kashimura, S. Electroreduction of Aromatics Using Magnesium Electrodes in Aprotic Solvents Containing Alcoholic Proton Donors. *Electrochim. Acta* **2003**, *48*, 2405−2409.
(99) Kashimura, S.; Yamashita, H.; Murai, Y.; Kera, Y.; Yamashita, N.; Murase, H.; Ishifune, M. Magnesium and Lanthanide Ions Promoted Electrochemical Coupling of Aliphatic Esters and Tetrahydrofuran for the Synthesis of Acetals. *Electrochim. Acta* **2002**, *48*, 7−10.

https://doi.org/10.1021/acs.chemrev.1c00471
Chem. Rev. XXXX, XXX, XXX−XXX

(100) Manabe, S.; Wong, C. M.; Sevov, C. S. Direct and Scalable Electroreduction of Triphenylphosphine Oxide to Triphenylphosphine. *J. Am. Chem. Soc.* **2020**, *142*, 3024−3031.
(101) Sherbo, R. S.; Delima, R. S.; Chiykowski, V. A.; MacLeod, B. P.; Berlinguette, C. P. Complete Electron Economy by Pairing Electrolysis with Hydrogenation. *Nat. Catal.* **2018**, *1*, 501−507.
(102) Llorente, M. J.; Nguyen, B. H.; Kubiak, C. P.; Moeller, K. D. Paired Electrolysis in the Simultaneous Production of Synthetic Intermediates and Substrates. *J. Am. Chem. Soc.* **2016**, *138*, 15110−15113.
(103) Wu, T.; Moeller, K. D. Organic Electrochemistry: Expanding the Scope of Paired Reactions. *Angew. Chem., Int. Ed.* **2021**, *60*, 12883−12890.
(104) Martínez, N. P.; Isaacs, M.; Nanda, K. K. Paired Electrolysis for Simultaneous Generation of Synthetic Fuels and Chemicals. *New J. Chem.* **2020**, *44*, 5617−5637.
(105) Hamann, C. H.; Hamnett, A.; Vielstich, W. *Electrochemistry*, 2nd ed.; Wiley: Weinheim, Germany, 2007.
(106) Jerkiewicz, G. Standard and Reversible Hydrogen Electrodes: Theory, Design, Operation, and Applications. *ACS Catal.* **2020**, *10*, 8409−8417.
(107) Safari, S.; Selvaganapathy, P. R.; Derardja, A.; Deen, M. J. Electrochemical Growth of High-Aspect Ratio Nanostructured Silver Chloride on Silver and Its Application to Miniaturized Reference Electrodes. *Nanotechnology* **2011**, *22*, 315601.
(108) Pavlishchuk, V. V.; Addison, A. W. Conversion Constants for Redox Potentials Measured Versus Difference Reference Electrodes in Acetonitrile Solutions at 25 °C. *Inorg. Chim. Acta* **2000**, *298*, 97−102.
(109) Larson, R. C.; Iwamoto, R. T.; Adams, R. N. Reference Electrodes for Voltammetry in Acetonitrile. *Anal. Chim. Acta* **1961**, *25*, 371−374.
(110) Izutsu, K.; Ito, M.; Sarai, E. Silver−Silver Cryptate(2,2) Ion Electrode as a Reference Electrode in Nonaqueous Solvents. *Anal. Sci.* **1985**, *1*, 341−344.
(111) Izutsu, K. *Electrochemistry in Nonaqueous Solutions*, 2nd ed.; Wiley: Weinheim, Germany, 2009.
(112) Hall, J. L.; Jennings, P. W. Modification of the Preparation of a Cadmium Amalgam Reference Electrode for Use in *N,N*-dimethylformamide. *Anal. Chem.* **1976**, *48*, 2026−2027.
(113) Bentley, C. L.; Perry, D.; Unwin, P. R. Stability and Placement of Ag/AgCl Quasi-Reference Counter Electrodes in Confined Electrochemical Cells. *Anal. Chem.* **2018**, *90*, 7700−7707.
(114) Gagne, R. R.; Koval, C. A.; Lisensky, G. C. Ferrocene as an Internal Standard for Electrochemical Measurements. *Inorg. Chem.* **1980**, *19*, 2854−2855.
(115) Hilt, G. Basic Strategies and Types of Applications in Organic Electrochemistry. *ChemElectroChem* **2020**, *7*, 395−405.
(116) Elgrishi, N.; Rountree, K. J.; McCarthy, B. D.; Rountree, E. S.; Eisenhart, T. T.; Dempsey, J. L. A Practical Beginner's Guide to Cyclic Voltammetry. *J. Chem. Educ.* **2018**, *95*, 197−206.
(117) Mann, C. K. Nonaqueous Solvents for Electrochemical Use. In *Electroanalytical Chemistry*; Bard, A. J., Ed.; Marcel Dekker: New York, 1969; Vol. *3*.
(118) Peters, B. K.; Rodriguez, K. X.; Reisberg, S. H.; Beil, S. B.; Hickey, D. P.; Kawamata, Y.; Collins, M.; Starr, J.; Chen, L.; Udyavara, S.; et al. Scalable and safe synthetic organic electroreduction inspired by Li-ion battery chemistry. *Science* **2019**, *363*, 838−845.
(119) Dahm, C. E.; Peters, D. G. Electrochemical Reduction of Tetraalkylammonium Tetrafluoroborates at Carbon Cathodes in Dimethylformamide. *J. Electroanal. Chem.* **1996**, *402*, 91−96.
(120) Fuchigami, T.; Arobe, M.; Inagi, S. New Methodology of Organic Electrochemical Synthesis. In *Fundamentals and Applications of Organic Electrochemistry: Synthesis, Materials, Devices*, 1st ed.; Wiley: West Sussex, U.K., 2015; pp 129−186.
(121) Schulz, L.; Waldvogel, S. R. Solvent Control in Electro-Organic Synthesis. *Synlett* **2019**, *30*, 275−286.
(122) Harvey, D. Analytical Chemisty 2.0—An Open-Access Digital Textbook. *Anal. Bioanal. Chem.* **2011**, *399*, 149−152.
(123) Kimura, K.; Horie, S.; Minato, I.; Odaira, Y. Small Ring Compouds. IV. Anodic Oxidation of Carbethoxycyclopropanecarboxylic Acids. *Chem. Lett.* **1973**, *2*, 1209−1212.
(124) Pletcher, D.; Green, R. A.; Brown, R. C. D. Flow Electrolysis Cells for the Synthetic Organic Chemistry Laboratory. *Chem. Rev.* **2018**, *118*, 4573−4591.
(125) Noël, T.; Cao, Y.; Laudadio, G. The Fundamentals Behind the Use of Flow Reactors in Electrochemistry. *Acc. Chem. Res.* **2019**, *52*, 2858−2869.
(126) Möhle, S.; Zirbes, M.; Rodrigo, E.; Gieshoff, T.; Wiebe, A.; Waldvogel, S. R. Modern Electrochemical Aspects for the Synthesis of Value-Added Organic Products. *Angew. Chem., Int. Ed.* **2018**, *57*, 6018−6041.
(127) Mitsudo, K.; Kurimoto, Y.; Yoshioka, K.; Suga, S. Miniaturization and Combinatorial Approach in Organic Electrochemistry. *Chem. Rev.* **2018**, *118*, 5985−5999.
(128) Pletcher, D. Electrolysis Cells for Laboratory Organic Synthesis. *Curr. Opin. Electrochem.* **2020**, *24*, 1−5.
(129) Gütz, C.; Stenglein, A.; Waldvogel, S. R. Highly Modular Flow Cell for Electroorganic Synthesis. *Org. Process Res. Dev.* **2017**, *21*, 771−778.
(130) Blanco, D. E.; Prasad, P. A.; Dunningan, K.; Modestino, M. A. Insights into membrane−separated organic electrosynthesis: the case of adiponitrile electrochemical production. *React. Chem. Eng.* **2020**, *5*, 136−144.
(131) Martin, E. T.; McGuire, C. M.; Mubarak, M. S.; Peters, D. G. Electroreductive Remediation of Halogenated Environmental Pollutants. *Chem. Rev.* **2016**, *116*, 15198−15234.
(132) Newman, J. S.; Thomas-Alyea, K. E. *Electrochemical Systems*, 3rd ed.; Wiley: Hoboken, NJ, 2004.
(133) *The Faraday Cage: What Is It? How Does It Work?* Technical Note for Gamry Instruments; Gamry Instruments: Warminster, PA, Dec 2010.
(134) *Organic Electrochemistry*; 4th ed.; Lund, H., Hammerich, O., Eds.; Marcel Dekker: New York, 2001.
(135) Peterson, B. M.; Lin, S.; Fors, B. P. Electrochemically Controlled Cationic Polymerization of Vinyl Ethers. *J. Am. Chem. Soc.* **2018**, *140*, 2076−2079.
(136) Marken, F.; Cresswell, A. J.; Bull, S. D. Recent Advances in Paired Electrosynthesis. *Chem. Rec.* **2021**, *21*, 2585−2600.
(137) Zhang, W.; Hong, N.; Song, L.; Fu, N. Reaching the Full Potential of Electroorganic Syntheis by Paired Electrolysis. *Chem. Rec.* **2021**, *21*, 2574−2584.
(138) Nguyen, B. H.; Perkins, R. J.; Smith, J. A.; Moeller, K. D. Solvolysis, Electrochemistry, and Development of Synthetic Building Blocks from Sawdust. *J. Org. Chem.* **2015**, *80*, 11953−11962.
(139) Rensing, D. T.; Nguyen, B. H.; Moeller, K. D. Considering Organic Mechanisms and the Optimization of Current Flow in an Electrochemical Oxidative Condensation Reaction. *Org. Chem. Front.* **2016**, *3*, 1236−1240.
(140) Wu, T.; Nguyen, B. H.; Daugherty, M. C.; Moeller, K. D. Paired Electrochemical Reactions and the On-Site Generation of a Chemical Reagent. *Angew. Chem.* **2019**, *131*, 3600−3603.
(141) Strehl, J.; Abraham, M. L.; Hilt, G. Linear Paired Electrolysis—Realizing 200% Current Efficiency for Stoichiometric Transformations—The Electrochemical Bromination of Alkenes. *Angew. Chem., Int. Ed.* **2021**, *60*, 9996−10000.
(142) Li, W.; Nonaka, T. Development of a Cathodic Oxidation System and Its Application to Paired Electrosynthesis of Sulfones and Nitrones. *J. Electrochem. Soc.* **1999**, *146*, 592−599.
(143) Rodrigo, S.; Um, C.; Mixdorf, J. C.; Gunasekera, D.; Nguyen, H. M.; Luo, L. Alternating Current Electrolysis for Organic Electrosynthesis: Trifluoromethylation of (Hetero)arenes. *Org. Lett.* **2020**, *22*, 6719−6723.
(144) Sattler, L. E.; Otten, C. J.; Hilt, G. Alternating Current Electrolysis for the Electrocatalytic Synthesis of Mixed Disulfide via Sulfur−Sulfur Bond Metathesis towards Dynamic Disulfide Libraries. *Chem. Eur. J.* **2020**, *26*, 3129−3136.

https://doi.org/10.1021/acs.chemrev.1c00471
Chem. Rev. XXXX, XXX, XXX−XXX

(145) Fry, A. J.; Little, R. D.; Leonetti, J. A General Mechanistic Scheme for Intramolecular Electrochemical Hydrocyclizations. Mechanism of Electroreductive Cyclization of ω-Keto-α,β-Unsaturated Esters. *J. Org. Chem.* **1994**, *59*, 5017−5026.
(146) Huynh, M. H. V.; Meyer, T. J. Proton-Coupled Electron Transfer. *Chem. Rev.* **2007**, *107*, 5004−5064.
(147) Costentin, C. Electrochemical Approach to the Mechanistic Study of Proton-Coupled Electron Transfer. *Chem. Rev.* **2008**, *108*, 2145−2179.
(148) Yi, H.; Zhang, G.; Wang, H.; Huang, Z.; Wang, J.; Singh, A. K.; Lei, A. Recent Advances in Radical C−H Activation/Radical Cross-Coupling. *Chem. Rev.* **2017**, *117*, 9016−9085.
(149) Andrieux, C. P.; Badoz-Lambling, J.; Combellas, C.; Lacombe, D.; Savéant, J.-M.; Thiebault, A.; Zann, D. Electron Transfer Catalyzed Reactions. Electrochemical Induction of the Hydrogen Atom Transfer Oxidation of Alcohols and Other Substrates by Aromatic Halides. *J. Am. Chem. Soc.* **1987**, *109*, 1518−1525.
(150) M'Halla, F.; Pinson, J.; Savéant, J.-M. The Solvent as Hydrogen-Atom Donor in Organic Electrochemical Reactions. Reduction of Aromatic Halides. *J. Am. Chem. Soc.* **1980**, *102*, 4120−4127.
(151) Gaudiello, J. G.; Wright, T. C.; Jones, R. A.; Bard, A. J. Electrochemical Reduction and Reoxidation Accompanied by Reversible Geometric Isomerization. Electrochemistry of $[Rh(\mu\text{-}t\text{-}Bu_2P)(CO)_2]_2$. Isolation and X-ray Crystal Structure of $[N(n\text{-}Bu)_4]_2^+[Rh(\mu\text{-}t\text{-}Bu_2P)(CO)_2]_2^{2-}$. *J. Am. Chem. Soc.* **1985**, *107*, 888−897.
(152) Rieke, R. D.; Kojima, H.; Oefele, K. Electrochemical Oxidation of Dicarbene Metal Carbonyl Complexes. Isomerization via an Electrochemical Reaction with No Net Current Flow. *J. Am. Chem. Soc.* **1976**, *98*, 6735−6737.
(153) Mabbott, G. A. An Introduction to Cyclic Voltammetry. *J. Chem. Educ.* **1983**, *60*, 697−702.
(154) Nicholson, R. S.; Shain, I. Theory of Stationary Electrode Polarography. Single Scan and Cyclic Methods Applied to Reversible, Irreversible, and Kinetic Systems. *Anal. Chem.* **1964**, *36*, 706−723.
(155) Evans, D. H.; O'Connell, K. M.; Petersen, R. A.; Kelly, M. J. Cyclic Voltammetry. *J. Chem. Educ.* **1983**, *60*, 290−293.
(156) Kissinger, P. T.; Heineman, W. R. Cyclic Voltammetry. *J. Chem. Educ.* **1983**, *60*, 702−706.
(157) Delahay, P. Theory of Irreversible Waves in Oscillographic Polarography. *J. Am. Chem. Soc.* **1953**, *75*, 1190−1196.
(158) Costentin, C.; Robert, M.; Savéant, J.-M. Catalysis of the Electrochemical Reduction of Carbon Dioxide. *Chem. Soc. Rev.* **2013**, *42*, 2423−2436.
(159) Costentin, C.; Drouet, S.; Robert, M.; Savéant, J.-M. A Local Proton Source Enhances CO_2 Electroreduction to CO by a Molecular Fe Catalyst. *Science* **2012**, *338*, 90−94.
(160) Bhugun, I.; Lexa, D.; Savéant, J.-M. Catalysis of the Electrochemical Reduction of Carbon Dioxide by Iron(0) Porphyrins: Synergystic Effect of Weak Brönsted Acids. *J. Am. Chem. Soc.* **1996**, *118*, 1769−1776.
(161) Hickey, D. P.; Sandford, C.; Rhodes, Z.; Gensch, T.; Fries, L. R.; Sigman, M. S.; Minteer, S. D. Investigating the Role of Ligand Electronics on Stabilizing Electrocatalytically Relevant Low-Valent Co(I) Intermediates. *J. Am. Chem. Soc.* **2019**, *141*, 1382−1392.
(162) Andrieux, C. P.; Hapiot, P.; Savéant, J.-M. Fast Chemical Steps Coupled with Outer-Sphere Electron Transfers. Application of Fast Scan Voltammetry at Ultramicroelectrodes to the Cleavage of Aromatic Halide Anion Radicals in the Microsecond Lifetime Range. *J. Phys. Chem.* **1988**, *92*, 5987−5992.
(163) McGuire, C. M.; Peters, D. G. Electrochemical Dechlorination of 4,4′-(2,2,2-trichloroethane-1,1-diyl)bis(chlorobenzene) (DDT) at Silver Cathodes. *Electrochim. Acta* **2014**, *137*, 423−430.
(164) Rathore, R.; Burns, C. L.; Deselnicu, M. I. Multiple-Electron Transfer in a Single Step. Design and Synthesis of Highly Charged Cation-Radical Salts. *Org. Lett.* **2001**, *3*, 2887−2890.
(165) Wang, V. C.-C.; Johnson, B. A. Interpreting the Electrocatalytic Voltammetry of Homogeneous Catalysts by the Foot of the Wave Analysis and Its Wider Implications. *ACS Catal.* **2019**, *9*, 7109−7123.
(166) Matheu, R.; Neudeck, S.; Meyer, F.; Sala, X.; Llobet, A. Foot of the Wave Analysis for Mechanistic Elucidation and Benchmarking Applications in Molecular Water Oxidation Catalysis. *ChemSusChem* **2016**, *9*, 3361−3369.
(167) Gonell, S.; Miller, A. J. M. Carbon Dioxide Electroreduction Catalyzed by Organometallic Complexes. In *Advances in Organometallic Chemistry*; Pérez, P. J., Stone, F. G. A., West, R., Eds.; Academic Press: Cambridge, MA, 2018; Vol. *70*, pp 1−69.
(168) Savéant, J.-M.; Vianello, E. Potential-Sweep Chronoamperometry: Kinetic Currents for First−Order Chemical Reaction Parallel to Electron-Transfer Process (Catalytic Currents). *Electrochim. Acta* **1965**, *10*, 905−920.
(169) Costentin, C.; Savéant, J.-M. Multielectron, Multistep Molecular Catalysis of Electrochemical Reactions: Benchmarking of Homogeneous Catalysts. *ChemElectroChem* **2014**, *1*, 1226−1236.
(170) Costentin, C.; Drouet, S.; Robert, M.; Savéant, J.-M. Turnover Numbers, Turnover Frequencies, and Overpotential in Molecular Catalysis of Electrochemical Reactions. Cyclic Voltammetry and Preparative-Scale Electrolysis. *J. Am. Chem. Soc.* **2012**, *134*, 11235−11242.
(171) Lee, K. J.; Elgrishi, N.; Kandemir, B.; Dempsey, J. L. Electrochemical and Spectroscopic Methods for Evaluating Molecular Electrocatalysts. *Nat. Rev. Chem.* **2017**, *1*, 0039.
(172) Rountree, E. S.; McCarthy, B. D.; Eisenhart, T. T.; Dempsey, J. L. Evaluation of Homogeneous Electrocatalysts by Cyclic Voltammetry. *Inorg. Chem.* **2014**, *53*, 9983−10002.
(173) Laviron, E. General Expression of the Linear Potential Sweep Voltammogram in the Case of Diffusionless Electrochemical Systems. *J. Electroanal. Chem. Interfacial Electrochem.* **1979**, *101*, 19−28.
(174) Hanna, C. M.; Sanborn, C. D.; Ardo, S.; Yang, J. Y. Interfacial Electron Transfer of Ferrocene Immobilized onto Indium Tin Oxide through Covalent and Noncovalent Interactions. *ACS Appl. Mater. Interfaces* **2018**, *10*, 13211−13217.
(175) Isse, A. A.; Mussini, P. R.; Gennaro, A. New Insights into Electrocatalysis and Dissociative Electron Transfer Mechanisms: The Case of Aromatic Bromides. *J. Phys. Chem. C* **2009**, *113*, 14983−14992.
(176) Antonello, S.; Musumeci, M.; Wayner, D. D.; Maran, F. Electroreduction of Dialkyl Peroxides. Activation-Driving Force Relationships and Bond Dissociation Free Energies. *J. Am. Chem. Soc.* **1997**, *119*, 9541−9549.
(177) Rountree, E. S.; Martin, D. J.; McCarthy, B. D.; Dempsey, J. L. Linear Free Energy Relationships in the Hydrogen Evolution Reaction: Kinetic Analysis of a Cobaloxime Catalyst. *ACS Catal.* **2016**, *6*, 3326−3335.
(178) Scialdone, O.; Galia, A.; Errante, G.; Isse, A. A.; Gennaro, A.; Filardo, G. Electrocarboxylation of Benzyl Chlorides at Silver Cathode at the Preparative Scale Level. *Electrochim. Acta* **2008**, *53*, 2514−2528.
(179) Elgrishi, N.; Kurtz, A. D.; Dempsey, J. L. Reaction Parameters Influencing Cobalt Hydride Formation Kinetics: Implications for Benchmarking H_2-Evolution Catalysts. *J. Am. Chem. Soc.* **2017**, *139*, 239−244.
(180) Imbeaux, J. C.; Savéant, J.-M. Convolutive Potential Sweep Voltammetry: I. Introduction. *J. Electroanal. Chem. Interfacial Electrochem.* **1973**, *44*, 169−187.
(181) Savéant, J.-M.; Tessier, D. Convolution Potential Sweep Voltammetry: Part IV. Homogeneous Follow-Up Chemical Reactions. *J. Electroanal. Chem. Interfacial Electrochem.* **1975**, *61*, 251−263.
(182) Ammar, F.; Savéant, J.-M. Convolution Potential Sweep Voltammetry: II. Multistep Nernstian Waves. *J. Electroanal. Chem. Interfacial Electrochem.* **1973**, *47*, 215−221.
(183) Savéant, J.-M.; Tessier, D. Convolution Potential Sweep Voltammetry V. Determination of Charge Transfer Kinetics Deviating from the Butler−Volmer Behaviour. *J. Electroanal. Chem.* **1975**, *65*, 57−66.
(184) Savéant, J.-M.; Tessier, D. Convolution Potential Sweep Voltammetry: Part VI. Experimental Evaluation in the Kilovolt per

https://doi.org/10.1021/acs.chemrev.1c00471
Chem. Rev. XXXX, XXX, XXX−XXX

Second Sweep Rate Range. *J. Electroanal. Chem. Interfacial Electrochem.* **1977**, *77*, 225−235.
(185) Nadjo, L.; Savéant, J.-M.; Tessier, D. Convolution Potential Sweep Voltammetry: III. Effect of Sweep Rate Cyclic Voltammetry. *J. Electroanal. Chem. Interfacial Electrochem.* **1974**, *52*, 403−412.
(186) Nicholson, R. S.; Shain, I. Experimental Verification of an ECE Mechanism for the Reduction of *p*-Nitrosophenol, Using Stationary Electrode Polarography. *Anal. Chem.* **1965**, *37*, 190−195.
(187) Nicholson, R. S.; Shain, I. Theory of Stationary Electrode Polarography for a Chemical Reaction Coupled Between Two Charge Transfers. *Anal. Chem.* **1965**, *37*, 178−190.
(188) Olmstead, M. L.; Hamilton, R. G.; Nicholson, R. S. Theory of Cyclic Voltammetry for a Dimerization Reaction Initiated Electrochemically. *Anal. Chem.* **1969**, *41*, 260−267.
(189) Kudirka, P. J.; Nicholson, R. S. Experimental Evaluation of Cyclic Voltammetry Theory for Disproportionation Reactions. *Anal. Chem.* **1972**, *44*, 1786−1794.
(190) Wipf, D. O.; Kristensen, E. W.; Deakin, M. R.; Wightman, R. M. Fast-Scan Cyclic Voltammetry as a Method To Measure Rapid, Heterogeneous Electron-Transfer Kinetics. *Anal. Chem.* **1988**, *60*, 306−310.
(191) Howell, J. O.; Wightman, R. M. Ultrafast Voltammetry and Voltammetry in Highly Resistive Solutions with Microvoltammetric Electrodes. *Anal. Chem.* **1984**, *56*, 524−529.
(192) Amatore, C.; Maisonhaute, E. When Voltammetry Reaches Nanoseconds. *Anal. Chem.* **2005**, *77*, 303A−311A.
(193) Johnson, J. A.; Hobbs, C. N.; Wightman, R. M. Removal of Differential Capacitive Interferences in Fast-Scan Cyclic Voltammetry. *Anal. Chem.* **2017**, *89*, 6166−6174.
(194) Amatore, C.; Lefrou, C.; Pflüger, F. On-line Compensation of Ohmic Drop in Submicrosecond Time Resolved Cyclic Voltammetry at Ultramicroelectrodes. *J. Electroanal. Chem. Interfacial Electrochem.* **1989**, *270*, 43−59.
(195) Pathirathna, P.; Balla, R. J.; Amemiya, S. Nanogap-Based Electrochemical Measurements at Double-Carbon-Fiber Ultramicroelectrodes. *Anal. Chem.* **2018**, *90*, 11746−11750.
(196) Ching, S.; Dudek, R.; Tabet, E. Cyclic Voltammetry with Ultramicroelectrodes. *J. Chem. Educ.* **1994**, *71*, 602−605.
(197) Keithley, R. B.; Takmakov, P.; Bucher, E. S.; Belle, A. M.; Owesson-White, C. A.; Park, J.; Wightman, R. M. Higher Sensitivity Dopamine Measurements with Faster-Scan Cyclic Voltammetry. *Anal. Chem.* **2011**, *83*, 3563−3571.
(198) Rodeberg, N. T.; Sandberg, S. G.; Johnson, J. A.; Phillips, P. E.; Wightman, R. M. Hitchhiker's Guide to Voltammetry: Acute and Chronic Electrodes for in Vivo Fast-Scan Cyclic Voltammetry. *ACS Chem. Neurosci.* **2017**, *8*, 221−234.
(199) Venton, B. J.; Cao, Q. Fundamentals of Fast-Scan Cyclic Voltammetry for Dopamine Detection. *Analyst* **2020**, *145*, 1158−1168.
(200) Andrieux, C. P.; Hapiot, P.; Savéant, J.-M. Fast Potential Step Techniques at Ultramicroelectrodes. Application to the Kinetic Characterization of Electrochemically Generated Short-Lived Species. *J. Phys. Chem.* **1988**, *92*, 5992−5995.
(201) Schmittel, M.; Peters, K.; Peters, E.-M.; Haeuseler, A.; Trenkle, H. Radical Cation Ester Cleavage in Solution. Mechanism of the Mesolytic O−CO Bond Scission. *J. Org. Chem.* **2001**, *66*, 3265−3276.
(202) Yang, H.; Bard, A. J. The Application of Fast Scan Cyclic Voltammetry. Mechanistic Study of the Initial Stage of Electropolymerization of Aniline in Aqueous Solutions. *J. Electroanal. Chem.* **1992**, *339*, 423−449.
(203) Rheinhardt, J. H.; Mubarak, M. S.; Foley, M. P.; Peters, D. G. Reduction of 4-(Bromomethyl)-2-oxo-2*H*-chromen-7-yl Acetate at Carbon Cathodes in Dimethylformamide and Acetonitrile: Lifetime of the Electrogenerated Radical−Anion. *J. Electroanal. Chem.* **2011**, *654*, 44−51.
(204) Andrieux, C. P.; Audebert, P.; Hapiot, P.; Savéant, J.-M. Observation of the Cation Radicals of Pyrrole and of Some Substituted Pyrroles in Fast-Scan Cyclic Voltammetry. Standard Potentials and Lifetimes. *J. Am. Chem. Soc.* **1990**, *112*, 2439−2440.
(205) Murray, R. W. Nanoelectrochemistry: Metal Nanoparticles, Nanoelectrodes, and Nanopores. *Chem. Rev.* **2008**, *108*, 2688−2720.
(206) Watkins, J. J.; Chen, J.; White, H. S.; Abruña, H. D.; Maisonhaute, E.; Amatore, C. Zeptomole Voltammetric Detection and Electron-Transfer Rate Measurements Using Platinum Electrodes of Nanometer Dimensions. *Anal. Chem.* **2003**, *75*, 3962−3971.
(207) Bruckenstein, S.; Miller, B. Unraveling Reactions with Rotating Electrodes. *Acc. Chem. Res.* **1977**, *10*, 54−61.
(208) Malachesky, P. A.; Prater, K. B.; Petrie, G.; Adams, R. N. Measurement of Chemical Reaction Rates Following Electron Transfer. An Empirical Approach Using Ring-Disk Electrodes. *J. Electroanal. Chem. Interfacial Electrochem.* **1968**, *16*, 41−46.
(209) Sunarso, J.; Torriero, A. A.; Zhou, W.; Howlett, P. C.; Forsyth, M. Oxygen Reduction Reaction Activity of La-Based Perovskite Oxides in Alkaline Medium: A Thin-Film Rotating Ring-Disk Electrode Study. *J. Phys. Chem. C* **2012**, *116*, 5827−5834.
(210) Zhou, R.; Zheng, Y.; Jaroniec, M.; Qiao, S.-Z. Determination of the Electron Transfer Number for the Oxygen Reduction Reaction: From Theory to Experiment. *ACS Catal.* **2016**, *6*, 4720−4728.
(211) Bard, A. J.; Parsons, R.; Jordan, J. *Standard Potentials in Aqueous Solution*; Marcel Dekker: New York, 1985.
(212) Amatore, C.; Jutand, A. Anionic Pd(0) and Pd(II) Intermediates in Palladium-Catalyzed Heck and Cross-Coupling Reactions. *Acc. Chem. Res.* **2000**, *33*, 314−321.
(213) Adamo, C.; Amatore, C.; Ciofini, I.; Jutand, A.; Lakmini, H. Mechanism of the Palladium-Catalyzed Homocoupling of Arylboronic Acids: Key Involvement of a Palladium Peroxo Complex. *J. Am. Chem. Soc.* **2006**, *128*, 6829−6836.
(214) Chen, G.; Liu, H. Understanding the Reduction Kinetics of Aqueous Vanadium(V) and Transformation Products Using Rotating Ring-Disk Electrodes. *Environ. Sci. Technol.* **2017**, *51*, 11643−11651.
(215) Marken, F.; Akkermans, R. P.; Compton, R. G. Voltammetry in the Presence of Ultrasound: the Limit of Acoustic Streaming Induced Diffusion Layer Thinning and the Effect of Solvent Viscosity. *J. Electroanal. Chem.* **1996**, *415*, 55−63.
(216) Compton, R. G.; Eklund, J. C.; Page, S. D.; Sanders, G. H. W.; Booth, J. Voltammetry in the Presence of Ultrasound. Sonovoltammetry and Surface Effects. *J. Phys. Chem.* **1994**, *98*, 12410−12414.
(217) Compton, R. G.; Eklund, J. C.; Page, S. D. Sonovoltammetry: Heterogeneous Electron-Transfer Processes with Coupled Ultrasonically Induced Chemical Reaction: The "Sono-EC" Reaction. *J. Phys. Chem.* **1995**, *99*, 4211−4214.
(218) Compton, R. G.; Eklund, J. C.; Marken, F. Sonoelectrochemical Processes: A Review. *Electroanalysis* **1997**, *9*, 509−522.
(219) Banks, C. E.; Compton, R. G. Ultrasonically Enhanced Voltammetric Analysis and Applications: An Overview. *Electroanalysis* **2003**, *15*, 329−346.
(220) Eklund, J. C.; Waller, D. N.; Rebbitt, T. O.; Marken, F.; Compton, R. G. Organic Sonoelectrochemistry: Reduction of Fluorescein in the Prescence of 20 kHz Power Ultrasound: An EC' reaction. *J. Chem. Soc., Perkin Trans. 2* **1995**, *2*, 1981−1984.
(221) *Laboratory Techniques in Electroanalytical Chemistry*; Kissinger, P. T., Heineman, W. R., Eds.; Marcel Dekker, Inc.: New York, 1984.
(222) Osteryoung, J. G.; Osteryoung, R. A. Square Wave Voltammetry. *Anal. Chem.* **1985**, *57*, 101A−110A.
(223) Roesel, A. F.; Ugandi, M.; Huyen, N. T. T.; Májek, M.; Broese, T.; Roemelt, M.; Francke, R. Electrochemically Catalyzed Newman−Kwart Rearrangement: Mechanism, Structure−Reactivity Relationship, and Parallels to Photoredox Catalysis. *J. Org. Chem.* **2020**, *85*, 8029−8044.
(224) Sperry, J. B.; Wright, D. L. The *gem*-Dialkyl Effect in Electron Transfer Reactions: Rapid Synthesis of Seven-Membered Rings through an Electrochemical Annulation. *J. Am. Chem. Soc.* **2005**, *127*, 8034−8035.
(225) Tang, T.; Sandford, C.; Minteer, S. D.; Sigman, M. S. Analyzing Mechanisms in Co(I) Redox Catalysis Using a Pattern Recognition Platform. *Chem. Sci.* **2021**, *12*, 4771−4778.

https://doi.org/10.1021/acs.chemrev.1c00471
Chem. Rev. XXXX, XXX, XXX−XXX

(226) Sandford, C.; Fries, L. R.; Ball, T. E.; Minteer, S. D.; Sigman, M. S. Mechanistic Studies into the Oxidative Addition of Co(I) Complexes: Combining Electroanalytical Techniques with Parameterization. *J. Am. Chem. Soc.* **2019**, *141*, 18877−18889.
(227) Tennyson, A. G.; Lynch, V. M.; Bielawski, C. W. Arrested Catalysis: Controlling Kumada Coupling Activity via a Redox-Active N-Heterocyclic Carbene. *J. Am. Chem. Soc.* **2010**, *132*, 9420−9429.
(228) Zevenbergen, M. A.; Krapf, D.; Zuiddam, M. R.; Lemay, S. G. Mesoscopic Concentration Fluctuations in a Fluidic Nanocavity Detected by Redox Cycling. *Nano Lett.* **2007**, *7*, 384−388.
(229) Mathwig, K.; Lemay, S. G. Mass Transport in Electrochemical Nanogap Sensors. *Electrochim. Acta* **2013**, *112*, 943−949.
(230) Zevenbergen, M. A.; Wolfrum, B. L.; Goluch, E. D.; Singh, P. S.; Lemay, S. G. Fast Electron-Transfer Kinetics Probed in Nanofluidic Channels. *J. Am. Chem. Soc.* **2009**, *131*, 11471−11477.
(231) Mathwig, K.; Zafarani, H. R.; Speck, J. M.; Sarkar, S.; Lang, H.; Lemay, S. G.; Rassaei, L.; Schmidt, O. G. Potential-Dependent Stochastic Amperometry of Multiferrocenylthiophenes in an Electrochemical Nanogap Transducer. *J. Phys. Chem. C* **2016**, *120*, 23262−23267.
(232) Mirkin, M. V.; Bulhoes, L. O. S.; Bard, A. J. Determination of the Kinetic Parameters for the Electroreduction of C_{60} by Scanning Electrochemical Microscopy and Fast Scan Cyclic Voltammetry. *J. Am. Chem. Soc.* **1993**, *115*, 201−204.
(233) Gavach, C. In *Biological Aspects of Electrochemistry*; Millazo, G., Jones, P. E., Rampazzo, L., Eds.; Springer: Basel, Switzerland, 1971; pp 321−331.
(234) Guastalla, J. Interface Hysteresis and Negative Differential Conductance at Liquid−Liquid Junction Between Non-miscible Ionic Solutions. *Nature* **1970**, *227*, 485−486.
(235) Gavach, C.; d'Epenoux, B. Chronopotentiometric Investigation of the Diffusion Overvoltage at the Interface Between Two Non-Miscible Solutions: II. Potassium Halide Aqueous Solution-Hexadecyl-Trimethylammonium Picrate Nitrobenzene Solution. *J. Electroanal. Chem. Interfacial Electrochem.* **1974**, *55*, 59−67.
(236) Gavach, C.; Mlodnicka, T.; Guastalla, J. Overvoltage Phenomena at Interfaces Between Organic and Aqueous Solutions. *C. R. Acad. Sci., Ser. C* **1968**, *266*, 1196−1199.
(237) Koryta, J. Electrochemical Polarization Phenomena at the Interface of Two Immiscible Electrolyte Solutions—III. Progress since 1983. *Electrochim. Acta* **1988**, *33*, 189−197.
(238) Koryta, J. Electrochemical Polarization Phenomena at the Interface of Two Immiscible Electrolyte Solutions—II. Progress Since 1978. *Electrochim. Acta* **1984**, *29*, 445−452.
(239) Koryta, J. Electrochemical Polarization Phenomena at the Interface of Two Immiscible Electrolyte Solutions. *Electrochim. Acta* **1979**, *24*, 293−300.
(240) Girault, H. H. J. Electrochemistry at the Interface Between Two Immiscible Electrolyte Solutions. *Electrochim. Acta* **1987**, *32*, 383−385.
(241) Girault, H. H. J.; Schiffrin, D. J. A New Approach for the Definition of Galvani Potential Scales and Ionic Gibbs Energies of Transfer Across Liquid-Liquid Interfaces. *Electrochim. Acta* **1986**, *31*, 1341−1342.
(242) Girault, H. H. J.; Schiffrin, D. J. Theory of the Kinetics of Ion Transfer Across Liquid/Liquid Interfaces. *J. Electroanal. Chem. Interfacial Electrochem.* **1985**, *195*, 213−227.
(243) Girault, H. H. J.; Schiffrin, D. J. Thermodynamics of a Polarised Interface Between Two Immiscible Electrolyte Solutions. *J. Electroanal. Chem. Interfacial Electrochem.* **1984**, *170*, 127−141.
(244) Lozeman, J. J. A.; Führer, P.; Olthuis, W.; Odijk, M. Spectroelectrochemistry, the Future of Visualizing Electrode Processes by Hyphenating Electrochemistry with Spectroscopic Techniques. *Analyst* **2020**, *145*, 2482−2509.
(245) Dunsch, L. Recent Advances in in situ multi-spectroelectrochemistry. *J. Solid State Electrochem.* **2011**, *15*, 1631−1646.
(246) Wain, A. J.; O'Connell, M. A. Advances in Surface-Enhanced Vibrational Spectroscopy at Electrochemical Interfaces. *Adv. Phys. X* **2017**, *2*, 188−209.
(247) Tong, Y. J. In Situ Electrochemical Nuclear Magnetic Resonance Spectroscopy for Electrocatalysis: Challenges and Prospects. *Curr. Opin. Electrochem.* **2017**, *4*, 60−68.
(248) Zhai, Y.; Zhu, Z.; Zhou, S.; Zhu, C.; Dong, S. Recent Advances in Spectroelectrochemistry. *Nanoscale* **2018**, *10*, 3089−3111.
(249) Garoz-Ruiz, J.; Perales-Rondon, J. V.; Heras, A.; Colina, A. Spectroelectrochemical Sensing: Current Trends and Challenges. *Electroanalysis* **2019**, *31*, 1254−1278.
(250) León, L.; Mozo, J. Designing Spectroelectrochemical Cells: A Review. *TrAC, Trends Anal. Chem.* **2018**, *102*, 147−169.
(251) Shah, A. H. A. UV−Vis Spectroelectrochemistry. In *Encyclopedia of Applied Electrochemistry*; Savinell, R. F., Ota, K.-I., Kreysa, G., Eds.; Springer: New York, 2014; pp 2099−2102.
(252) Bauhofer, J. Electrochemical Applications of Internal Reflection Spectroscopy. In *Internal Reflection Spectroscopy: Theory and Applications*; Mirabella, F. M., Jr., Ed.; Marcel Dekker: New York, 1992; pp 233−254.
(253) Robinson, R. S.; McCurdy, C. W.; McCreery, R. L. Microsecond Spectroelectrochemistry by External Reflection from Cylindrical Microelectrodes. *Anal. Chem.* **1982**, *54*, 2356−2361.
(254) Robinson, R. S.; McCreery, R. L. Submicrosecond Spectroelectrochemistry Applied to Chlorpromazine Cation Radical Charge-Transfer Reactions. *J. Electroanal. Chem. Interfacial Electrochem.* **1985**, *182*, 61−72.
(255) Mayausky, J. S.; McCreery, R. L. Spectroelectrochemical Examination of Charge Transfer Between Chlorpromazine Cation Radical and Catecholamines. *Anal. Chem.* **1983**, *55*, 308−312.
(256) Pilkington, M. B. G.; Coles, B. A.; Compton, R. G. Construction of an Optically Transparent Thin-Layer-Electrode Cell for Use with Oxygen-Sensitive Species in Aqueous and Nonaqueous solvents. *Anal. Chem.* **1989**, *61*, 1787−1789.
(257) Yogendra, S.; Schulz, S.; Hennersdorf, F.; Kumar, S.; Fischer, R.; Weigand, J. J. Reductive Ring Opening of a Cyclo-Tri-(phosphonio)methanide Dication to a Phosphanylcarbodiphosphorane: In Situ UV−vis Spectroelectrochemistry and Gold Coordination. *Organometallics* **2018**, *37*, 748−754.
(258) Malinauskas, A.; Holze, R. In Situ UV−Vis Spectroelectrochemical Evidence of an EC Mechanism in the Electrooxidation of *N*-Methylaniline. *Ber. Bunsenges. Phys. Chem.* **1997**, *101*, 1859−1864.
(259) Zhao, M.; Tang, X.; Zhang, H.; Gu, C.; Ma, Y. Characterization of Complicated Electropolymerization Using UV−Vis Spectroelectrochemistry and an Electrochemical Quartz-Crystal Microbalance with Dissipation: A Case Study of Tricarbazole Derivatives. *Electrochem. Commun.* **2021**, *123*, 106913.
(260) Molina, A.; Laborda, E.; Gómez-Gil, J.; Martínez-Ortiz, F.; Compton, R. Analytical Solutions for the Study of Homogeneous First-Order Chemical Kinetics via UV−Vis Spectroelectrochemistry. *J. Electroanal. Chem.* **2018**, *819*, 202−213.
(261) Gora, M.; Pluczyk, S.; Zassowski, P.; Krzywiec, W.; Zagorska, M.; Mieczkowski, J.; Lapkowski, M.; Pron, A. EPR and UV−vis Spectroelectrochemical Studies of Diketopyrrolopyrroles Disubstituted with Alkylated Thiophenes. *Synth. Met.* **2016**, *216*, 75−82.
(262) Pluczyk, S.; Zassowski, P.; Rybakiewicz, R.; Wielgosz, R.; Zagorska, M.; Lapkowski, M.; Pron, A. UV−Vis and EPR Spectroelectrochemical Investigations of Triarylamine Functionalized Arylene Bisimides. *RSC Adv.* **2015**, *5*, 7401−7412.
(263) Zhang, J.; Wang, J.; Wei, C.; Wang, Y.; Xie, G.; Li, Y.; Li, M. Rapidly Sequence-Controlled Electrosynthesis of Organometallic Polymers. *Nat. Commun.* **2020**, *11*, 2530.
(264) Seifert, T. P.; Klein, J.; Gamer, M. T.; Knöfel, N. D.; Feuerstein, T. J.; Sarkar, B.; Roesky, P. W. Synthesis, Spectroscopy, and Redox Studies of Ferrocene-Functionalized Coinage Metal Alkyne Complexes. *Inorg. Chem.* **2019**, *58*, 2997−3006.
(265) Das, A.; Scherer, T.; Maji, S.; Mondal, T. K.; Mobin, S. M.; Urbanos, F. A.; Jiménez-Aparicio, R.; Kaim, W.; Lahiri, G. K. Reductive Approach to Mixed Valency (n = 1-) in the Pyrazine Ligand-Bridged $[(acac)_2Ru(\mu\text{-}L^{2-})Ru(acac)_2]^n$ (L^{2-} = 2,5−Pyrazine-

https://doi.org/10.1021/acs.chemrev.1c00471
Chem. Rev. XXXX, XXX, XXX−XXX

Dicarboxylate) Through Experiment and Theory. *Inorg. Chem.* **2011**, *50*, 7040−7049.
(266) Sazanovich, I. V.; Alamiry, M. A. H.; Best, J.; Bennett, R. D.; Bouganov, O. V.; Davies, E. S.; Grivin, V. P.; Meijer, A. J. H. M.; Plyusnin, V. F.; Ronayne, K. L.; et al. Excited State Dynamics of a Pt^{II} Diimine Complex Bearing a Naphthalene-Diimide Electron Acceptor. *Inorg. Chem.* **2008**, *47*, 10432−10445.
(267) Ito, T.; Hamaguchi, T.; Nagino, H.; Yamaguchi, T.; Kido, H.; Zavarine, I. S.; Richmond, T.; Washington, J.; Kubiak, C. P. Electron Transfer on the Infrared Vibrational Time Scale in the Mixed Valence State of 1,4-Pyrazine- and 4,4′-Bipyridine-Bridged Ruthenium Cluster Complexes. *J. Am. Chem. Soc.* **1999**, *121*, 4625−4632.
(268) Wain, A. J.; O'Connell, M. A.; Attard, G. A. Insights into Self-Poisoning During Catalytic Hydrogenation on Platinum Surfaces Using ATR-IR Spectroelectrochemistry. *ACS Catal.* **2018**, *8*, 3561−3570.
(269) Pander, J. E., III; Baruch, M. F.; Bocarsly, A. B. Probing the Mechanism of Aqueous CO_2 Reduction on Post-Transition-Metal Electrodes Using ATR-IR Spectroelectrochemistry. *ACS Catal.* **2016**, *6*, 7824−7833.
(270) Koca, A.; Kalkan, A.; Bayır, Z. A. Electrocatalytic oxygen reduction and hydrogen evolution reactions on phthalocyanine modified electrodes: Electrochemical, in situ spectroelectrochemical, and in situ electrocolorimetric monitoring. *Electrochim. Acta* **2011**, *56*, 5513−5525.
(271) Pastor, E.; Le Formal, F.; Mayer, M. T.; Tilley, S. D.; Francàs, L.; Mesa, C. A.; Grätzel, M.; Durrant, J. R. Spectroelectrochemical Analysis of the Mechanism of (Photo)electrochemical Hydrogen Evolution at a Catalytic Interface. *Nat. Commun.* **2017**, *8*, 14280.
(272) Zhang, Q.; Song, W.-L.; Hossain, A. M. S.; Liu, Z.-D.; Hu, G.-J.; Tian, Y.-P.; Wu, J.-Y.; Jin, B.-K.; Zhou, H.-P.; Yang, J.-X.; Zhang, S.-Y. Synthesis, crystal structure, electrochemistry and in situ FTIR spectroelectrochemistry of a bisferrocene pyrazole derivative. *Dalton Trans.* **2011**, *40*, 3510−3516.
(273) Foley, J. K.; Pons, S. In Situ Infrared Spectroelectrochemistry. *Anal. Chem.* **1985**, *57*, 945A−956A.
(274) Borg, S. J.; Behrsing, T.; Best, S. P.; Razavet, M.; Liu, X.; Pickett, C. J. Electron Transfer at a Dithiolate-Bridged Diiron assembly: Electrocatalytic Hydrogen Evolution. *J. Am. Chem. Soc.* **2004**, *126*, 16988−16999.
(275) Zahran, Z. N.; Shaw, M. J.; Khan, M. A.; Richter-Addo, G. B. Fiber-Optic Infrared Spectroelectrochemical Studies of Six-Coordinate Manganese Nitrosyl Porphyrins in Nonaqueous Media. *Inorg. Chem.* **2006**, *45*, 2661−2668.
(276) Stoll, M. E.; Geiger, W. E. In-Situ IR Spectroelectrochemistry Study of One-Electron Oxidations of Bis(cyclopentadienyl) Molybdenum(II)-Alkyne or -Alkene Compounds. *Organometallics* **2004**, *23*, 5818−5823.
(277) Petek, M.; Neal, T. E.; Murray, R. W. Spectroelectrochemistry. Application of Optically Transparent Minigrid Electrodes Under Semiinfinite Diffusion Conditions. *Anal. Chem.* **1971**, *43*, 1069−1074.
(278) Krejčik, M.; Daněk, M.; Hartl, F. Simple Construction of an Infrared Optically Transparent Thin-Layer Electrochemical Cell: Applications to the Redox Reactions of Ferrocene, $Mn_2(CO)_{10}$ and $Mn(CO)^3$(3,5-di-*t*-butyl-catecholate)$^-$. *J. Electroanal. Chem. Interfacial Electrochem.* **1991**, *317*, 179−187.
(279) Yun, K.-S.; Joo, S.; Kim, H.-J.; Kwak, J.; Yoon, E. Silicon Micromachined Infrared Thin-Layer Cell for in Situ Spectroelectrochemical Analysis of Aqueous and Nonaqueous Solvent System. *Electroanalysis* **2005**, *17*, 959−964.
(280) Kaim, W.; Fiedler, J. Spectroelectrochemistry: The Best of Two Worlds. *Chem. Soc. Rev.* **2009**, *38*, 3373−3382.
(281) Lins, E.; Read, S.; Unni, B.; Rosendahl, S. M.; Burgess, I. J. Microsecond Resolved Infrared Spectroelectrochemistry Using Dual Frequency Comb IR Lasers. *Anal. Chem.* **2020**, *92*, 6241−6244.
(282) Ashley, K.; Pons, S. Infrared Spectroelectrochemistry. *Chem. Rev.* **1988**, *88*, 673−695.
(283) Machan, C. W.; Sampson, M. D.; Chabolla, S. A.; Dang, T.; Kubiak, C. P. Developing a Mechanistic Understanding of Molecular Electrocatalysts for CO_2 Reduction Using Infrared Spectroelectrochemistry. *Organometallics* **2014**, *33*, 4550−4559.
(284) Jin, B.-K.; Li, L.; Huang, J.-L.; Zhang, S.-Y.; Tian, Y.-P.; Yang, J.-X. IR Spectroelectrochemical Cyclic Voltabsorptometry and Derivative Cyclic Voltabsorptometry. *Anal. Chem.* **2009**, *81*, 4476−4481.
(285) Cheng, W.-X.; Jin, B.-K.; Huang, P.; Cheng, L.-J.; Zhang, S.-Y.; Tian, Y.-P. Investigation on the π-Dimer/σ-Dimer of 1,8-Dihydroxy-9,10-anthracenedione in the Process of Electrochemical Reduction by Using IR Spectroelectrochemical Cyclic Voltabsorptometry and Derivative Cyclic Voltabsorptometry. *J. Phys. Chem. C* **2013**, *117*, 3940−3948.
(286) Hashimoto, K.; Badarla, V. R.; Kawai, A.; Ideguchi, T. Complementary Vibrational Spectroscopy. *Nat. Commun.* **2019**, *10*, 4411.
(287) Jones, R. R.; Hooper, D. C.; Zhang, L.; Wolverson, D.; Valev, V. K. Raman Techniques: Fundamentals and Frontiers. *Nanoscale Res. Lett.* **2019**, *14*, 231.
(288) Le Ru, E.; Etchegoin, P. *Principles of Surface-Enhanced Raman Spectroscopy*; Elsevier: Oxford, U.K., 2009.
(289) Aroca, R. *Surface-Enhanced Vibrational Spectroscopy*; Wiley: West Sussex, England, 2006.
(290) Fleischmann, M.; Hendra, P. J.; McQuillan, A. J. Raman Spectra of Pyridine Adsorbed at a Silver Electrode. *Chem. Phys. Lett.* **1974**, *26*, 163−166.
(291) Niaura, G.; Gaigalas, A. K.; Vilker, V. L. Moving Spectroelectrochemical Cell for Surface Raman Spectroscopy. *J. Raman Spectrosc.* **1997**, *28*, 1009−1011.
(292) Yamada, H.; Amamiya, T.; Tsubomura, H. Resonance Raman Spectra of Rose Bengal Adsorbed on a ZnO Electrode. *Chem. Phys. Lett.* **1978**, *56*, 591−594.
(293) dos Santos, M. F.; Katic, V.; dos Santos, P. L.; Pires, B. M.; Formiga, A. L. B.; Bonacin, J. A. 3D-printed Low-Cost Spectroelectrochemical Cell for in Situ Raman Measurements. *Anal. Chem.* **2019**, *91*, 10386−10389.
(294) Blacha-Grzechnik, A.; Karon, K.; Data, P. Raman and IR Spectroelectrochemical Methods as Tools to Analyze Conjugated Organic Compounds. *J. Visualized Exp.* **2018**, *140*, No. e56653.
(295) McCreery, R. L.; Packard, R. T. Raman Monitoring of Dynamic Electrochemical Events. *Anal. Chem.* **1989**, *61*, 775A−789A.
(296) Packard, R. T.; McCreery, R. L. Raman Monitoring of Reactive Electrogenerated Species: Kinetics of Halide Addition to *o*-Quinones. *J. Phys. Chem.* **1988**, *92*, 6345−6351.
(297) Wang, A.; Huang, Y.-F.; Sur, U. K.; Wu, D.-Y.; Ren, B.; Rondinini, S.; Amatore, C.; Tian, Z.-Q. In Situ Identification of Intermediates of Benzyl Chloride Reduction at a Silver Electrode by SERS Coupled with DFT Calculations. *J. Am. Chem. Soc.* **2010**, *132*, 9534−9536.
(298) Itoh, T.; McCreery, R. L. In Situ Raman Spectroelectrochemistry of Azobenzene Monolayers on Glassy Carbon. *Anal. Bioanal. Chem.* **2007**, *388*, 131−134.
(299) Itoh, T.; McCreery, R. L. In situ Raman Spectroelectrochemistry of Electron Transfer Between Glassy Carbon and a Chemisorbed Nitroazobenzene Monolayer. *J. Am. Chem. Soc.* **2002**, *124*, 10894−10902.
(300) Richards, J. A.; Evans, D. H. Flow cell for Electrolysis Within the Probe of a Nuclear Magnetic Resonance Spectrometer. *Anal. Chem.* **1975**, *47*, 964−966.
(301) Cao, S.-H.; Ni, Z.-R.; Huang, L.; Sun, H.-J.; Tang, B.; Lin, L.-J.; Huang, Y.-Q.; Zhou, Z.-Y.; Sun, S.-G.; Chen, Z. In Situ Monitoring Potential-Dependent Electrochemical Process by Liquid NMR Spectroelectrochemical Determination: A Proof-of-Concept Study. *Anal. Chem.* **2017**, *89*, 3810−3813.
(302) Bussy, U.; Boujtita, M. Review of Advances in Coupling Electrochemistry and Liquid State NMR. *Talanta* **2015**, *136*, 155−160.
(303) Bussy, U.; Giraudeau, P.; Silvestre, V.; Jaunet-Lahary, T.; Ferchaud-Roucher, V.; Krempf, M.; Akoka, S.; Tea, I.; Boujtita, M. In Situ NMR Spectroelectrochemistry for the Structure Elucidation of

https://doi.org/10.1021/acs.chemrev.1c00471
Chem. Rev. XXXX, XXX, XXX−XXX

Unstable Intermediate Metabolites. *Anal. Bioanal. Chem.* **2013**, *405*, 5817−5824.
(304) Klod, S.; Ziegs, F.; Dunsch, L. In Situ NMR Spectroelectrochemistry of Higher Sensitivity by Large Scale Electrodes. *Anal. Chem.* **2009**, *81*, 10262−10267.
(305) Falck, D.; Niessen, W. M. A. Solution-Phase Electrochemistry-Nuclear Magnetic Resonance of Small Organic Molecules. *TrAC, Trends Anal. Chem.* **2015**, *70*, 31−39.
(306) Klod, S.; Dunsch, L. A combination of in situ ESR and in situ NMR spectroelectrochemistry for mechanistic studies of electrode reactions: the case of *p*-benzoquinone. *Magn. Reson. Chem.* **2011**, *49*, 725−729.
(307) da Silva, P. F.; Gomes, B. F.; Lobo, C. M. S.; Queiroz Júnior, L. H. K.; Danieli, E.; Carmo, M.; Blümich, B.; Colnago, L. A. Electrochemical NMR Spectroscopy: Electrode Construction and Magnetic Sample Stirring. *Microchem. J.* **2019**, *146*, 658−663.
(308) Hinds, G.; Spada, F. E.; Coey, J. M. D.; Ní Mhíochán, T. R.; Lyons, M. E. G. Magnetic Field Effects on Copper Electrolysis. *J. Phys. Chem. B* **2001**, *105*, 9487−9502.
(309) Monzon, L. M. A.; Coey, J. M. D. Magnetic Fields in Electrochemistry: The Lorentz Force. A Mini-Review. *Electrochem. Commun.* **2014**, *42*, 38−41.
(310) Boisseau, R.; Bussy, U.; Giraudeau, P.; Boujtita, M. In Situ Ultrafast 2D NMR Spectroelectrochemistry for Real-Time Monitoring of Redox Reactions. *Anal. Chem.* **2015**, *87*, 372−375.
(311) Berliner, L. J.; Khramtsov, V.; Fujii, H.; Clanton, T. L. Unique in vivo applications of spin traps. *Free Radical Biol. Med.* **2001**, *30*, 489−499.
(312) Adams, R. N. Application of Electron Paramagnetic Resonance Techniques in Electrochemistry. *J. Electroanal. Chem.* **1964**, *8*, 151−162.
(313) Davies, M. J. Detection and Characterisation of Radicals Using Electron Paramagnetic Resonance (EPR) Spin Trapping and Related Methods. *Methods* **2016**, *109*, 21−30.
(314) Drago, R. S. *Physical Methods in Chemistry*; W.B. Saunders Co.: Philadelphia, PA, 1977.
(315) Roessler, M. M.; Salvadori, E. Principles and Applications of EPR Spectroscopy in the Chemical Sciences. *Chem. Soc. Rev.* **2018**, *47*, 2534−2553.
(316) Weil, J. A.; Bolton, J. R. *Electron Paramagnetic Resonance: Elementary Theory and Practical Applications*; 2nd ed.; Wiley: Hoboken, NJ, 2006.
(317) Bunce, N. J. Introduction to the Interpretation of Electron Spin Resonance Spectra of Organic Radicals. *J. Chem. Educ.* **1987**, *64*, 907−914.
(318) Geske, D. H.; Maki, A. H. Electrochemical Generation of Free Radicals and Their Study by Electron Spin Resonance Spectroscopy; The Nitrobenzene Anion Radical. *J. Am. Chem. Soc.* **1960**, *82*, 2671−2676.
(319) Murray, P. R.; Collison, D.; Daff, S.; Austin, N.; Edge, R.; Flynn, B. W.; Jack, L.; Leroux, F.; McInnes, E. J. L.; Murray, A. F.; et al. An in situ electrochemical cell for Q- and W-band EPR spectroscopy. *J. Magn. Reson.* **2011**, *213*, 206−209.
(320) Wang, B.; Fielding, A. J.; Dryfe, R. A. W. In Situ Electrochemical Electron Paramagnetic Resonance Spectroscopy as a Tool to Probe Electrical Double Layer Capacitance. *Chem. Commun.* **2018**, *54*, 3827−3830.
(321) Martínez Suárez, J. F.; Caram, J. A.; Echeverría, G. A.; Piro, O. E.; Gennaro, A. M.; Mirífico, M. V. Electrosynthesis of *N*-Methylisatin. *J. Org. Chem.* **2019**, *84*, 6879−6885.
(322) Liu, Q.; Sun, B.; Liu, Z.; Kao, Y.; Dong, B.-W.; Jiang, S.-D.; Li, F.; Liu, G.; Yang, Y.; Mo, F. A General Electrochemical Strategy for the Sandmeyer Reaction. *Chem. Sci.* **2018**, *9*, 8731−8737.
(323) Eaton, G. R.; Eaton, S. S.; Barr, D. P.; Weber, R. T. *Quantitative EPR*; Springer: Germany, 2010.
(324) Tamski, M. A.; Dale, M. W.; Breeze, B. G.; Macpherson, J. V.; Unwin, P. R.; Newton, M. E. Quantitative Measurements in Electrochemical Electron Paramagnetic Resonance. *Electrochim. Acta* **2016**, *213*, 802−810.
(325) Holland, J. P.; Barnard, P. J.; Collison, D.; Dilworth, J. R.; Edge, R.; Green, J. C.; McInnes, E. J. L. Spectroelectrochemical and Computational Studies on the Mechanism of Hypoxia Selectivity of Copper Radiopharmaceuticals. *Chem. Eur. J.* **2008**, *14*, 5890−5907.
(326) Sarneski, J. E.; Thorp, H. H.; Brudvig, G. W.; Crabtree, R. H.; Schulte, G. K. Assembly of High-Valent Oxomanganese Clusters in Aqueous Solution. Redox equilibrium of Water-Stable $Mn_3O_4^{4+}$ and $Mn_2O_2^{3+}$ Complexes. *J. Am. Chem. Soc.* **1990**, *112*, 7255−7260.
(327) Virmani, Y. P.; Zeller, E. J. Analysis of Background Copper Concentration in Sea Water by Electron Spin Resonance. *Anal. Chem.* **1974**, *46*, 324−325.
(328) *Modern Practice of Gas Chromatography*, 4th ed.; Grob, R. L., Barry, E. F., Eds.; Wiley: New York, 2004.
(329) Miller, J. M. *Chromatography: Concepts and Contrasts*, 2nd ed.; Wiley: Hoboken, NJ, 2005.
(330) Snyder, L. R.; Kirkland, J. J.; Dolan, J. W. *Introduction to Modern Liquid Chromatography*, 3rd ed.; Wiley: Hoboken, NJ, 2010.
(331) Snyder, L. R.; Kirkland, J. J.; Glajch, J. L. *Practical HPLC Method Development*; Wiley: New York, 2012.
(332) Stein, S. Mass Spectral Reference Libraries: An Ever-Expanding Resource for Chemical Identification. *Anal. Chem.* **2012**, *84*, 7274−7282.
(333) McLafferty, F. W.; Stauffer, D. A.; Loh, S. Y.; Wesdemiotis, C. Unknown Identification Using Reference Mass Spectra. Quality Evaluation of Databases. *J. Am. Soc. Mass Spectrom.* **1999**, *10*, 1229−1240.
(334) Milman, B. L. General Principles of Identification by Mass Spectrometry. *TrAC, Trends Anal. Chem.* **2015**, *69*, 24−33.
(335) Little, J. L.; Cleven, C. D.; Brown, S. D. Identification of "Known Unknowns" Utilizing Accurate Mass Data and Chemical Abstracts Service Databases. *J. Am. Soc. Mass Spectrom.* **2011**, *22*, 348−359.
(336) Dresen, S.; Gergov, M.; Politi, L.; Halter, C.; Weinmann, W. ESI-MS/MS Library of 1,253 Compounds for Application in Forensic and Clinical Toxicology. *Anal. Bioanal. Chem.* **2009**, *395*, 2521−2526.
(337) Pritts, W. A.; Vieira, K. L.; Peters, D. G. Quantitative Determination of Volatile Products Formed in Electrolyses of Organic Compounds. *Anal. Chem.* **1993**, *65*, 2145−2149.
(338) Xu, Y.; Zhu, Y.; Zhao, F.; Ma, C.−A. Electrocatalytic Reductive Dehalogenation of Polyhalogenated Phenols in Aqueous Solution on Ag Electrodes. *Appl. Catal., A* **2007**, *324*, 83−86.
(339) Verlato, E.; He, W.; Amrane, A.; Barison, S.; Floner, D.; Fourcade, F.; Geneste, F.; Musiani, M.; Seraglia, R. Preparation of Silver-Modified Nickel Foams by Galvanic Displacement and Their Use as Cathodes for the Reductive Dechlorination of Herbicides. *ChemElectroChem* **2016**, *3*, 2084−2092.
(340) Jahn, S.; Karst, U. Electrochemistry Coupled to (Liquid Chromatography/) Mass Spectrometry—Current State and Future Perspectives. *J. Chromatogr. A* **2012**, *1259*, 16−49.
(341) Oberacher, H.; Pitterl, F.; Erb, R.; Plattner, S. Mass Spectrometric Methods for Monitoring Redox Processes in Electrochemical Cells. *Mass Spectrom. Rev.* **2015**, *34*, 64−92.
(342) Iwahashi, H.; Ishii, T. Detection of the Oxidative Products of 3-Hydroxykynurenine Using High-Performance Liquid Chromatography−Electrochemical Detection−Ultraviolet Absorption Detection−Electron Spin Resonance Spectrometry and High-Performance Liquid Chromatography−Electrochemical Detection−Ultraviolet Absorption Detection−Mass Spectrometry. *J. Chromatogr. A* **1997**, *773*, 23−31.
(343) Iwahashi, H. 3-Hydroxyanthranilic Acid-Derived Compounds Formed Through Electrochemical Oxidation. *J. Chromatogr., Biomed. Appl.* **1999**, *736*, 237−245.
(344) Gamache, P. H.; Meyer, D. F.; Granger, M. C.; Acworth, I. N. Metabolomic Applications of Electrochemistry/Mass Spectrometry. *J. Am. Soc. Mass Spectrom.* **2004**, *15*, 1717−1726.
(345) Lohmann, W.; Karst, U. Electrochemistry Meets Enzymes: Instrumental On-Line Simulation of Oxidative and Conjugative Metabolism Reactions of Toremifene. *Anal. Bioanal. Chem.* **2009**, *394*, 1341−1348.

https://doi.org/10.1021/acs.chemrev.1c00471
Chem. Rev. XXXX, XXX, XXX−XXX

(346) Moghaddam, A. B.; Ganjali, M. R.; Norouzi, P.; Niasari, M. A Green Method on the Electro-Organic Synthesis of New Caffeic Acid Derivatives: Electrochemical Properties and LC−ESI−MS Analysis of Products. *J. Electroanal. Chem.* **2007**, *601*, 205−210.
(347) Zettersten, C.; Co, M.; Wende, S.; Turner, C.; Nyholm, L.; Sjöberg, P. J. R. Identification and Characterization of Polyphenolic Antioxidants Using On-Line Liquid Chromatography, Electrochemistry, and Electrospray Ionization Tandem Mass Spectrometry. *Anal. Chem.* **2009**, *81*, 8968−8977.
(348) Li, K.-M.; Byun, J.; Gross, M. L.; Zamzow, D.; Jankowiak, R.; Rogan, E. G.; Cavalieri, E. L. Synthesis and Structure Determination of the Adducts Formed by Electrochemical Oxidation of Dibenzo[*a*, *l*]pyrene in the Presence of Adenine. *Chem. Res. Toxicol.* **1999**, *12*, 749−757.
(349) Erb, R.; Plattner, S.; Pitterl, F.; Brouwer, H.-J.; Oberacher, H. An Optimized Electrochemistry-Liquid Chromatography-Mass Spectrometry Method for Studying Guanosine Oxidation. *Electrophoresis* **2012**, *33*, 614−621.
(350) Plattner, S.; Erb, R.; Pitterl, F.; Brouwer, H.-J.; Oberacher, H. Formation and Characterization of Covalent Guanosine Adducts with Electrochemistry−Liquid Chromatography−Mass Spectrometry. *J. Chromatogr. B: Anal. Technol. Biomed. Life Sci.* **2012**, *883*−*884*, 198−204.
(351) Roeser, J.; Alting, N. F.; Permentier, H. P.; Bruins, A. P.; Bischoff, R. Boron-Doped Diamond Electrodes for the Electrochemical Oxidation and Cleavage of Peptides. *Anal. Chem.* **2013**, *85*, 6626−6632.
(352) McClintock, C.; Kertesz, V.; Hettich, R. L. Development of an Electrochemical Oxidation Method for Probing Higher Order Protein Structure with Mass Spectrometry. *Anal. Chem.* **2008**, *80*, 3304−3317.
(353) Roeser, J.; Permentier, H. P.; Bruins, A. P.; Bischoff, R. Electrochemical Oxidation and Cleavage of Tyrosine- and Tryptophan-Containing Tripeptides. *Anal. Chem.* **2010**, *82*, 7556−7565.
(354) Basile, F.; Hauser, N. Rapid Online Nonenzymatic Protein Digestion Combining Microwave Heating Acid Hydrolysis and Electrochemical Oxidation. *Anal. Chem.* **2011**, *83*, 359−367.
(355) Faber, H.; Lutze, H.; Lareo, P. L.; Frensemeier, L.; Vogel, M.; Schmidt, T. C.; Karst, U. Liquid Chromatography/Mass Spectrometry to Study Oxidative Degradation of Environmentally Relevant Pharmaceuticals by Electrochemistry and Ozonation. *J. Chromatogr. A* **2014**, *1343*, 152−159.
(356) Torres, S.; Brown, R.; Zelesky, T.; Scrivens, G.; Szucs, R.; Hawkins, J. M.; Taylor, M. R. Electrochemical Oxidation Coupled with Liquid Chromatography and Mass Spectrometry to Study the Oxidative Stability of Active Pharmaceutical Ingredients in Solution: A Comparison of Off-Line and On-Line Approaches. *J. Pharm. Biomed. Anal.* **2016**, *131*, 71−79.
(357) Torres, S.; Brown, R.; Szucs, R.; Hawkins, J. M.; Scrivens, G.; Pettman, A.; Kraus, D.; Taylor, M. R. Rapid Synthesis of Pharmaceutical Oxidation Products Using Electrochemistry: A Systematic Study of *N*-Dealkylation Reactions of Fesoterodine Using a Commercially Available Synthesis Cell. *Org. Process Res. Dev.* **2015**, *19*, 1596−1603.
(358) Torres, S.; Brown, R.; Szucs, R.; Hawkins, J. M.; Zelesky, T.; Scrivens, G.; Pettman, A.; Taylor, M. R. The Application of Electrochemistry to Pharmaceutical Stability Testing−Comparison with in Silico Prediction and Chemical Forced Degradation Approaches. *J. Pharm. Biomed. Anal.* **2015**, *115*, 487−501.
(359) Faber, H.; Melles, D.; Brauckmann, C.; Wehe, C. A.; Wentker, K.; Karst, U. Simulation of the Oxidative Metabolism of Diclofenac by Electrochemistry/(Liquid Chromatography/) Mass Spectrometry. *Anal. Bioanal. Chem.* **2012**, *403*, 345−354.
(360) Mekonnen, T. F.; Panne, U.; Koch, M. Electrochemistry Coupled Online to Liquid Chromatography-Mass Spectrometry for Fast Simulation of Biotransformation Reactions of the Insecticide Chlorpyrifos. *Anal. Bioanal. Chem.* **2017**, *409*, 3359−3368.
(361) Polcaro, A. M.; Mascia, M.; Palmas, S.; Vacca, A. Electrochemical Degradation of Diuron and Dichloroaniline at BDD Electrode. *Electrochim. Acta* **2004**, *49*, 649−656.
(362) Alves, S. A.; Ferreira, T. C.; Migliorini, F. L.; Baldan, M. R.; Ferreira, N. G.; Lanza, M. R. Electrochemical Degradation of the Insecticide Methyl Parathion using a Boron-Doped Diamond Film Anode. *J. Electroanal. Chem.* **2013**, *702*, 1−7.
(363) Mekonnen, T. F.; Panne, U.; Koch, M. Prediction of biotransformation products of the fungicide fluopyram by electrochemistry coupled online to liquid chromatography-mass spectrometry and comparison with in vitro microsomal assays. *Anal. Bioanal. Chem.* **2018**, *410*, 2607−2617.
(364) Lohmann, W.; Hayen, H.; Karst, U. Covalent Protein Modification by Reactive Drug Metabolites Using Online Electrochemistry/Liquid Chromatography/Mass Spectrometry. *Anal. Chem.* **2008**, *80*, 9714−9719.
(365) Santi, M.; Seitz, J.; Cicala, R.; Hardwick, T.; Ahmed, N.; Wirth, T. Memory of Chirality in Flow Electrochemistry: Fast Optimisation with DoE and Online 2D-HPLC. *Chem. Eur. J.* **2019**, *25*, 16230−16235.
(366) Chen, C. S.; Wan, J. H.; Yeo, B. S. Electrochemical Reduction of Carbon Dioxide to Ethane Using Nanostructured Cu_2O-Derived Copper Catalyst and Palladium(II) Chloride. *J. Phys. Chem. C* **2015**, *119*, 26875−26882.
(367) Xiang, K.; Zhu, F.; Liu, Y.; Pan, Y.; Wang, X.; Yan, X.; Liu, H. A Strategy to Eliminate Carbon Deposition on a Copper Electrode in Order to Enhance Its Stability in CO_2RR Catalysis by Introducing Crystal Defects. *Electrochem. Commun.* **2019**, *102*, 72−77.
(368) de Koning, S.; Janssen, H.-G.; Brinkman, U. A. T. Modern Methods of Sample Preparation for GC Analysis. *Chromatographia* **2009**, *69*, 33−78.
(369) Pasciak, E. M.; Hochstetler, S. E.; Mubarak, M. S.; Evans, D. H.; Peters, D. G. Electrochemical Reduction of Phthalide at Carbon Cathodes in Dimethylformamide: Effects of Supporting Electrolyte and Gas Chromatographic Injector-Port Chemistry on the Product Distribution. *Electrochim. Acta* **2013**, *113*, 557−563.
(370) Wang, Q.; Wang, Q.; Zhang, Y.; Mohamed, Y. M.; Pacheco, C.; Zheng, N.; Zare, R. N.; Chen, H. Electrocatalytic Redox Neutral [3 + 2] Annulation of *N*-Cyclopropylanilines and Alkenes. *Chem. Sci.* **2021**, *12*, 969−975.
(371) Ye, X.; Zhao, P.; Zhang, S.; Zhang, Y.; Wang, Q.; Shan, C.; Wojtas, L.; Guo, H.; Chen, H.; Shi, X. Facilitating Gold Redox Catalysis with Electrochemistry: An Efficient Chemical-Oxidant-Free Approach. *Angew. Chem., Int. Ed.* **2019**, *58*, 17226−17230.
(372) Bruckenstein, S.; Gadde, R. R. Use of a Porous Electrode for in Situ Mass Spectrometric Determination of Volatile Electrode Reaction Products. *J. Am. Chem. Soc.* **1971**, *93*, 793−794.
(373) Diehl, G.; Karst, U. On-Line Electrochemistry−MS and Related Techniques. *Anal. Bioanal. Chem.* **2002**, *373*, 390−398.
(374) Hoffmann, T.; Hofmann, D.; Klumpp, E.; Küppers, S. Electrochemistry-Mass Spectrometry for Mechanistic Studies and Simulation of Oxidation Processes in the Environment. *Anal. Bioanal. Chem.* **2011**, *399*, 1859−1868.
(375) Karst, U. Electrochemistry/Mass Spectrometry (EC/MS)—A New Tool to Study Drug Metabolism and Reaction Mechanisms. *Angew. Chem., Int. Ed.* **2004**, *43*, 2476−2478.
(376) Ashton, S. J. *Design, Construction and Research Application of a Differential Electrochemical Mass Spectrometer (DEMS)*; Springer: Berlin, Germany, 2012.
(377) Baltruschat, H. Differential Electrochemical Mass Spectrometry. *J. Am. Soc. Mass Spectrom.* **2004**, *15*, 1693−1706.
(378) Wolter, O.; Heitbaum, J. Differential Electrochemical Mass Spectroscopy (DEMS)—A New Method for the Study of Electrode Processes. *Ber. Bunsenges. Phys. Chem.* **1984**, *88*, 2−6.
(379) Herl, T.; Matysik, F.-M. Recent Developments in Electrochemistry−Mass Spectrometry. *ChemElectroChem* **2020**, *7*, 2498−2512.
(380) Clark, E. L.; Bell, A. T. Direct Observation of the Local Reaction Environment During the Electrochemical Reduction of CO_2. *J. Am. Chem. Soc.* **2018**, *140*, 7012−7020.
(381) Peverly, A. A.; Karty, J. A.; Peters, D. G. Electrochemical Reduction of (1*R*, 2*r*, 3*S*, 4*R*, 5*r*, 6*S*)-Hexachlorocyclohexane

https://doi.org/10.1021/acs.chemrev.1c00471
Chem. Rev. XXXX, XXX, XXX−XXX

(Lindane) at Silver Cathodes in Organic and Aqueous−Organic Media. *J. Electroanal. Chem.* **2013**, *692*, 66−71.
(382) Couto Petro, A. G.; Thapa, B.; Karty, J. A.; Raghavachari, K.; Baker, L. A.; Peters, D. G. Direct Electrochemical Reduction of Acetochlor at Carbon and Silver Cathodes in Dimethylformamide. *J. Electrochem. Soc.* **2020**, *167*, 155517.
(383) De, R.; Gonglach, S.; Paul, S.; Haas, M.; Sreejith, S. S.; Gerschel, P.; Apfel, U.-P.; Vuong, T. H.; Rabeah, J.; Roy, S.; Schöfberger, W. Electrocatalytic Reduction of CO_2 to Acetic Acid by a Molecular Manganese Corrole Complex. *Angew. Chem.* **2020**, *132*, 10614−10621.
(384) Engstrom, R. C.; Weber, M.; Wunder, D. J.; Burgess, R.; Winquist, S. Measurements Within the Diffusion Layer Using a Microelectrode Probe. *Anal. Chem.* **1986**, *58*, 844−848.
(385) Bard, A. J.; Fan, F.-R. F.; Kwak, J.; Lev, O. Scanning Electrochemical Microscopy. Introduction and Principles. *Anal. Chem.* **1989**, *61*, 132−138.
(386) Liu, H.-Y.; Fan, F.-R. F.; Lin, C. W.; Bard, A. J. Scanning Electrochemical and Tunneling Ultramicroelectrode Microscope for High-Resolution Examination of Electrode Surfaces in Solution. *J. Am. Chem. Soc.* **1986**, *108*, 3838−3839.
(387) Amemiya, S.; Bard, A. J.; Fan, F.-R. F.; Mirkin, M. V.; Unwin, P. R. Scanning Electrochemical Microscopy. *Annu. Rev. Anal. Chem.* **2008**, *1*, 95−131.
(388) Bard, A. J. Introduction and Principles. In *Scanning electrochemical microscopy*; Bard, A. J., Mirkin, M. V., Eds.; CRC Press: Boca Raton, FL, 2012; pp 1−15.
(389) Eckhard, K.; Schuhmann, W. Alternating Current Techniques in Scanning Electrochemical Microscopy (AC-SECM). *Analyst* **2008**, *133*, 1486−1497.
(390) Polcari, D.; Dauphin-Ducharme, P.; Mauzeroll, J. Scanning Electrochemical Microscopy: A Comprehensive Review of Experimental Parameters from 1989 to 2015. *Chem. Rev.* **2016**, *116*, 13234−13278.
(391) Wipf, D. O.; Bard, A. J.; Tallman, D. E. Scanning Electrochemical Microscopy. 21. Constant−Current Imaging with an Autoswitching Controller. *Anal. Chem.* **1993**, *65*, 1373−1377.
(392) Zhou, F.; Unwin, P. R.; Bard, A. J. Scanning Electrochemical Microscopy. 16. Study of Second-Order Homogeneous Chemical Reactions via the Feedback and Generation/Collection Modes. *J. Phys. Chem.* **1992**, *96*, 4917−4924.
(393) Wuu, Y.-M.; Fan, F.-R. F.; Bard, A. J. High Resolution Deposition of Polyaniline on Pt with the Scanning Electrochemical Microscope. *J. Electrochem. Soc.* **1989**, *136*, 885−886.
(394) Cao, F.; Kim, J.; Bard, A. J. Detection of the Short-Lived Cation Radical Intermediate in the Electrochemical Oxidation of *N,N*-Dimethylaniline by Scanning Electrochemical Microscopy. *J. Am. Chem. Soc.* **2014**, *136*, 18163−18169.
(395) Yang, H.; Wipf, D. O.; Bard, A. J. Application of Rapid Scan Cyclic Voltammetry to a Study of the Oxidation and Dimerization of *N,N*-Dimethylaniline in Acetonitrile. *J. Electroanal. Chem.* **1992**, *331*, 913−924.
(396) Marck, C.; Borgwarth, K.; Heinze, J. Generation of Polythiophene Micropatterns by Scanning Electrochemical Microscopy. *Chem. Mater.* **2001**, *13*, 747−752.
(397) Kai, T.; Zoski, C. G.; Bard, A. J. Scanning Electrochemical Microscopy at the Nanometer Level. *Chem. Commun.* **2018**, *54*, 1934−1947.
(398) Izquierdo, J.; Knittel, P.; Kranz, C. Scanning Electrochemical Microscopy: An Analytical Perspective. *Anal. Bioanal. Chem.* **2018**, *410*, 307−324.
(399) Ahn, H. S.; Bard, A. J. Switching Transient Generation in Surface Interrogation Scanning Electrochemical Microscopy and Time-of-Flight Techniques. *Anal. Chem.* **2015**, *87*, 12276−12280.
(400) Rodríguez-López, J.; Alpuche-Avilés, M. A.; Bard, A. J. Interrogation of Surfaces for the Quantification of Adsorbed Species on Electrodes: Oxygen on Gold and Platinum in Neutral Media. *J. Am. Chem. Soc.* **2008**, *130*, 16985−16995.
(401) Barker, A. L.; Gonsalves, M.; Macpherson, J. V.; Slevin, C. J.; Unwin, P. R. Scanning Electrochemical Microscopy: Beyond the Solid/Liquid Interface. *Anal. Chim. Acta* **1999**, *385*, 223−240.
(402) Shao, Y.; Mirkin, M. V. Scanning Electrochemical Microscopy (SECM) of Facilitated Ion Transfer at the Liquid|Liquid Interface. *J. Electroanal. Chem.* **1997**, *439*, 137−143.
(403) Barker, A. L.; Unwin, P. R.; Amemiya, S.; Zhou, J.; Bard, A. J. Scanning Electrochemistry Microscopy (SECM) in the Study of Electron Transfer Kinetics at Liquid/Liquid Interfaces: Beyond the Constant Composition Approximation. *J. Phys. Chem. B* **1999**, *103*, 7260−7269.
(404) Li, F.; Unwin, P. R. Scanning Electrochemical Microscopy (SECM) of Photoinduced Electron Transfer Kinetics at Liquid/Liquid Interfaces. *J. Phys. Chem. C* **2015**, *119*, 4031−4043.
(405) Zhang, Z.; Ye, J.; Sun, P.; Yuan, Y.; Tong, Y.; Hu, J.; Shao, Y. Study of Electron Transfer Across the Liquid/Ice-Like Matrix Interface by Scanning Electrochemical Microscopy. *Anal. Chem.* **2002**, *74*, 1530−1536.
(406) Selzer, Y.; Mandler, D. Probing the Coupling of Charge-Transfer Processes Across Liquid/Liquid Interfaces by the Scanning Electrochemical Microscope. *J. Phys. Chem. B* **2000**, *104*, 4903−4910.
(407) Kanoufi, F.; Cannes, C.; Zu, Y.; Bard, A. J. Scanning Electrochemical Microscopy. 43. Investigation of Oxalate Oxidation and Electrogenerated Chemiluminescence Across the Liquid-Liquid Interface. *J. Phys. Chem. B* **2001**, *105*, 8951−8962.
(408) Randles, J. E. B. A Cathode Ray Polarograph. Part II.—The Current-Voltage Curves. *Trans. Faraday Soc.* **1948**, *44*, 327−338.
(409) Hohenberg, P.; Kohn, W. Inhomogeneous Electron Gas. *Phys. Rev.* **1964**, *136*, B864−B871.
(410) Becke, A. D. Perspective: Fifty years of Density-Functional Theory in Chemical Physics. *J. Chem. Phys.* **2014**, *140*, 18A301.
(411) Fry, A. J. Computational Applications in Organic Electrochemistry. *Curr. Opin. Electrochem.* **2017**, *2*, 67−75.
(412) Baseden, K. A.; Tye, J. W. Introduction to Density Functional Theory: Calculations by Hand on the Helium Atom. *J. Chem. Educ.* **2014**, *91*, 2116−2123.
(413) Geerlings, P.; De Proft, F.; Langenaeker, W. Conceptual Density Functional Theory. *Chem. Rev.* **2003**, *103*, 1793−1874.
(414) Alfonso, D. R.; Tafen, D. N.; Kauffmann, D. R. First-Principles Modeling in Heterogeneous Electrocatalysis. *Catalysts* **2018**, *8*, 424.
(415) Marenich, A. V.; Ho, J.; Coote, M. L.; Cramer, C. J.; Truhlar, D. G. Computational Electrochemistry: Prediction of Liquid-Phase Reduction Potentials. *Phys. Chem. Chem. Phys.* **2014**, *16*, 15068−15106.
(416) Hicks, L. D.; Fry, A. J.; Kurzweil, V. C. Ab Initio Computation of Electron Affinities of Substituted Benzalacetophenones (Chalcones): A New Approach to Substituent Effects in Organic Electrochemistry. *Electrochim. Acta* **2004**, *50*, 1039−1047.
(417) Zuman, P. *Substituent Effects in Organic Polarography*; Springer: New York, 1967.
(418) Frontana, C.; Vázquez-Mayagoitia, Á.; Garza, J.; Vargas, R.; González, I. Substituent Effect on a Family of Quinones in Aprotic Solvents: An Experimental and Theoretical Approach. *J. Phys. Chem. A* **2006**, *110*, 9411−9419.
(419) Haya, L.; Sayago, F. J.; Mainar, A. M.; Cativiela, C.; Urieta, J. S. Quantum-Chemical Predictions of Redox Potentials of Carbamates in Methanol. *Phys. Chem. Chem. Phys.* **2011**, *13*, 17696−17703.
(420) Hammerich, O.; Hansen, T.; Thorvildsen, A.; Christensen, J. B. Electrochemical One-Electron Oxidation of Low-Generation Polyamidoamine-Type Dendrimers with a 1,4-Phenylenediamine Core. *ChemPhysChem* **2009**, *10*, 1805−1824.
(421) Alligrant, T. M.; Hackett, J. C.; Alvarez, J. C. Acid/Base and Hydrogen Bonding Effects on the Proton-Coupled Electron Transfer of Quinones and Hydroquinones in Acetonitrile: Mechanistic Investigation by Voltammetry, ^{1}H NMR and Computation. *Electrochim. Acta* **2010**, *55*, 6507−6516.
(422) Morton, K. W. Finite Difference and Finite Element Methods. *Comput. Phys. Commun.* **1976**, *12*, 99−108.

https://doi.org/10.1021/acs.chemrev.1c00471
Chem. Rev. XXXX, XXX, XXX−XXX

(423) Kobus, J. Finite-Difference versus Finite-Element Methods. *Chem. Phys. Lett.* **1993**, *202*, 7−12.
(424) Blazek, J. *Computational Fluid Dynamics: Principles and Applications*, 3rd ed.; Butterworth−Heinemann: Oxford, U.K., 2015.
(425) Rudolph, M. A Fast Implicit Finite Difference Algorithm for the Digital Simulation of Electrochemical Processes. *J. Electroanal. Chem. Interfacial Electrochem.* **1991**, *314*, 13−22.
(426) Rudolph, M. Digital simulations with the Fast Implicit Finite Difference (FIFD) Algorithm: Part II. An Improved Treatment of Electrochemical Mechanisms with Second-Order Reactions. *J. Electroanal. Chem.* **1992**, *338*, 85−98.
(427) Rudolph, M. Digital Simulations with the Fast Implicit Finite-Difference (FIFD) Algorithm. Part 4. Simulation of Electrical Migration and Diffuse Double-Layer Effects. *J. Electroanal. Chem.* **1994**, *375*, 89−99.
(428) Rudolph, M. Digital Simulation with the Fast Implicit Finite Difference (FIFD) Algorithm: Part 5: Digital Simulations of Square Wave Voltammetry for Any User Defined Electrochemical Mechanism Comprising First- and Second-Order Chemical Reactions. *J. Electroanal. Chem.* **2001**, *503*, 15−27.
(429) Nepomnyashchii, A. B.; Bröring, M.; Ahrens, J.; Bard, A. J. Synthesis, Photophysical, Electrochemical, and Electrogenerated Chemiluminescence Studies. Multiple Sequential Electron Transfers in BODIPY Monomers, Dimers, Trimers, and Polymer. *J. Am. Chem. Soc.* **2011**, *133*, 8633−8645.
(430) Batchelor-McAuley, C.; Kätelhön, E.; Barnes, E. O.; Compton, R. G.; Laborda, E.; Molina, A. Recent Advances in Voltammetry. *ChemistryOpen* **2015**, *4*, 224−260.
(431) Batchelor-McAuley, C.; Compton, R. G. Voltammetry of Multi-Electron Electrode Processes of Organic Species. *J. Electroanal. Chem.* **2012**, *669*, 73−81.
(432) Batchelor-McAuley, C.; Li, Q.; Dapin, S. M.; Compton, R. G. Voltammetric Characterization of DNA Intercalators Across the Full pH Range: Anthraquinone-2,6-disulfonate and Anthraquinone-2-sulfonate. *J. Phys. Chem. B* **2010**, *114*, 4094−4100.
(433) Cutress, I. J.; Dickinson, E. J.; Compton, R. G. Analysis of Commercial General Engineering Finite Element Software in Electrochemical Simulations. *J. Electroanal. Chem.* **2010**, *638*, 76−83.
(434) Zienkiewicz, O. C.; Taylor, R. L.; Zhu, J. Z. *The Finite Element Method: Its Basis and Fundamentals*, 6th ed.; Butterworth−Heinemann: Oxford, U.K., 2005.
(435) Reddy, J. N. *Introduction to the Finite Element Method*, 3rd ed.; McGraw-Hill: New York, 2006.
(436) Dickinson, E. J.; Ekström, H.; Fontes, E. COMSOL Multiphysics®: Finite Element Software for Electrochemical Analysis. A Mini-Review. *Electrochem. Commun.* **2014**, *40*, 71−74.
(437) Nioradze, N.; Kim, J.; Amemiya, S. Quasi-Steady-State Voltammetry of Rapid Electron Transfer Reactions at the Macroscopic Substrate of the Scanning Electrochemical Microscope. *Anal. Chem.* **2011**, *83*, 828−835.
(438) Petr, A.; Dunsch, L.; Neudeck, A. In Situ UV−Vis ESR Spectroelectrochemistry. *J. Electroanal. Chem.* **1996**, *412*, 153−158.
(439) Ibañez, D.; Garoz-Ruiz, J.; Heras, A.; Colina, A. Simultaneous UV−Visible Absorption and Raman Spectroelectrochemistry. *Anal. Chem.* **2016**, *88*, 8210−8217.
(440) Patten, H. V.; Meadows, K. E.; Hutton, L. A.; Iacobini, J. G.; Battistel, D.; McKelvey, K.; Colburn, A. W.; Newton, M. E.; Macpherson, J. V.; Unwin, P. R. Electrochemical Mapping Reveals Direct Correlation Between Heterogeneous Electron Transfer Kinetics and Local Density of States in Diamond Electrodes. *Angew. Chem., Int. Ed.* **2012**, *51*, 7002−7006.
(441) Bentley, C. L.; Kang, M.; Unwin, P. R. Scanning Electrochemical Cell Microscopy (SECCM) in Aprotic Solvents: Practical Considerations and Applications. *Anal. Chem.* **2020**, *92*, 11673−11680.
(442) Guell, A. G.; Ebejer, N.; Snowden, M. E.; McKelvey, K.; Macpherson, J. V.; Unwin, P. R. Quantitative Nanoscale Visualization of Heterogeneous Electron Transfer Rates in 2D Carbon Nanotube Networks. *Proc. Natl. Acad. Sci. U. S. A.* **2012**, *109*, 11487−11492.

https://doi.org/10.1021/acs.chemrev.1c00471
Chem. Rev. XXXX, XXX, XXX−XXX